Dissertation

submitted to the

Combined Faculty of Natural Sciences and Mathematics

of the Ruperto-Carola University Heidelberg, Germany

for the degree of

Doctor of Natural Sciences

Presented by,

Master of Science (M.Sc.) Amol Tandon
Born in Sitapur, India
Oral examination: 21.11.2018

ADP dependent glucokinase as a novel onco-target for haematological malignancies

Referees: Prof. Dr. Michael Brunner

PD Dr. Sven Wolfgang Sauer

ACKNOWLEDGEMENTS

My deep gratitude goes towards my supervisor PD Dr. Sven Sauer, who provided me the opportunity to work on this project and provided me help and guidance throughout. He stood like a pillar, providing selfless support, especially during the last phase of my PhD which made me focus away from all the difficult situations. His unwavering enthusiasm for my work constantly engaged me with my research and made my stay in the lab pleasant and fruitful.

Besides, I would also like to thank my first supervisor Prof. Dr. Michael Brunner and TAC member PD Dr. Karsten Gülow for all the suggestions and guidance during our meetings. I would also like to thank Prof. Dr. Stefan Wiemann and Dr. med. Mirko Völkers for joining my thesis committee in the final phase of my PhD.

Many thanks to Prof. Dr. Stefan Kölker, Prof. Dr. Georg Hoffman and PD Dr. Jürgen Okun for all the support provided during my project. I would like to give a big set of thanks to Brigitte Schmidt-Mader, Tanja Lunczer and Eleni Filiousi for helping me with metabolic measurements. Their support is really appreciated.

In addition I would also like to thank all my laboratory colleagues and the good friends whom I met during my stay in Heidelberg and their generous support throughout my PhD. Special thanks to Fr. Sigrid Gensichen for all her support and motivation starting from the first day of my arrival in Germany until now.

I am indebted to my family, whose sacrifices and prayers made my growth possible besides making me the person I am today. Words cannot say how grateful I am to my beautiful wife, Nagalla Deepthi Tandon, who provided endless days of non-tiring support and guidance and motivation at every single step; for the constant love and support, for all the late nights and mornings and for all the past months keeping me healthy and sane to complete my thesis.

SUMMARY

In this study we aimed at studying the tumor aggressiveness and differentiation potential of Ramos Burkitt's lymphoma cells upon mitogenic stimulation in light of a novel regulator of immune cell metabolism and activation, ADPGK.

We have identified the role of ADPGK in regulation of aerobic glycolysis in Burkitt's Lymphoma cells and shown that its knock-out leads to reduced tumor aggressiveness, as measured *in-vitro* via co-culture, migration experiments and metabolic profile, and *in-vivo* Zebrafish. We found significantly reduced *MYC* transcription in ADPGK knock-out Burkitt's lymphoma cells and importantly, several folds reduction in accumulated random mutations in translocated *MYC* in these cells. We additionally observed a stalled pathway to differentiation of ADPGK knock out B-cells into plasma cells upon stimulation by mitogenic signals. Overall, the study provided the first insights into the role of a novel ER resident protein acting as a regulator of two complementary phenomenon, cell-differentiation and cancer aggressiveness, and thereby opens up new possibilities of therapeutic interventions for hematopoietic malignancies.

ZUSAMMENFASSUNG

Ziel dieser Studie war es, die Tumoraggressivität und das Differenzierungspotential von Ramos Burkitts Lymphomzellen bei der mitogenen Stimulation im Lichte eines neuartigen Regulators des Immunzellstoffwechsels und der Aktivierung, ADPGK, zu untersuchen.

Wir haben die Rolle von ADPGK bei der Regulation der aeroben Glykolyse in Burkitt-Lymphom-Zellen identifiziert und gezeigt, dass dessen Knock-out zu reduzierter Aggressivität des Tumors führt, gemessen in-vitro über Co-Kultur- und Migrationsexperimente, metabolische Profile sowie in-vivo in Zebrafischen . Wir fanden eine signifikant reduzierte MYC Transkription in ADPGK Knock-Out Burkitt Lymphomzellen und eine verminderte Akkumulation zufälliger Mutationen in translozierten MYC in diesen Zellen. Wir beobachteten zusätzlich eine blockierte Differenzierung von ADPGK Knockout B-Zellen in Plasmazellen bei Stimulierung durch mitogene Signale. Insgesamt lieferte die Studie erste Einblicke in die Rolle eines neuen ER-residenten Proteins, das als Regulator zweier komplementärer Phänomene, Zelldifferenzierung und Krebsaggressivität agiert, und eröffnet damit neue Möglichkeiten therapeutischer Interventionen für hämatopoetische Malignome.

ABBREVIATIONS

Ab	Antibody
ADP	Adenosine diphosphate
ADPGK	ADP dependent glucokinase
ASC	Antibody secreting cell
ATP	Adenosine triphosphate
BL	Burkitt's lymphoma
Cas9	CRISPR-associated nuclease 9
CRISPR	Clustered Regularly Interspaced Short Palindromic Repeats
CSR	Class switch recombination
ER	Endoplasmic reticulum
FDG	Fluorodeoxyglucose
G6PD	Glucose-6-phsophate dehydrogenase
Gata1	GATA Binding Protein 1
GC	Germinal centre
GFAT	Glutamine:fructose-6-phosphate amidotransferase
GFP	Green fluorescence
HK	Hexokinase
Hpf	Hour post fertilization
Ig	Immunoglobulin
IP_3R	Inositol triphosphate receptor
IRE	Inositol requiring enzyme
KO	Knockout

LDH	Lactate dehydrogenase
MYC	Myelocytomatosis oncogene
NADH	Nicotinamide adenine dinucleotide
NADPH	Nicotinamide adenine dinucleotide phosphate
NBDG	2-(*N*-(7-Nitrobenz-2-oxa-1,3-diazol-4-yl)Amino)-2-Deoxyglucose glucose
OXPHOS	Oxidative phosphorylation
PAM	Protospacer adjacent motif
PMA	Phorbol 12-myristate 13-acetate
PPP	Pentose phosphate pathway
PYR	Pyruvate
ROS	Reactive oxygen species
SHM	Somatic hypermutation
TAM	Tumor associated macrophage
TCA cycle	Tricarboxylic acid cycle
VDJ	Variable diversity joining segment
WT	Wild type
XBP	X-box binding protein

Contents

Introduction 1
Warburg Effect or aerobic glycolysis 1
Burkitt's lymphoma 3
Somatic hypermutation and translocated *MYC* mutations 5
B-cell differentiation 8
ADP dependent glucokinase 13
Tumor microenvironment 14
Macrophage polarization 16
Zebrafish as xenograft model 17
Aims 18
Materials 20
Chemicals 20
Reagents 22
Kits 23
Machines and Devices 24
Disposables 25
Primer Sequences 26
Antibodies 27
Methods 28
Cell culture 28
ADPGK knock-out 28
ADPGK localization studies 29
Immunoblot Analysis 30
Quantitative RT PCR Analysis 31
Macrophage Migration Assay 31
Macrophage-Ramos co-culture 32
Amino-acid analysis 34
Lactate/Pyruvate measurements 34
Flow cytometric analysis for differentiation markers 34
Glucose uptake assay 35
Enzyme kinetics 35
Mutational analysis of translocated *MYC* 36

Zebrafish xenograft studies....36
Statistical analysis....38
Results....39
Preliminary studies....39
ADPGK knock-out and localization studies....39
ADPGK expression upon B-cell activation....41
PMA stimulation induced differentiation is hampered in *ADPGK* KO cells....43
Flow cytometric profiling signalled stalled differentiation and increased apoptosis in *ADPGK* KO cells....43
Activation associated homotypic aggregation is lost in *ADPGK* KO cells....44
ER stress-based differentiation markers are more expressed in *ADPGK* WT cells....47
ADPGK KO B-cells are metabolically toxified....51
ADPGK KO cells display reduced glycolysis in initial phases of stimulation driven differentiation....51
ADPGK KO cells are less 'glucoholic' than the wild type Ramos cells....51
Amino-acid uptake and metabolite secretion is remnant of activation driven metabolism in ADPGK KO cells....53
c-*MYC* expression and mutational status are dependent on glucose metabolism....55
ADPGK KO cells exhibit a near complete loss of c-Myc post activation....55
Translocated and wild-type c-*Myc* are expressed differentially in Ramos cells....57
Translocated c-*Myc* is highly mutated in WT cells compared to *ADPGK* KO....57
ADPGK KO leads to reduced migration of macrophages to tumor....60
Macrophage M1 polarization increases with KO of *ADPGK*....60
ADPGK KO affects the growth of lymphoma xenografts in Zebrafish larvae....63
Discussion....65
Perturbation of differentiation markers in ADPGK KO and WT cells....65
Metabolic catastrophe was bestowed upon *ADPGK* KO cells....67
c-*MYC* expression and mutational status are hampered by *ADPGK* KO....69
ADPGK KO cells resemble a nutrient starved condition....70
In-vitro and *in-vivo* models of reduced tumor aggressiveness in ADPGK KO cells....70
Outlook....72
Conclusion....73
Bibliography....74

INTRODUCTION

Warburg Effect or aerobic glycolysis

Normal somatic cells have a strict control of cell cycle and metabolism and possess numerous checkpoints to regulate the growth and differentiation status of the cell during its life cycle. However, through rare events, cells can acquire traits which leads them to a fully transformed cancerous state which is marked by uncontrolled growth and proliferation (Fouad & Aanei, 2017). The most common of these traits found in cancer is a metabolic state enabling the cells to upregulate glucose uptake and utilization several folds even in the presence of oxygen. The process, termed as Warburg effect or aerobic glycolysis, provides an evolutionary growth advantage to cancer cells and has in recent years become increasingly important as a target for curbing aggressively growing malignancies (Cairns, Harris, & Mak, 2011; DeBerardinis, Lum, Hatzivassiliou, & Thompson, 2008; Gatenby & Gillies, 2004; Liberti & Locasale, 2016). Glycolysis, or lytic metabolism of glucose, involves the conversion of glucose to pyruvate with production of ATP. Pyruvate is further converted into lactic acid as a waste product. In the presence of oxygen, glycolysis is redirected at the step of pyruvate, which is oxidised into CO_2 and H_20 by mitochondrial oxidative phosphorylation. This process of reduced lactate production by inhibition of the cycle at pyruvate in presence of oxygen is termed as 'Pasteur effect'. Under anaerobic conditions, such as in muscle cells during bursts of short intense exercise, enough oxygen is not present for oxidation of pyruvate and NADH produced in glycolysis. In such cases, NAD+ is reobtained from NADH by reduction of pyruvate to lactate, using the enzyme lactate dehydrogenase (Proia, Di Liegro, Schiera, Fricano, & Di Liegro, 2016). Thus, different fates of glucose over range of oxygen concentrations help the cells in adapting to the microenvironmental conditions prevalent at that time and continue the process of energy generation, although with varying efficiencies (Phan, Yeung, & Lee, 2014). In addition to these common occurrences, there arises a condition, mostly observed in fast proliferating cells or cancer, where glucose is converted to lactic acid even in the presence of sufficient amounts of oxygen. Known as aerobic glycolysis or Warburg effect, it is known to provide a growth advantage to tumors with respect to their microenvironment and additionally aides in selection of resistant and malignant cells in the developing tumor (Gatenby & Gillies, 2004; Liberti & Locasale, 2016).

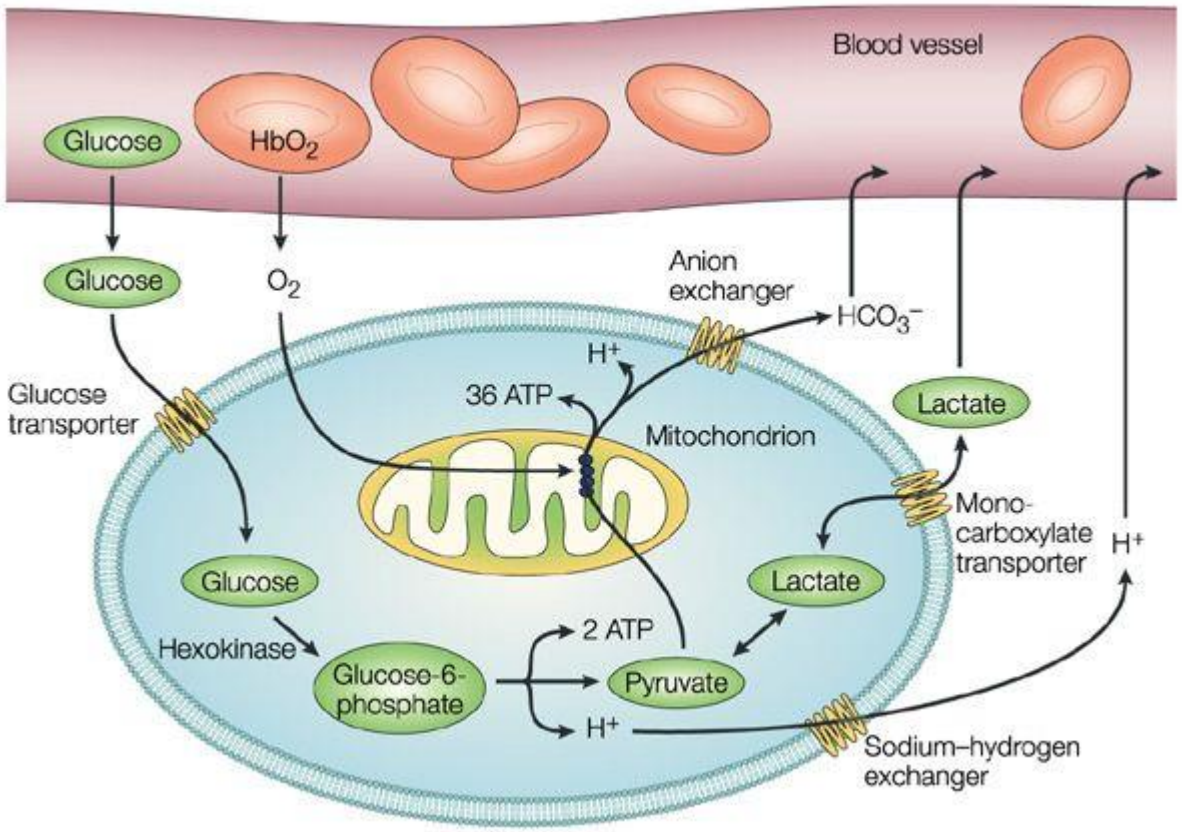

Figure 1.1 : Delivery of glucose and oxygen to tissues in the body, entering the cells via specific glucose transporters. The glucose taken up is primed into Glucose-6 phosphate by hexokinases to prevent its exit from the cell, and further through glycolysis converted to pyruvate with generation of 2 ATP molecules per glucose. In the presence of oxygen, mitochondrial oxidative phosphorylation oxidises pyruvate to HCO_3, and generates 36 additional ATP molecules per glucose. In anoxic conditions, pyruvate is reduced to lactic acid, which is then exported from the cell as a waste product. Hydrogen ions (H^+) are produced by both the processes and causes acidification of the extracellular space. HbO_2 represents oxygenated haemoglobin. Image adapted from (Gatenby & Gillies, 2004).

The importance of glucose metabolism for cancer cells was diminished shortly after the discovery of Warburg effect but has recently gained significance in the past decade, due to the widely known clinical imaging technique positron-emission tomography (PET) (Gatenby & Gillies, 2004). PET employs tracer molecule ^{18}fluorodeoxyglucose (FdG) as a glucose analogue and has proven with majority of lesions the increased glucose uptake and

accumulation of the tracer compared to non-malignant tissues in the body (Cox, Mackie, & Eliceiri, 2015). Another piece of information conveyed by PET scans is the avid trapping of fluorescent-glucose by immune cells owing to their increased proliferative phenotype and thereby upregulated glycolysis under inflammatory conditions (Escuin-Ordinas et al., 2013). Nonetheless, there exists a major difference between immune cell metabolism and cancer, in that the aerobic glycolytic phenotype is only transiently expressed in the former whereas it is stably and epigenetically switched on in case of the latter. Owing to this phenotypic switching to aerobic glycolysis, immune cells serve as an effective tool for modelling cancer cell metabolism.

Burkitt's lymphoma

Burkitt's lymphoma (BL), a malignancy of germinal centre B-cells, is the fastest growing human cancer (Molyneux et al., 2012) and owing its growth to one of the most widely studied oncogenes and regulator of glycolysis, *MYC*, provides a perfect model for study of Warburg effect (Buttgereit, Burmester, & Brand, 2000; Schmitz, Ceribelli, Pittaluga, Wright, & Staudt, 2014). The cancer, a non-Hodgkin's type Lymphoma, is one of the most commonly found paediatric cancer in regions of Africa and South America (Molyneux et al., 2012). The tumor is characterized by a very high proliferation rate with mostly monomorphic, medium-sized cells. The cells express markers typical of germinal-centre B-cells such as CD20, IgM, CD19, PAX5, CD10 and BCL6, but do not express nuclear TdT, CD5 and BCL2 (Dozzo et al., 2017). Under the microscope, upon H&E staining of tumor biopsies, a typical starry sky appearance is appreciated due to the presence of tangible-body macrophages (Andrade-Filho, 2014). The dense involvement of macrophages in almost all cases of Burkitt's lymphoma provides an additional advantage of studying tumor-microenvironment interrelationship (Scott & Gascoyne, 2014).

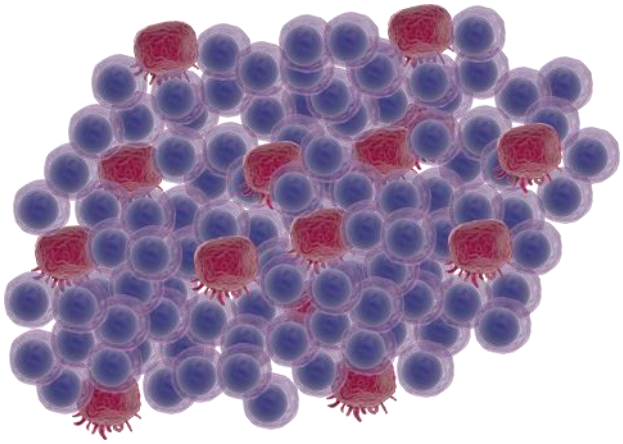

Figure 1.2: Dense involvement of tumor microenvironment in Burkitt's lymphoma with upto 10% of cells in the tumor occurring as immune cells (macrophages). Macrophages are depicted in red and in purple are the tumor cells with a large prominent nucleus and minimal cytoplasm.

The translocation t(8;14)(q24;q32) is the characteristic genetic hallmark of Burkitt's lymphoma, identified in most of the patient biopsies (Bemark & Neuberger, 2000; Cowling, Turner, & Cole, 2014; Eick & Bornkamm, 1989; Xu-Monette et al., 2016). This translocation brings *MYC* proto-oncogene into proximity with the immunoglobulin locus (H/L chain). Owing to the influence of heavy transcriptional activity of this locus, *MYC* expression is dysregulated and leads to a constitutive overexpression of *MYC* in Burkitt's lymphoma (Bemark & Neuberger, 2000). The overexpression of this proto-oncogene affects its downstream target genes, i.e. almost 15 percent of all genes; involved in cell proliferation, growth, differentiation, apoptosis and stem-cell renewal (Cowling et al., 2014). However, along with *MYC* translocation and overexpression, there are several other factors responsible for driving lymphomagenesis. Targeting *MYC* expression, nonetheless, remains as an attractive strategy to curbing haematological malignancies and its expression used as a prognostic marker.

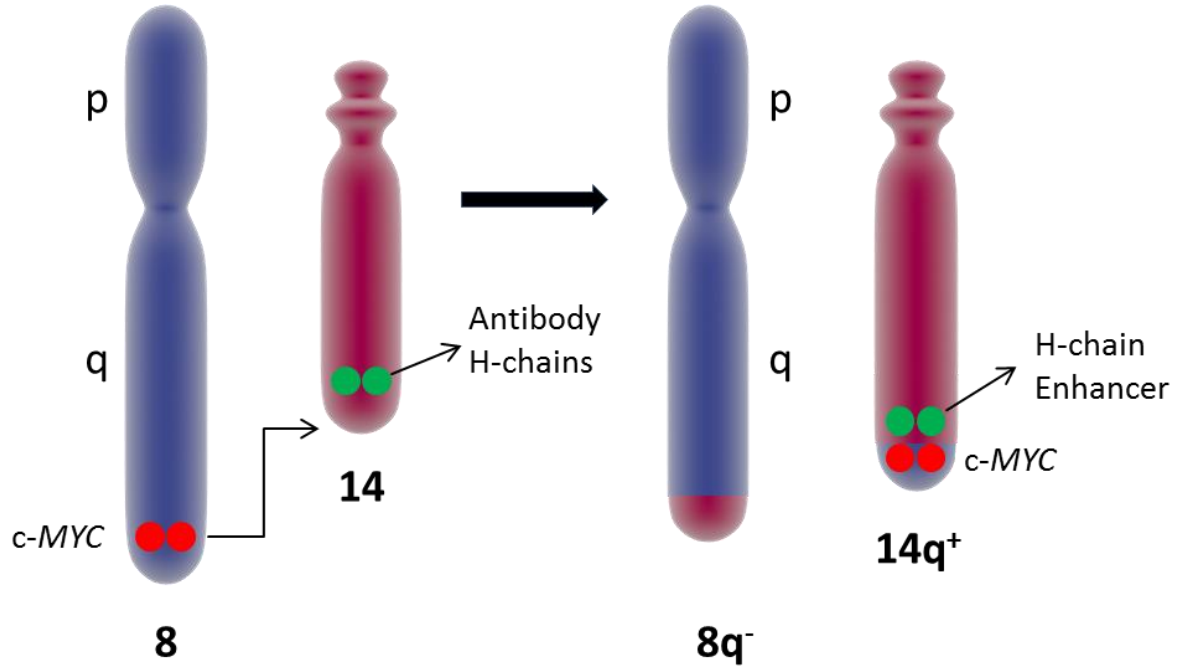

Figure 1.3: Diagrammatic representation of *MYC* translocation (t(8;14)(q24;q32)) in Burkitt's lymphoma placing c-MYC under the locus of heavy chain immunoglobulin promoter.

Somatic hypermutation and translocated *MYC* mutations

The genetic information leading to production of the vast repertoire of structural and functional diversity in antibodies was a mystery for long time in immunology. The discovery of the basic four-chain structure of antibodies established a huge amount of heterogeneity in amino-terminal domains of polypeptide chains and was probably the first clue towards an inlying genetic mechanism responsible for introducing somatic diversification in antibodies (Li, Woo, Iglesias-Ussel, Ronai, & Scharff, 2004). A limited number of genetic elements are responsible for generation of antibody diversity through a process called Somatic hypermutation (SHM). Somatic hypermutation is the process of modification of a germline immunoglobulin genetic sequence by introduction of nucleotide editions, mainly in the form of point mutations, in the locality around the rearranged variable immunoglobulin (Ig V) domain (Clark, Ganesan, Papp, & van Vlijmen, 2006; Mao et al., 2004; Peled et al., 2008).

Somatic hypermutation takes place in humans after V-D-J recombination and is found to occur during different phases of the immune response. Genetic rearrangement takes place during B-cell development and is required to generate a primary pool of antibodies for

targeting foreign antigens (Peled et al., 2008). This is usually provided via IgM antibodies exhibiting low binding affinity to the antigen, however the binding is often enough to trigger a physiological response against the antigen (Li et al., 2004). Upon binding of antigens to B-cells and their recognition by specific receptors, B-cells undergo rapid proliferation and form discrete structures within immunological areas in the body; called Germinal centres (GC). It is within these GCs that somatic hypermutation takes place and an alternative repetition of SHM and antibody binding mediated selection leads to affinity maturation of antibodies (Wagner & Neuberger, 1996). Thereafter, in surplus to the introduction of point mutations in the IgV region via SHM, Class-switch-recombination (CSR) takes place in the IgH (immunoglobulin heavy) locus. CSR involves recombination based deletion of regions of IgH locus, removing the exons of IgM constant region and thereby brings the segments surrounding the deleted portions (such as VDJ and IgC (immunoglobulin constant) regions) together, to form a functional antibody gene but of a different isotype. Thus, whereas SHM serves to increase the heterogeneity and repertoire of antibody variable region, CSR serves to increase the interaction options of antibodies with same variable region to different effector molecules (Di Noia & Neuberger, 2007; Peled et al., 2008; Wagner & Neuberger, 1996).

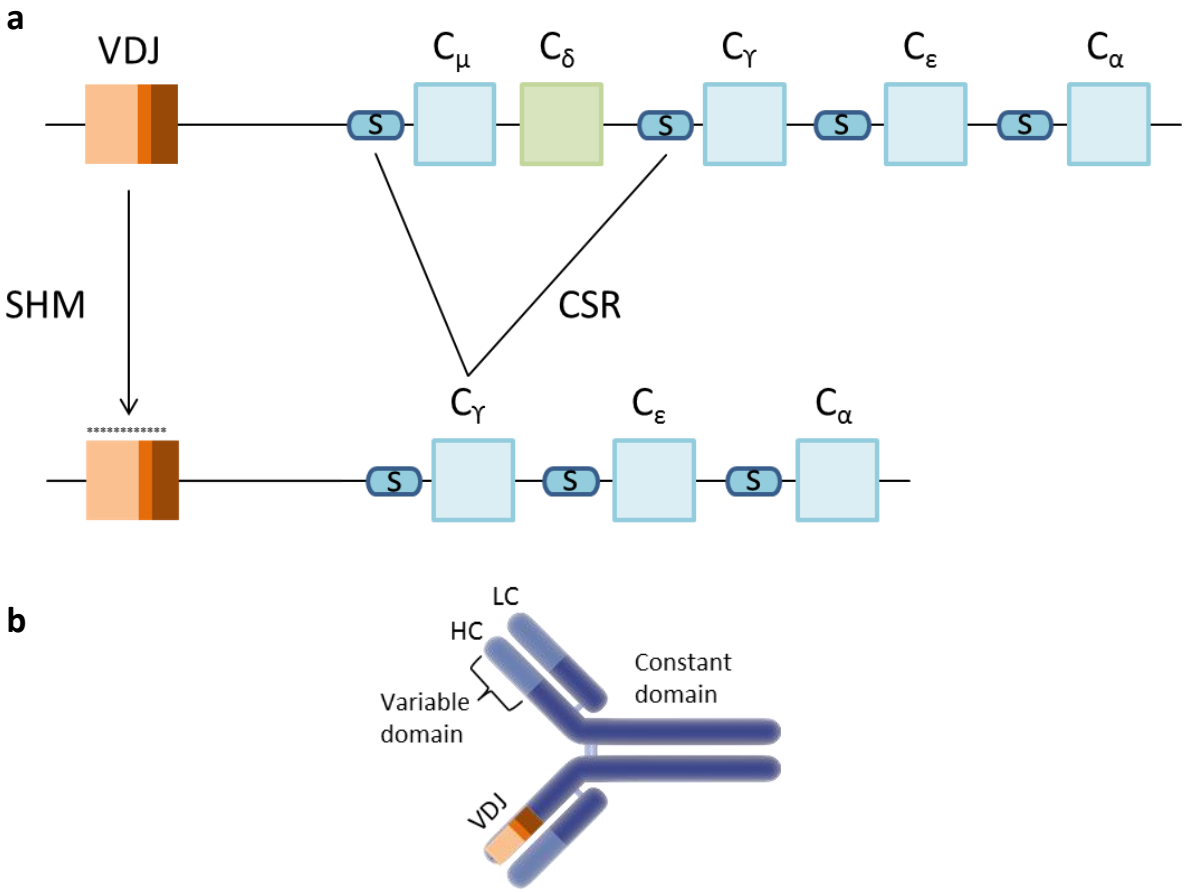

Figure 1.4: **a**: Schematic illustration of the process of Somatic hypermutation (SHM) and class-switch-recombination (CSR). SHM introduces point mutations in VDJ region (indicated by *), resulting in affinity maturation while CSR between switch (S) regions in the antibody leads to isotype switching. Different constant regions are denoted by C. **b**: Antibody assembly, showing the Heavy chains (HC), Light chains (LC), constant and variable regions and the VDJ domain located in the HC region (on both arms).

The process of SHM and CSR is performed through targeted deamination of deoxycytidine residues, which converts them to deoxyuridine and subsequently the C:G nucleotide pairs are transformed into U:G mismatches. This deamination of deoxycytidine to deoxyuridine is catalysed by an enzyme called Activation induced cytidine deaminase (AID). The enzyme is expressed specifically in B-cells and acts only on single stranded DNA templates, (Bransteitter, Pham, Scharff, & Goodman, 2003; Duquette, Pham, Goodman, & Maizels, 2005) thus highlighting its role upon increased transcriptional activity of the locus. Overall,

the enzyme is likely to introduce increasing number of mutations in a highly proliferating (transcriptionally active cell), such as B-cells activated by antigen.

Post discovery of translocated *MYC* allele in Burkitt's lymphoma, it was noted that the allele in most of the Burkitt's lymphoma lines had acquired several mutations and most of the observed mutations were conserved across tumor biopsy samples (Bemark & Neuberger, 2000; Mao et al., 2004; Vincent et al., 2009). Translocation of *MYC* into the immunoglobulin locus transforms the *MYC* into becoming a target for antibody hypermutation associated with the locus. The process has been observed *in-vitro* as well, such as for the Burkitt's lymphoma cell line Ramos (Bemark & Neuberger, 2000). Ramos cells in culture under standard lab conditions have been found to accumulate mutations at a high rate in its translocated *MYC* allele (Bemark & Neuberger, 2000). The process is constitutive for the cell line and the accumulation of mutations increases with the length of culturing of these cells. Thus, the cell line provides a perfect model to assess mutability and expression status of translocated *MYC* under various external conditions such as metabolic state of the cell. The mutability and expression of *MYC* could consequently be analysed with respect to changes in tumor aggressiveness of this cell line in *in-vitro* conditions.

B-cell differentiation

B-cell differentiation can be split into two phase, early and terminal B-cell differentiation. Early phase of B-cell differentiation is a tightly scrutinized process which occurs in liver of the developing foetus or in the bone marrow (BM) of adults, from common lymphoid progenitor cells (Roth et al., 2014; Zhang, Garcia-Ibanez, & Toellner, 2016). Commitment to B-cell lineage is dependent on a multitude of transcription factors such as early B-cell factor (COE1*,* encoded by *EBF1*), PU.1 (encoded by *SPI1*), E2A (encoded by *TCF3*) and paired box protein 5(*PAX5*) (Pieper, Grimbacher, & Eibel, 2013). Positive selection post rearrangement of IgH and IgL genes leads to a population of pre (precursor)-B cells. These cells express transmembrane form of the heavy chain μ, known as μM, which is an important checkpoint in the pre-B-cell receptor for B-cell development. Entry through this checkpoint allows for IgL gene segment rearrangement and clonal expansion. Second checkpoint is the presence of surface IgM where through negative selection, tolerance mechanisms act on autoreactive clones by deleting, anergizing or editing them. Cells surviving the negative selection, the immature B-cells, leave the bone marrow and migrate to secondary lymphoid organs such

as spleen where they continue their development. In the spleen, cells pass through transitional stages T1 and T2, and undergo further negative selection to become mature B-cells. Transitional B-cells can additionally be homed to splenic marginal zone (MZ) where they remain as non-circulating MZ B-cells, or like in case of most of the transitional cells, they could mature into naïve follicular B-cells, which circulate freely follicles, lymph nodes and BM until their death or undergo further differentiation upon antigen encounter (Pieper et al., 2013; Zhang et al., 2016).

The next phase of B-cell differentiation typically involves encounter with antigen and the response type depends on the type of antigen. Fully differentiated plasma cell (short-lived or long-lived) can thus develop from MZ B-cells, follicular cells, Germinal centre (GC) B-cells and from memory cells. Germinal centre cells are derived from follicular B-cells when the latter encounter an antigen and at the same time receive help from T-cells (T-cell dependent activation (TD)). There exists another pathway of activation via T-cell independent activation (TDI), known to occur in response to certain lipopolysaccharides and phorbol esters. The TDI is preferentially followed by a subset of B-cells called the B1 cells and are responsible for providing first line of defence by producing natural IgM. B-cells undergo extensive proliferation along with affinity maturation and CSR in germinal centres, which are specialized follicular areas for differentiation of GC B-cells. GC based response peaks between day 10 and 14 after encounter of antigen and then diminishes. The response gives rise to Plasma cells and Memory cells. Plasma cells are terminally differentiated antibody secreting cells (ASCs) and memory cells have the capability to differentiate into PCs if provided appropriate signals. However, the differentiation from GC cells to plasma cells involves several intermediate stages. Activated GC B-cells (T-cell dependent/independent (TD/TDI) stimulation) undergo a high proliferative phase characterized by Warburg like upregulation of metabolism and growth, and subsequent differentiation to plasma/memory cells (Brand, Leibold, Luppa, Schoerner, & Schulz, 1986; DeFranco, Raveche, & Paul, 1985; Garcia-Manteiga et al., 2011; Semmel et al., 1988; Shapiro-Shelef & Calame, 2005). These stages of proliferation and differentiation also thereby furnish ideal scenarios to analyse the regulation of metabolic activity of a fast-growing cancer under activated and quiescent states.

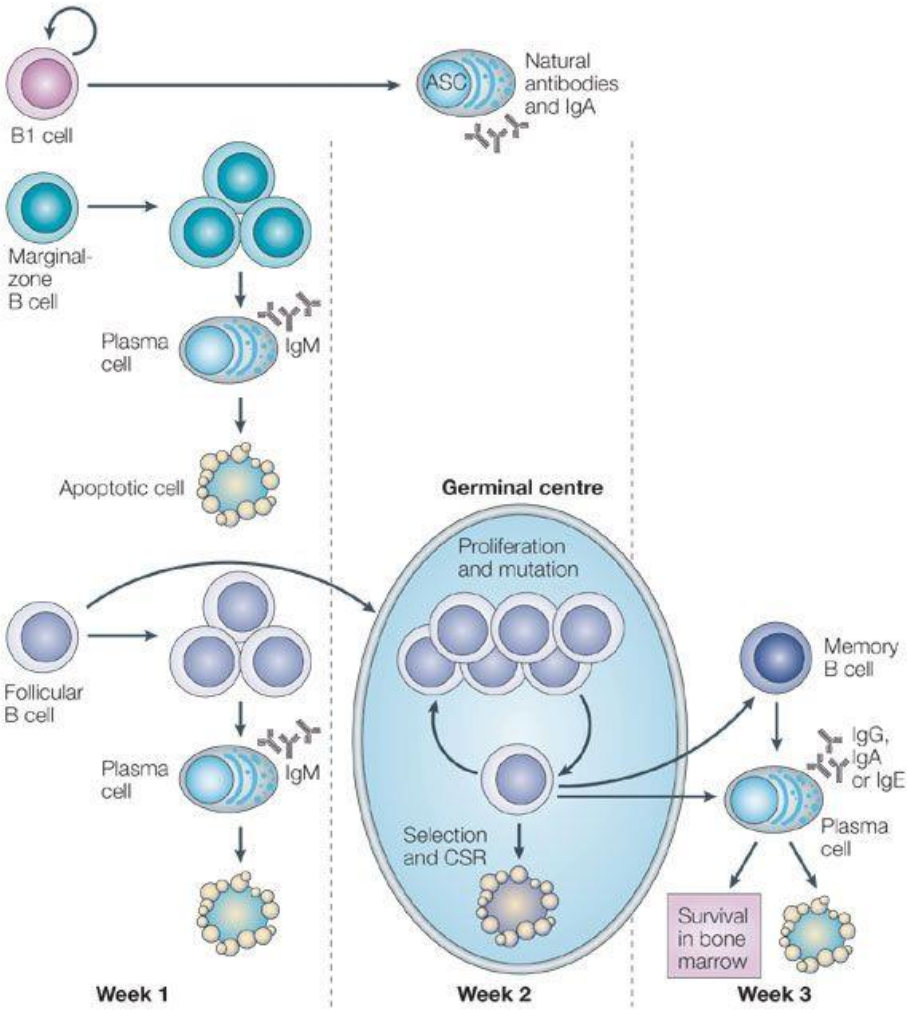

Figure 1.5: B-cell differentiation from B1 cells: On encounter with foreign antigens, marginal zone, follicular zone cells can differentiate into short-lived plasma cells. Activated follicular cells can form a germinal centre from which Plasma cells can either form directly or through a memory B-cell stage. Plasma cells resulting from germinal centres can become long-lived if they detect suitable survival niches in the bone marrow. (CSR: class-switch recombination). Image adapted from (Shapiro-Shelef & Calame, 2005)

Several transcription factors are necessary to drive the irreversible process of differentiation of GC B-cells to plasma cells. BLIMP1, the most widely studied transcription factor, is sufficient under appropriate conditions and at appropriate developmental stage of B-cells to induce differentiation into plasma cells (Ding, Bi, Chen, Yu, & Ye, 2013). It is expressed mainly by bone marrow and splenic plasma cells and is required for terminal differentiation and immunoglobulin secretion. It leads to termination of cell cycle (by repression of proliferative genes such as *MYC*), repression of genes characteristic of mature and GC B-cells and the induction of immunoglobulin secretion. It also represses expression of two important GC transcription factors, BCL-6 and PAX5. PAX5 repression is an important event in differentiation, leading to derepression of XBP1 (X-box binding protein 1), which is one of the first transcription factors shown to be necessary for plasmacytic differentiation. XBP1 is a primary regulator of immunoglobulin secretion in plasma cells. Along with these, IRF4 is another transcription factor known to be involved in early plasma cell development, being required in the activated B-cells for the proliferative phase (Bertolotti et al., 2010; Garcia-Manteiga et al., 2011; Jourdan et al., 2011; Reimold et al., 2001; Shaffer et al., 2002; Todd et al., 2009; Zhang et al., 2016). A list of important B-cell differentiation markers and transcription factors, and their expression status at different stages of differentiation is provided in Table 1.

	Pre-B	Imm-B cell	Trans-B cell	MZ	FL-B cell	Act B cell	GC-B cell	Memory B cell	PC long lived
Immunoglobulin	IgM^-	IgM^+, IgD^-	IgM^{high}, IgD^{low}	IgM^+, IgD^{low}	IgM^{low}, IgD^+	IgM^+, IgD^+	$IgM/G/A/E^+$, IgD^{var}	$IgM/G/A/E^+$, IgD^-	Ig^-
Positive markers	CD10, CD19, CD20, CD24, CD38, IL7/4/3R	CD10, CD19, CD20, CD21, $CD24^{high}$, $CD38^{high}$, CD40, CD268, IL4R	CD5, CD19, CD20, CD21, $CD24^{high}$, $CD38^{high}$, CD268, CCR7	CD1c, CD19, CD20, $CD21^{high}$, $CD27^{low}$	CD19, CD20, CD21, CD22, CD23, CD24, CD268, CCR7, CXCR5	CD19, CD20, CD25, CD27, CD30, CD69, CD80, CD86, CD95, CD135, CD268, CXCR5	CD10, CD19, CD20, CD23, CD27, $CD38^{high}$, CD95, CD135, CD268, CXCR5	CD19, CD20, $CD27^{var}$, CD40, CD268, CCR7, CXCR4, 5, 7	CD27, CD28, $CD38^{high}$, CD138, CD268, CD269, CXCR4
Enzymes	RAG-1,2 $EZH2^{low}$						AID EZH2		
Transcription factors	**Ikaros, Aiolos** **Pax5** **EBF1, E2A** **IRF4**						**BCL6**	**Pax5**	**BLIMP1** **IRF4** **XBP-1S**

Table 1: **Markers for B-cell development**. Imm: Immature, Trans: Transitional, MZ: Marginal zone, FL: Follicular zone, Act: Activated, GC: Germinal centre, PC: Plasma cell.

ADP dependent glucokinase

ADP-dependent glucokinase (UniProtKB-Q9BRR6) uses ADP to convert a molecule of glucose to glucose-6-phosphate. Human *ADPGK* is located at chromosome 15 (15q24.1) and is localized in the lumen of rough ER. Initially identified in Archaea, it was shown to be important in glucose breakdown with a modified Embeden-Meyerhof-Parnas pathway (EMP), typical for Archaea (Kengen et al., 1994). Human ADPGK has been shown to be highly specific for utilization of ADP, unlike the Archael ADPGK, which can employ other nucleotide diphosphates too as the phophoryl donor (M. M. Kaminski et al., 2012; J. P. Richter, Goroncy, Ronimus, & Sutherland-Smith, 2016; S. Richter et al., 2012). ADPGK has a very high specificity for glucose as a substrate and does not show any activity with other carbohydrates or even with 2-deoxyglucose. Despite the similarity in function to hexokinases in priming of glucose, it shows significant differences in enzyme kinetics. Whereas hexokinases (I to IV) are inhibited by their product, glucose-6-phosphate, ADPGK is inhibited by high concentrations of glucose and AMP. Also, ADPGK has an optimal temperature for its enzyme activity at 42^{o}C and a bimodal optimum pH at around 5.75 to 6.5 and 8.75 to 9 (M. M. Kaminski et al., 2012).

ADPGK is known to be a master regulator of Warburg effect and has been shown to play a role in T-cell activation and induction of glycolytic phenotype by our lab in previous studies (M. M. Kaminski et al., 2012). Seated in the lumen of rough-ER (Endoplasmic Reticulum), serving as a glucose sensor and regulating protein glycosylation, the protein is also hypothesized to play an important role in activation-based differentiation of B-cells which are highly dependent on ER biogenesis and extensive protein shuttling upon activation by mitogenic signals. Use of ADP instead of ATP by ADPGK for priming glucose hints at its role in nutrient deprived and hypoxic conditions, such as those prevalent in tumor growth, where ATP is available in lean amounts (M. M. Kaminski et al., 2012; J. P. Richter et al., 2016; S. Richter et al., 2012). Thus, knowing the importance of this protein in immune cell metabolism and cancer, it will be interesting to find out the effect bestowed upon Burkitt's lymphoma cells such as Ramos (ATCC CRL-1596) by *ADPGK* with respect to their oncogenic, differentiation potential.

Tumor microenvironment

The term tumor microenvironment implies to the presence of non-malignant cells and tissues present in the tumor and its immediate vicinity. These cells could be immune cells, fibroblasts and cells/tissues comprising the vasculature. The context is also used to refer to the proteins secreted by the cells existing in the tumor, which support the growth of tumor cells (Scott & Gascoyne, 2014).

For B-cell lymphomas, the microenvironment is highly infiltrated with variety of immune cells, stroma, ECM (extracellular matrix) and blood vessels. However, the degree of involvement of these components with the cancer cells depends on the genetic profile (aberrations) of the cancer cells, as it decides the extent to which these cancer cells depend on presence of external factors for survival and growth and not to forget, the inflammatory response by the host (Burger & Peled, 2009; Scott & Gascoyne, 2014). A cumulative effect of all these factors dictates the wide variations found in tumor microenvironments between different lymphoma subtypes.

Burkitt's lymphoma, characterized by a strong regulation from translocated, overexpressed *MYC,* has an autonomous survival instinct, which implies that actions are planned by the cell and depend much lesser on various microenvironmental constituents compared to other lymphomas. The only microenvironment observed in case of Burkitt's lymphoma is the presence of large number of tangible-body macrophages (Scott & Gascoyne, 2014; M. L. Xu & Fedoriw, 2016). These macrophages are known to decide the fate of tumor aggressiveness by transforming into tumor-promoting (M2) or tumor-killing (M1) phenotypes (Galvan-Pena & O'Neill, 2014; Gensel, Kopper, Zhang, Orr, & Bailey, 2017), and thus become exceedingly important in research based on targeting Burkitt's lymphoma.

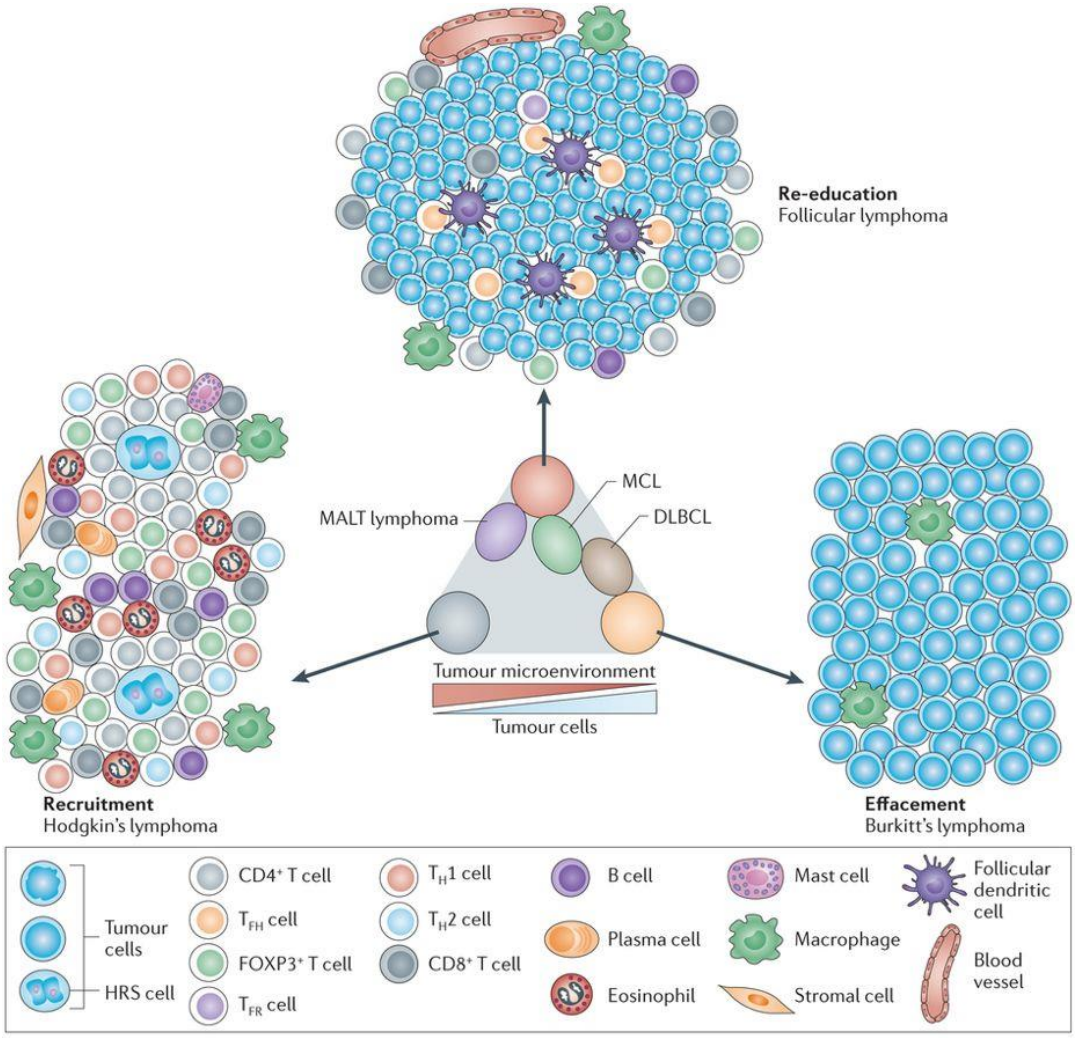

Figure 1.6: Figure shows the microenvironmental differences between three lymphoma subtypes. Microenvironmental constituent content ranges from 99% in Hodgkin's lymphoma to about 10% in Burkitt's lymphoma. FOXP3, forkhead box protein P3; MCL, mantle cell lymphoma; DLBCL, diffuse large B cell lymphoma; T_H, T helper; MALT, mucosa-associated lymphoid tissue; T_{FH}, follicular T helper; T_{FR}, follicular regulatory T;HRS, Hodgkin Reed–Sternberg. Image adapted from (Scott & Gascoyne, 2014).

Macrophage polarization

Macrophages form an indispensable part of the innate immune system owing to their antigen-presenting and phagocytic capabilities. They possess the capability to respond to various signals from foreign antigens in the body and perform phagocytosis and killing of bacteria and other harmful organisms. They are also known to present antigens to T-cells and initiate the process of inflammation by release of cytokines. Macrophages are basically the differentiated form of blood monocytes, and depending on the type of antigen encountered and the signals received, they present a great amount of heterogeneity in morphology, cytokines released and the effect induced (Szulzewsky et al., 2015). They likewise respond to signals produced by different tumors and can be polarized (activated) into pro-inflammatory (known as M1 or classical type) or anti-inflammatory (known as M2 or alternative type) macrophages. M1 polarized macrophages are responsible for Th1 cell response, killing of pathogens and type I inflammation, whereas M2 macrophages induce tissue growth and wound healing besides inducing cessation of inflammation (Colegio et al., 2014; Galvan-Pena & O'Neill, 2014; Subei & Cohen, 2015; Szulzewsky et al., 2015).

Aggressively growing tumors are known to employ myeloid-derived macrophages as tumor-promoting agents in the microenvironment (Colegio et al., 2014). A massive accumulation of these drivers of tumor growth and immune suppressors is often found in the advanced growth stages of cancerous lesions. These macrophages are termed as tumor-associated macrophages (TAMs) and are shown to be of important prognostic value, with some cancers showing regressions by the presence of TAMs while most others linked to a poor prognosis (Szulzewsky et al., 2015). In regressing tumors, most of the TAMs are detected to be of M1-subtype whereas malignant, aggressively growing tumors have an overwhelming presence of M2-TAMs (Allavena, Sica, Solinas, Porta, & Mantovani, 2008; Mantovani, Sozzani, Locati, Allavena, & Sica, 2002; Murdoch, Muthana, Coffelt, & Lewis, 2008).

M2 macrophages have a reduced antigen-presenting capability, suppress immune response mediated by T-cells by limiting their proliferation, and promote angiogenesis, to name a few factors by which they promote the growth of the associated tumor (Mantovani et al., 2002). Observed phenotypic differences between M1 and M2 macrophages can also be linked to their underlying metabolic differences, where M1 macrophages are characterized by a high glycolytic profile, increased glutamine uptake and anaplerosis, and high NO (nitric oxide) and

ROS generation for clearance of foreign cells (Fig. 1.7) (Galvan-Pena & O'Neill, 2014; Ghesquiere, Wong, Kuchnio, & Carmeliet, 2014). M2 macrophages on the other hand rely on oxidative phosphorylation for energy generation, use glutamine for synthesis of polyamines and generate proline and citrulline which promote tissue growth.

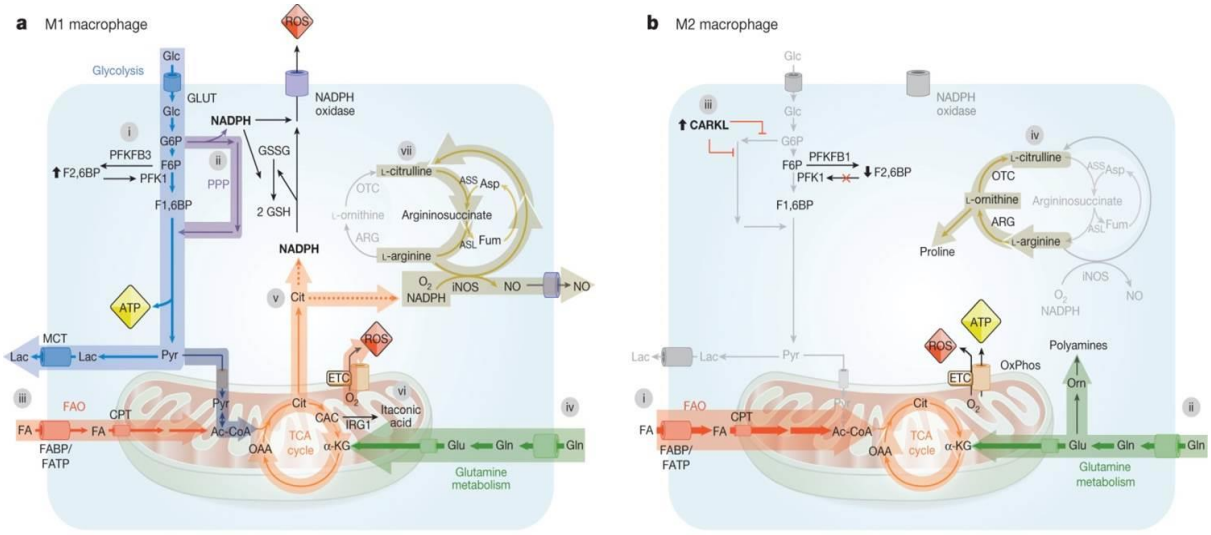

Figure 1.7: Metabolic profile of M1 and M2 macrophages. **a** M1 macrophages are characterized by: 1) High glycolytic rate (blue), 2) Increased pentose phosphate pathway (PPP) (purple) to generate NADPH for maintaining redox homeostasis and generating ROS (reactive oxygen species) via NADPH oxidase. ROS is additionally generated from mitochondria. 3) Basal rate of fatty acid oxidation (FAO) (red), 4) Glutamine uptake to fuel the TCA cycle anaplerotically (green), 5) Arginine is metabolized by iNOS (inducible nitric oxide synthase) to generate NO (nitric oxide) (tan) **b** M2 macrophages display: 1) Increased FAO to fuel energy demands (red), 2) Reduced glycolysis due to expression of PFKFB1 (grey), 3) Reduced PPP by CARL (carbohydrate kinase-like protein), 4) Arginine metabolism by arginase-1 to generate proline and citrulline. Image adapted from (Ghesquiere et al., 2014).

Zebrafish as xenograft model

Zebrafish (*Danio rerio*) belongs to the family Cyprinidae and are native of Indian rivers with distribution across South-Asia. Zebrafish models are being extensively used in biomedical research for studying developmental biology, neuroscience, oncology and metabolism to name a few (Bradbury, 2004). They have a life span of 4-5 years and retain sexual activity

throughout their lifetime, with a single female capable of giving hundreds of eggs in a week, making the organism very useful for high-throughput studies (Kalueff, Stewart, & Gerlai, 2014; Spence, Gerlach, Lawrence, & Smith, 2008). The zebrafish embryos undergo primary development within 48 hours and with lack of an adaptive immune system until 4 weeks post fertilization, the larvae serve as a perfect model to study growth of cancer xenografts (Barriuso, Nagaraju, & Hurlstone, 2015; van der Ent et al., 2014).

The model serves as a much more sophisticated alternative for tumor growth compared to 2D culture arrays or matrix systems and at the same time providing a natural dynamic environment to the xenografted cells. Cancer cells injected in zebrafish larvae provide rapid growth analysis with much wider and feasible imaging possibilities compared to other lab animals owing to the transparent nature of larvae in initial days of growth. The fishes can also be induced to be non-pigmented in later stages of growth using chemicals such as PTU (1-phenyl 2-thiourea) or employing *casper* pigmentation mutant strains (Antinucci & Hindges, 2016). Transgenic zebrafish lines such as *kdrl:GFP* or *mpeg1:mcherry* enable fluorescent labelling of vasculature and immune cells (macrophages) respectively and serve as excellent options for studying tumor microenvironment (Ellett, Pase, Hayman, Andrianopoulos, & Lieschke, 2011; Ibrahim & Richardson, 2017).

Though the optimum growth temperature of zebrafish is 28^{o}C, the fishes can be maintained at temperatures upto 34^{o}C to provide an optimum growth temperature to xenografted mammalian cells, without apparent negative effects to zebrafish larvae.

Aims

Activation induced proliferation and differentiation of B-cells furnishes ideal scenarios to analyse the regulation of metabolic activity of a fast-growing cancer under activated and quiescent states. Employing Burkitt's lymphoma derived Ramos BL (Burkitt's lymphoma) cells for this study, we will try to decipher the metabolic phenotype of these cells and their potential to differentiate in the light of ADPGK (ADP dependent glucokinase), which is known to be highly expressed in immune cells and cancer and has been shown to play a role in activation of T-cells.

Correspondingly, we hypothesize in this study that knock-out of *ADPGK* from Ramos BL cells will induce a metabolic catastrophe upon these cells, which will affect the tumor aggressiveness of these cells *in-vitro* and *in-vivo* zebrafish. The knock-out is also proposed to stall the activation mediated differentiation of these cells and thereby providing a novel regulator of two mutually complementary pathways, malignancy and differentiation.

We aim to achieve this by several investigations such as:

1. To study the differentiation status of Ramos BL cells and their *ADPGK* knock-out counterparts upon activation.
2. Overviews of metabolic changes such as glycolytic enzyme expression, kinetics, amino-acid and glucose uptake in *ADPGK* knock-out cells.
3. Study of the expression and mutational status of translocated *MYC* (t(8;14)(q24;q32)) in *ADPGK* knock-out and wild type cells.
4. Effect of *ADPGK* knock-out on tumor-microenvironment (tumor associated macrophages (TAMs)) *in-vitro*.
5. Finally, for *in-vivo* characterization of tumor developing capability of *ADPGK* knock-out cells, we will study the growth of Ramos BL xenografts in zebrafish.

MATERIALS

Chemicals

Name	Company
2-mercaptoethanol	Merck, Darmstadt, Germany
2-propanol	Carl Roth, Karlsruhe, Germany
6-aminocaproic acid	Sigma-Aldrich, St. Louis, U.S.A.
Acetic acid	Carl Roth, Karlsruhe, Germany
Acetone	Sigma-Aldrich, St. Louis, U.S.A.
Agarose	Carl Roth, Karlsruhe, Germany
Amino persulfate (APS)	Sigma-Aldrich, St. Louis, U.S.A.
Ammonium bicarbonate	Sigma-Aldrich, St. Louis, U.S.A.
Ampicilin	PanReac AppliChem, Darmstadt, Germany
Bacteriological agar	Sigma-Aldrich, St. Louis, U.S.A.
Bovine serum albumin (BSA)	Santa Cruz Biotechnology, Dallas, U.S.A.
Bromophenoblue	Merck, Darmstadt, Germany
Calcium chloride (CaCl)	Sigma-Aldrich, St. Louis, U.S.A.
Citric acid monohydrate	Carl Roth, Karlsruhe, Germany
Diethyl pyrocarbonate (DEPC)	Sigma-Aldrich, St. Louis, U.S.A.
Dipotassium phosphate (K_2HPO_4)	Sigma-Aldrich, St. Louis, U.S.A.
Dithiothreitol (DTT)	Merck, Darmstadt, Germany
Ethanol	Carl Roth, Karlsruhe, Germany
Ethylenediaminetetraacetic acid disodium salt dihydrate (EDTA)	Carl Roth, Karlsruhe, Germany

MATERIALS

Formaldehyde	Sigma-Aldrich, St. Louis, U.S.A.
Formamide	Sigma-Aldrich, St. Louis, U.S.A.
Fructose-1,6-bisphosphate (FBP)	Sigma-Aldrich, St. Louis, U.S.A.
Glucose-6-phosphate (G6P)	Sigma-Aldrich, St. Louis, U.S.A.
Glyceraldehyde-3-phosphate (GAP)	Sigma-Aldrich, St. Louis, U.S.A.
Glycerol	Sigma-Aldrich, St. Louis, U.S.A.
Glycine	Sigma-Aldrich, St. Louis, U.S.A.
Perchloric acid ($HClO_4$)	Sigma-Aldrich, St. Louis, U.S.A.
Hydrogen chloride	Sigma-Aldrich, St. Louis, U.S.A.
Lithium chloride (LiCl)	Applichem, Darmstadt , Germany
Magnesium chloride 6-hydrate (MgCl)	PanReac AppliChem, Gatersleben, Germany
Methanol	Carl Roth, Karlsruhe, Germany
Milk powder	Carl Roth, Karlsruhe, Germany
Monopotassium phosphate (KH_2PO_4)	Sigma-Aldrich, St. Louis, U.S.A.
N,N,N',N'-Tetramethylethylenediamine (TEMED)	Sigma-Aldrich, St. Louis, U.S.A.
Nicotinamide adenine dinucleotide (NADH)	Sigma-Aldrich, St. Louis, U.S.A.
Paraformaldehyde (PFA)	Merck, Darmstadt, Germany
Phosphoenolpyruvate (PEP)	Sigma-Aldrich, St. Louis, U.S.A.
Potassium bicarbonate ($KHCO_3$)	Sigma-Aldrich, St. Louis, U.S.A.
Potassium chloride (KCl)	Carl Roth, Karlsruhe, Germany
Potassium hydroxide (KOH)	Sigma-Aldrich, St. Louis, U.S.A.
Potassium phosphate (K_3PO_4)	Sigma-Aldrich, St. Louis, U.S.A.

Proteinase inhibitor	Roche, Basel, Switzerland
Proteinase K	Carl Roth, Karlsruhe, Germany
Pyruvate (PYR)	Sigma-Aldrich, St. Louis, U.S.A.
Sodium bicarbonate ($NaHCO_3$)	PanReac AppliChem, Gatersleben, Germany
Sodium carbonate anhydrous (Na_2CO_3)	Carl Roth, Karlsruhe, Germany
Sodium chloride (NaCl)	Carl Roth, Karlsruhe, Germany
Sodium deoxycholate	Sigma-Aldrich, St. Louis, U.S.A.
Sodium dodecyl sulfate (SDS) pellet	SERVA, Heidelberg, Germany
Sodium hydroxide	Carl Roth, Karlsruhe, Germany
Sulfosalicylic acid	Sigma-Aldrich, St. Louis, U.S.A.
Tributylamine	Sigma-Aldrich, St. Louis, U.S.A.
Tris base	Carl Roth, Karlsruhe, Germany
Triton X-100	Carl Roth, Karlsruhe, Germany
Trypton	Carl Roth, Karlsruhe, Germany
Tween 20	Carl Roth, Karlsruhe, Germany
Urea	Sigma-Aldrich, St. Louis, U.S.A.
Yeast extract	Sigma-Aldrich, St. Louis, U.S.A.

Reagents

Name	**Company**
40% acrylamide and bis-acrylamide solution	Bio-Rad, Hercules, U.S.A.
Braford Assay	Bio-Rad, Hercules, U.S.A.
DNase I, RNase free	Thermo Fisher Scientific, Waltham, U.S.A.

EcoRI restriction enzyme	Thermo Fisher Scientific, Waltham, U.S.A.
GeneRuler 1 kb DNA Ladder	Thermo Fisher Scientific, Waltham, U.S.A
GeneRuler 100 bp DNA Ladder	Thermo Fisher Scientific, Waltham, U.S.A
Latate dehydrogenase (LDH)	Sigma-Aldrich, St. Louis, U.S.A.
Lowry assay	Bio-Rad, Hercules, U.S.A.
MyTaq HS red mix	Bioline, London, UK
PageRuler prestained protein ladder	New England BioLabs, Ipswich, U.S.A.
Phusion PCR	New England BioLabs, Ipswich, U.S.A.
Q5® High-Fidelity DNA polymerase	New England BioLabs, Ipswich, U.S.A.
RNase inhibitor	Roche, Basel, Switzerland
S.O.C. medium	New England BioLabs, Ipswich, U.S.A.
SensiFAST™ SYBR®	Bioline, London, UK
SuperSignal™ West Pico chemiluminescent substrate	Thermo Fisher Scientific, Waltham, U.S.A.
T4 ligase	New England BioLabs, Ipswich, U.S.A.
Trizol reagent	Thermo Fisher Scientific, Waltham, U.S.A.

Kits

Name	**Company**
GeneJET plasmid miniprep kit	Thermo Fisher Scientific, Waltham, U.S.A.
GenElute(TM) gel extraction kit	Sigma-Aldrich, St. Louis, U.S.A.
Glucose colorimetric kit	Cayman, Ellsworth, U.S.A.
HiSpeed plasmid midi kit	Qiagen, Hilden, Germany

Maxima first strand cDNA synthesis kit for RT-qPCR	Thermo Fisher Scientific, Waltham, U.S.A.
NEB 5-α competent E.coli	New England BioLabs, Ipswich, U.S.A.
Topo-TA Zero blunt cloning kit dual promotor	Invitrogen/Thermo Fisher Scientific, Waltham, U.S.A.

Machines and Devices

Name	**Company**
Autoclave	Systec, Linden, Germany
Biochrom 30+ cation exchange chromatography	Biochrom, Cambridge, UK
BD FACS Verse Flow cytometer	BD Biosciences, USA
Blotting semidry system	PeqLab, Erlangen, Germany
C1000 Touch Thermo Cycler	Bio-Rad,Hercules, U.S.A.
Centrifuge	Heraeus, Hanau, Germany
CFX Connect Real Time System	Bio-Rad, Hercules, U.S.A.
Electrophoresis chamber	Bio-Rad, Hercules, U.S.A.
FemtoJet micro-injector	Eppendorf, Hamburg, Germany
Fluorescence microscope	Leica microsystems, Germany
Fusion-SL Advance 4.2 MP	Peqlab, Erlangen, Germany
Herathermo incubator	Thermo Fisher Scientific, Waltham, U.S.A.
Microloader 20 µL	Eppendorf, Hamburg, Germany
Microscope	Leica microsystems, Germany

Microwave	Sharp, Osaka, Japan
NanoDrop LiTe spectrophotometer	Thermo Fisher Scientific, Waltham, U.S.A.
Beckman Coulter AU400	Beckman Coulter, Brea, U.S.A.
pH-Meter	WTW, Weilheim , Germany
SDS PAGE electrophoresis system	Bio-Rad, Hercules, U.S.A.
Sonicator	Branson, Dietzenbach, Germany
SpectraMax Plus 384	Molecular Devices, Sunnyvale, U.S.A.
Ultracentrifuge Typ Optima TLX	Beckman Coulter, Brea, U.S.A.
UV-Handlamp VL-4.LC	Vilber, Eberhardzell, Germany
UV-Transilluminator CN-TFX	Vilber, Eberhardzell, Germany
Weighing machine PH204L	Mettler Toledo, Greifensee, Switzerland
Weighing machine XP56	Mettler Toledo, Greifensee, Switzerland

Disposables

Name	**Company**
PVDF membrane	Neolab, Heidelberg, Germany
10 cm dish	Sarstedt, Nümbrecht,Germany
Hard-Shell® 96-well PCR Plates, thin wall	Bio-Rad, Hercules, U.S.A
Microseal® 'B' PCR plate sealing film	Bio-Rad, Hercules, U.S.A
PCR tube (0.2 ml)	Sarstedt, Nümbrecht,Germany
Thin wall capillary, 1.0 mm	World Precision Instruments, Berlin, Germany
Transwell inserts 0.4µm 6-well	Sarstedt AG, Germany

Transwell inserts 5µm 24 well	Corning Incorporated, U.S.A.

Primer Sequences

Name	**Sequence**
18s Forward	GTAACCCGTTGAACCCCATT
18s Reverse	CCATCCAATCGGTAGTAGCG
ADPGK exon-2 Forward	GCTTCTTCCAGATCATTCCTTGA
ADPGK exon-2 Reverse	TTCAGGTTTCAGACCTACTTCCT
ADPGK CRISPR/Cas9 guide RNA	GTCAATGCATGTGTTGATGTGG
Arginase-1 Forward	ACTTAAAGAACAAGAGTGTGATGTG
Arginase-1 Reverse	GCATCCACCCAGATGACTCC
Hexokinase-2 Forward	CAAAGTGACAGTGGGTGTGG
Hexokinase-2 Reverse	GCCAGGTCCTTCACTGTCTC
Il-8 Forward	GAATGGGTTTGCTAGAATGTGATA
Il-8 Reverse	CAGACTAGGGTTGCCAGATTTAAC
iNOS Forward	GTCCCGAAGTTCTCAAGGCA
iNOS Reverse	CTGTGTCACTGGACTGGAGG
c-Myc proto oncogene Forward	AAAGGCCCCCAAGGTAGTTA
c-Myc proto oncogene Reverse	GCACAAGAGTTCCGTAGCTG
Translocated MYC Forward	CACTTTGCACTGGAACTTACAACA
Translocated MYC Reverse	TCACCATGTCTCCTCCCAGCA
XBP-1 unspliced Forward	CCTTGTAGTTGAGAACCAGGAG
XBP-1 unspliced Reverse	GGTCCAAGTTGTCCAGAATGC
XBP-1 spliced Forward	GGTCTGCTGAGTCCGCAGCAGG

XBP-1 spliced Reverse	GGGCTTGGTATATATGTGG

Antibodies

Name	**Company**
CD20-PE	BD Biosciences, U.S.A.
CD138-PE	BD Biosciences, U.S.A.
β-Actin	Santa Cruz, U.S.A.
ADPGK	Sigma Aldrich, U.S.A.
AnnexinV-FITC	BD Biosciences, U.S.A.
Calreticulin	Abcam, Cambridge, UK
GFAT-2	Santa Cruz, U.S.A.
IP3-receptor	Abcam, Cambridge, UK
IRE-1	Abcam, Cambridge, UK
MYC proto-oncogene	Abcam, Cambridge, UK
PDI	Cell Signalling Technologies, U.S.A.
Secondary, chicken anti-rabbit	Abcam, Cambridge, UK
Secondary, chicken anti-mouse	Abcam, Cambridge, UK
SRPR-β	Abcam, Cambridge, UK

Methods

Cell culture

Ramos (RA-1, ATCC CRL-1596) B-lymphocytes and THP-1 (ATCC TIB-202) monocytes were maintained as a suspension culture in RPMI-1640 media supplemented with GlutaMax (Thermo Fisher Scientific), 10% fetal bovine serum (FBS) and 1% Penicillin/Streptomycin. Cell cultures were incubated for optimum growth at 37^{o} C and 5% CO_2 in a humidified atmosphere and fresh media added every 2-3 days. For generation of ADPGK knockouts, CRISPR/Cas9 technique was used. Guide RNA was designed targeting exon 2 in the *ADPGK*. Ramos cells were transfected with the guide RNA containing GFP-linked CRISPR/Cas9 plasmid via Electroporation (Bio-Rad). Transfected cells were selected with the help of FACS into 96 well plates. Single cell clones were grown further and sequenced to analyze the presence of mutations in exon-2 near the PAM site of CRISPR guide RNA. *ADPGK* knockout was further confirmed by western blots with the selected clones using anti-ADPGK antibody and analyzing the loss of ADPGK activity by enzyme assays. Stimulation of cells was induced by PMA (phorbol 12-myristate 13-acetate) at 10 ng/ml for THP-1 cells and at 50 ng/ml for B-cells.

ADPGK knock-out

ADPGK knock-out Ramos cells were generated using the CRISPR/Cas9 technology. Exon-2 in *ADPGK* gene was targeted, which also codes for the glucose binding site of the translated protein and hence its catalytic function. CRISPR/Cas9 plasmid expressed guide-RNA designed against exon-2 under a U6 promoter and a GFP (green fluorescent protein) under the CMV (cytomegalovirus) promoter. We used un-transfected and GFP-plasmid transfected cells as positive control for ADPGK and as transfection control (TC) respectively for subsequent experiments. All transfections were performed using Bio-Rad Gene Pulsar Electroporation system at recommended conditions for lymphocytes. Transfected cells were sorted using FACS (Fluorescence-activated cell sorting) for GFP into 96 well plates. Sorted single cells were allowed to grow in standard cell culture conditions until the visible formation of colonies. Clones were selected by detection of 55 kDa ADPGK band in protein lysates obtained from the colonies by western blots using anti-ADPGK antibody (Sigma-Aldrich, HPA045194) and additionally by DNA sequencing. For sequencing, DNA was obtained from clones using DNeasy Blood and Tissue Kit (Qiagen) following the

manufacturer's protocol and PCR (polymerase chain reaction) amplified using the Q5 High-Fidelity DNA polymerase (New England Biolabs). The PCR products were sent for sequencing to Microsynth SEQLAB (Göttingen, Germany). Sequencing results were analyzed via BLAST (Basic local alignment search tool, NCBI) against *ADPGK* wild-type sequence.

ADPGK localization studies

From the previously performed studies in our lab showing ER (endoplasmic reticulum) presence of ADPGK, we wanted to distinguish between the smooth and rough ER localization of this protein. We used Endoplasmic Reticulum isolation kit (ER0100, Sigma-Aldrich) for this purpose and isolated microsomes as per manufacturer's guidelines. Briefly, the post mitochondrial fraction (PMF) obtained post disruption and differential centrifugation (standard protocols), and containing the microsomes, was dissolved in 20% OptiPrep sucrose density gradient medium and laid over a layer of 30% OptiPrep gradient medium (without PMF) in an ultracentrifuge tube. The layers were topped with 15% OptiPrep solution and the tube spun down in an ultracentrifuge at 150,000 x g for 3 hours. A total of 14 fractions were isolated from the gradient with a needle going by layers and stored in separate Eppendorf tubes. The protein concentration in the samples (1-14) was measured and the samples were later analysed via western blot for different rough ER markers, Calreticulin (Abcam, ab22683) and ADPGK. The principle of the experiment is depicted in Figure 2.1 and follows from the procedure described in (Alberts, 2017).

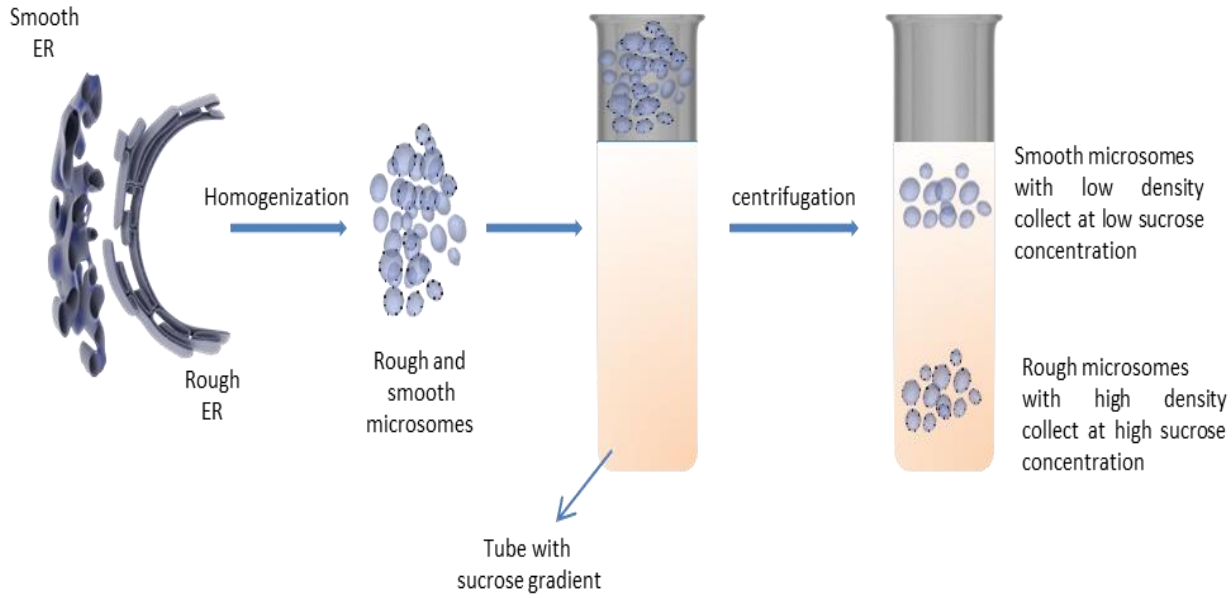

Figure 2.1: ADPGK localization experiment for rough and smooth ER: Cultured lymphocytes were homogenized and subjected to differential centrifugation to obtain microsomes. The microsomes were dissolved in 20% sucrose solution and ultra-centrifuged in a gradient of sucrose solution, with density increasing downwards. Figure represents the principle behind the experiment with low density smooth microsomes accumulating at upper layers of the sucrose gradient and high density rough microsomes preferentially sedimenting to the lower layers.

Immunoblot Analysis

Sodium dodecyl sulfate polyacrylamide gel electrophoresis (SDS PAGE) was used for separating the proteins in cell lysates. The separated proteins were immunoblotted on PVDF (Polyvinylidene fluoride) membranes according to standard procedure and labelled with antibodies. Cell lysis was performed with RIPA (radioimmunoprecipitation) buffer using a pellet of 5 million cells suspended in the buffer and subjected to 10 x 5-second cycles of sonication. Supernatant containing the extracted proteins was resolved by SDS PAGE in 10% polyacrylamide gels. Prior to loading, protein concentration of all samples was determined by Lowry assay. Equal volume for all samples adjusted to 40 µg protein content was loaded in the gels. Proteins were transferred to PVDF membranes, blocked in TBST (tris-buffered saline plus 0.1% tween-20) with 5% non-fat dry milk. Membranes were incubated overnight in primary antibody in blocking buffer and analyzed by HRP-conjugated secondary antibody next day using chemiluminescent substrate (ECL). Phusion GelDoc system was used for

visualization of results and quantification of band intensity was performed with ImageJ software (NIH, http://rsbweb.nih.gov/ij/).

Quantitative RT PCR Analysis

Total RNA was extracted from cells using TRIzol reagent (Thermo Fisher Scientific) using supplier's protocol. Approximately 5 million cells were used per extraction. Isolated RNA was subjected to DNase treatment (DNase1-Recombinant, Sigma-Aldrich) to remove contaminating DNA. We then used 1 µg of resulting purified RNA to prepare cDNA with the help of Maxima cDNA synthesis kit (Thermo Scientific). For expression analysis by RT-QPCR, we used SensiMix SYBR Hi-ROX Kit (Bioline) with template cDNA and primer concentration according to the manufacturer's protocol. All primers were previously verified for specificity by gel electrophoresis. PCRs were run on Bio-Rad CFX Connect RT-PCR Detection system at a preset melting cycle with annealing temperature specific for the primer set. For quantification, 18s ribosomal RNA expression was used as an endogenous reference. Expression data was quantified using $2^{-\Delta\Delta CT}$ method and stated as fold change in gene expression for each individual gene.

Macrophage Migration Assay

Migration assays were performed with 24-well Transwell inserts of 5 µm pore size purchased from Costar, Corning Incorporated, USA. THP-1 macrophages were seeded in Transwell inserts at 50,000 cells in 200 µl culture medium and stimulated by PMA for 24 hours. Post stimulation, transwell inserts were placed in wells containing 5 x 10^5 wild-type and *ADPGK* KO Ramos cells which were stimulated for 48 hours in 500µl total culture media. The THP-1 macrophages were allowed to migrate for 6 hours. After the completion of migration, Transwell inserts were washed with PBS and the un-migrated cells present on the upper side of the inserts were removed with a cotton swab. The migrated cells on the lower side of the transwells were fixed overnight with 4% paraformaldehyde (PFA) at 4^{o}C and then stained with DAPI (1:10000) (Figure 2.2). The DAPI-stained cells were imaged using Fluorescent microscopy (Leica) and later counted using the ImageJ software. Inserts incubated with media (no lymphocytes) were used as control.

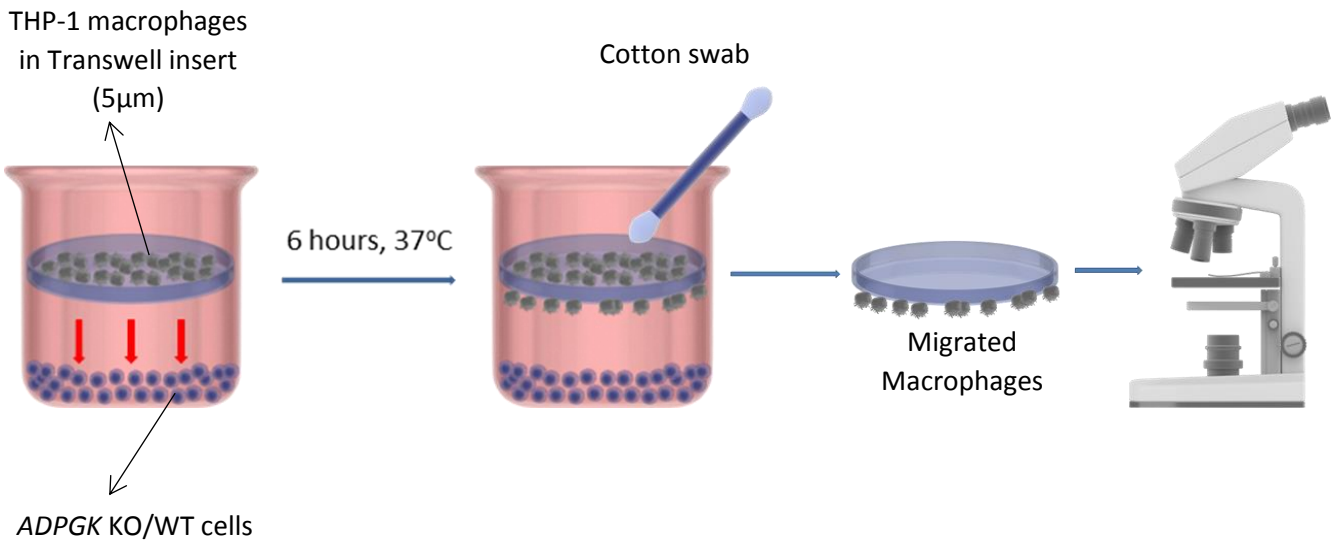

Figure 2.2: Macrophage migration experiment: Diagram representing the setup and work flow of a macrophage migration experiment. 50,000 THP-1 monocytes were seeded in 5µm transwell inserts and stimulated with PMA (phorbol 12-myristate 13-acetate) for 24 hours. Transwell inserts were placed in wells containing 48-hour stimulated 5 x 10^5 wild-type and *ADPGK* KO Ramos cells. Migrated macrophages post 6 hours of incubation, collected after wiping off the non-migrated cells with a cotton swab, were labelled with DAPI and observed under a microscope.

Macrophage-Ramos co-culture

To reproduce the tumor-macrophage interaction at in-vitro scale, THP-1 monocytes were co-cultured with *ADPGK* KO or WT Ramos cells and their polarization into M1/M2 macrophages was studied. In the setup, Ramos wild type or *ADPGK* KO cells were seeded on 0.4 µm Transwell inserts at a density of 1 million cells/ml. The cells in inserts were stimulated with PMA and moved into wells of 6-well plate containing 24 hour PMA stimulated monocytes seeded at 2x10^5 cells/well in 2.5 ml of complete media. Cells were physically separated from each other, and migration was not possible due to small pore size of inserts, but the design of the setup permitted free sharing of media and soluble factors/nutrients between the cells (Figure 2.3). After 48 hours of co-culture, macrophages were collected and analyzed for M1/M2 markers of polarization (hexokinase, Il-8, iNOS1 and

Arg1) by RT-qPCR. Stimulated macrophages, without insert in co-culture, were used as control.

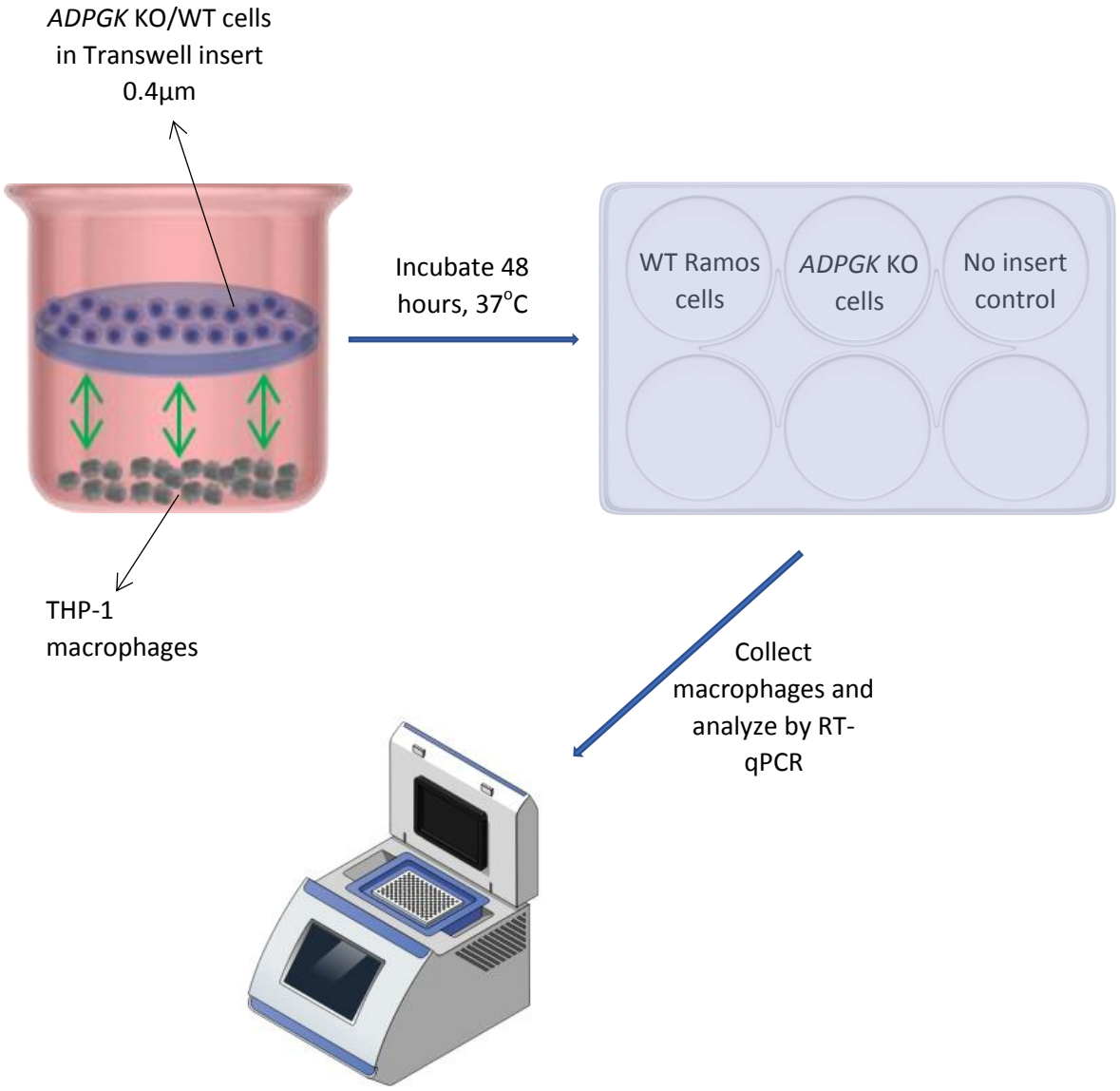

Figure 2.3: Ramos-macrophage co-culture: Diagram representing the setup and work flow of a Burkitt's lymphoma-macrophage *in-vitro* co-culture experiment. THP-1 monocytes were seeded in 6-well plate and stimulated with PMA (phorbol 12-myristate 13-acetate) for 24 hours. Transwell inserts containing stimulated lymphocytes were placed in the wells.

Macrophages were collected post 48 hours of incubation, and analyzed by RT-qPCR for expression of M1/M2 polarization markers. Well without insert served as control.

Amino-acid analysis

Ramos wild type and ADPGK KO cells were seeded at 1 million cells/ml in 6-well plates and stimulated with PMA for two days and seven days, at the end of which, cells were harvested, and media collected in separate 15-ml falcons. Media was further centrifuged at high speed and additionally passed through 0.35 µm filters to remove residual cells. 200µl of the sample was mixed with 50 µl Sulfosalicylic acid and centrifuged at maximum speed on a table-top centrifuge. Supernatant was collected, and amino acid analysis was performed by injecting the samples into a Biochrom 30+ Amino acid analyser (Biochrom ,UK) based on ion exchange chromatography, with resulting data expressed as µmol/litre.

Lactate/Pyruvate measurements

Media obtained from cells, as described in amino-acid analysis, was analyzed for lactate and pyruvate content. For pyruvate measurement the samples were mixed with pyruvate reagent 1 containing NADH, 1.5M Tris Base and 0.2 % $HClO_4$ and added to reagent 2 containing LDH (lactate dehydrogenase). For lactate measurement, the samples were mixed with NADH, 0.6M Glycine buffer and LDH. The completed samples were fed into and measured on a Beckman Coulter AU480 system (Beckman Coulter, USA), with final values obtained as mmol/litre.

Flow cytometric analysis for differentiation markers

Ramos wild type and *ADPGK* KO, stimulated (2 and 7 days) and unstimulated, cells were stained with CD20 and CD138 fluorochrome conjugated antibodies (BD Biosciences) according to the manufacturer's protocol. Cells from each study sample were also stained with FITC-Annexin V and Propidium Iodide (BD Biosciences), for analysis of apoptosis. Flow cytometry measurements were performed on BD FACS Verse cytometer using BD FACS Suite application software. At least 100,000 cells were analyzed for each sample and appropriate gating was applied to the populations to exclude cell debris and doublets. Data generated from positive gating was analysed using FlowJo software (Tree Star, Ashland, OR, USA).

Bound antigens for each sample were expressed as Relative Fluorescence Intensity (RFI), which is the ratio of the Median fluorescence intensity (MFI) of cells labelled with a specific Ab to that of unlabelled cells.

Glucose uptake assay

Uptake of 2-NBDG (2-(*N*-(7-Nitrobenz-2-oxa-1,3-diazol-4-yl)Amino)-2-Deoxyglucose glucose) glucose analog was measured flow-cytometrically using "Glucose uptake cell based assay kit" (Cayman chemicals, Europe) according to the manufacturer's protocol. Briefly, 5 million *ADPGK* KO and WT cells were seeded in 6 well plates and stimulated with PMA for up to seven days. Analysis was performed with unstimulated, 2-day and 7-day stimulated cells. Cells were incubated in glucose free media for 4 hours before analysis. At the end of glucose free incubation, 2-NBDG was provided at recommended concentration for 10 minutes and uptake measured via FITC measurement on flow cytometer. Cells incubated with Apigenin served as negative control for the experiment.

Enzyme kinetics

For analysis of glycolytic enzyme activities, Ramos wild type and KO cells (unstimulated, 2 and 7 days PMA stimulated) were lysed in Respiratory Chain Buffer (RCB). Around 15 million cells per sample were washed once with cold PBS (4^{o}C) post harvesting and dissolved in 700 µl cold RCB buffer. Samples were passed through 1 ml syringes fitted with 27G needles at least thirty times. Lysate was centrifuged at 300 g for 10 minutes to remove the debris and then at 7.5k in a table top centrifuge to get rid of mitochondrial pellet. The supernatant was then spun at 13k for 20 minutes to separate the Endoplasmic Reticulum pellet from the cytoplasmic supernatant. Supernatant, containing the glycolytic enzymes was used for analysis of Hexokinase and Gluocse-6-phosphate dehydrogenase enzyme activities using a colorimetric assay on a SpectraMax Plus 384 microplate reader (Molecular Devices) using SoftMax Pro Data Acquisition software in a 96-well plate. The enzyme activities were recorded as difference in absorbance at 340 nm to the absorbance at 400 nm and normalized to total protein content of the particular sample.

Mutational analysis of translocated *MYC*

cDNA obtained from unstimulated, 2-day and 7-day PMA stimulated *ADPGK* KO and WT cells was used to obtain *MYC* region coding for 3' segment of exon-1 and 5' plus middle segment of exon-2 via PCR using Q5 DNA polymerase. The product was purified using agarose gel electrophoresis and gel elution and cloned into TOPO-TA zero blunt vector (Thermo Fisher) as per kit guidelines. The plasmid was transformed into NEB-5alpha competent *E.coli* (New England Biolabs) and plated for colony formation in LB-plates. 65 colonies from WT and *ADPGK* KO plate colonies were picked and directly sent for sequencing using "Ecoli NightSeq service" (Microsynth Seqlab). The obtained sequences were aligned with wild-type *MYC* and analyzed for mutations using Geneious software (Biomatters Ltd., New Zealand).

Zebrafish xenograft studies

Zebrafish lines care and breeding were done under standardized and controlled conditions. Zebrafish *kdrl:GFP* line, used for xenografting, was raised at 28°C in a dedicated Zebrafish facility available at our institute. Embryos obtained via in-cross matings were maintained in E3 Embryo medium. Twenty-three hours post fertilization, media was supplemented with 0.2 mM 1-phenyl-2- thiourea (PTU, Sigma-Aldrich), to prevent pigmentation of larvae. For xenotransplantation, Ramos wild type and *ADPGK* KO cells were counted with a haemocytometer and stimulated with PMA. For injection, cells were fluorescently labelled by incubation with Cell Tracker CM-diI dye (C7001, Thermo Fisher) for 5 min at 37°C and further 15 minutes at 4-degree celsius. After the incubation, cells were washed once with PBS, and resuspended to a final concentration of 1.0×10^8 cell/ml in RPMI. Zebrafish larvae, 48 hpf, were anesthetized with tricaine (0.02%, 168 mg/L, Sigma) and aligned on agarose moulds (1% agarose) in a lateral position. Around 200-250 CM-diI labelled cells were injected into the yolk sac of each zebrafish larva using glass microinjection needles (World Precision instruments, USA) with a FemtoJet microinjector (Eppendorf, Hamburg, Germany). Maximum pressure applied in the microinjector was 180 psi. Larvae were incubated at 28^{o} C for 1 hour and then transferred to 34°C incubator for observing the growth of tumor cells.

Xenografts were analyzed by fluorescence microscopy (Leica DMI 4000B, Leica microsystems) on the day of injection and 48 hours post injection. Larvae were transferred to individual wells in 96-well plates in fresh E3 Embryo medium supplemented with PTU, for

observation of tumor growth. At the time of microscopy, the E3 media was removed and larvae were embedded in freshly prepared 0.1% Agarose in embryo medium. Tricaine was added at a final concentration of 168 mg/L to anaesthetize the larvae. The low agarose concentration prevented movement of larvae during microscopy and assisted in their proper alignment and at the same time kept the larvae alive by keeping the fluid circulation intact. At the end of microscopy, larvae were resuspended in fresh E3 media. The embryo medium was replaced daily. Growth of xenografted cells in the larvae was assessed with the help of ImageJ software.

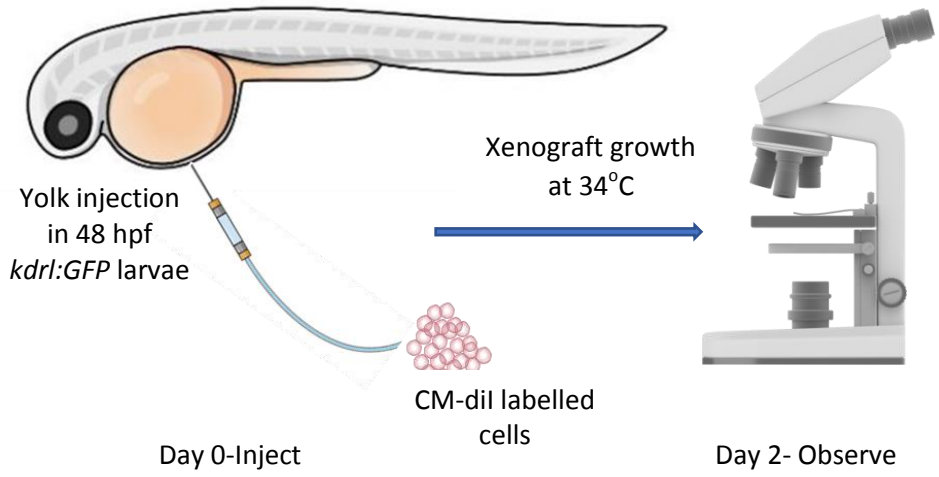

Figure 2.4: Zebrafish xenograft studies: *kdrl:GFP* larvae were grown at 28°C for 48 hours post fertilization and injected with 200-250 CM-dil labelled *ADPGK* KO/WT cells in the yolk. Larvae were transferred in 96-well plates post injection and kept for 1 hour at 28°C and imaged under a microscope, and then at 34°C for two days, at the end of which xenograft growth was observed and quantified. 50 larvae were injected for KO and WT conditions each.

Statistical analysis

Statistical analysis for all data presented in the study was performed using GraphPad Prism (7.04). Welch's t-test (unpaired) was used for significance analysis. A p value less than 0.05 were considered significant. If not stated otherwise in the text, analyzed data is presented as mean ± standard deviation of at least three independent experiments.

RESULTS

Preliminary studies

ADPGK knock-out and localization studies

ADPGK knockouts were generated in Ramos BL cells (Burkitt's lymphoma) using CRISPR/Cas9 technology and analyzed via Western blots. Two knockouts were finally selected for further experiments based on loss of 55 kDa ADPGK band in western blot and additionally confirmed by sequencing (Fig. 3.1a). Sequencing confirmed the presence of heterozygous deletion/insertion in one clone (KO1: 316_317del and 319_320insC) and homozygous four base deletion in the other (KO2: 314_317del).

Intracellular localization of ADPGK was performed using sucrose gradient centrifugation (Alberts, 2017). A total of 14 ER fractions (1-14 numbered) were obtained post gradient ultracentrifugation with 1 representing the least and 14 as the highest median density for the sample. Rough ER is bound to be present in the higher numbered fraction due to its high density and was accordingly detected in fractions 8-10 using markers such as SRPR-β (signal recognition particle receptor) and GFAT-2 (glutamine:fructose-6-phosphate aminotransferase). ADPGK was found to be present only in the fractions positive for rough ER markers and hence confirmed its presence in rough Endoplasmic reticulum (Fig. 3.1b).

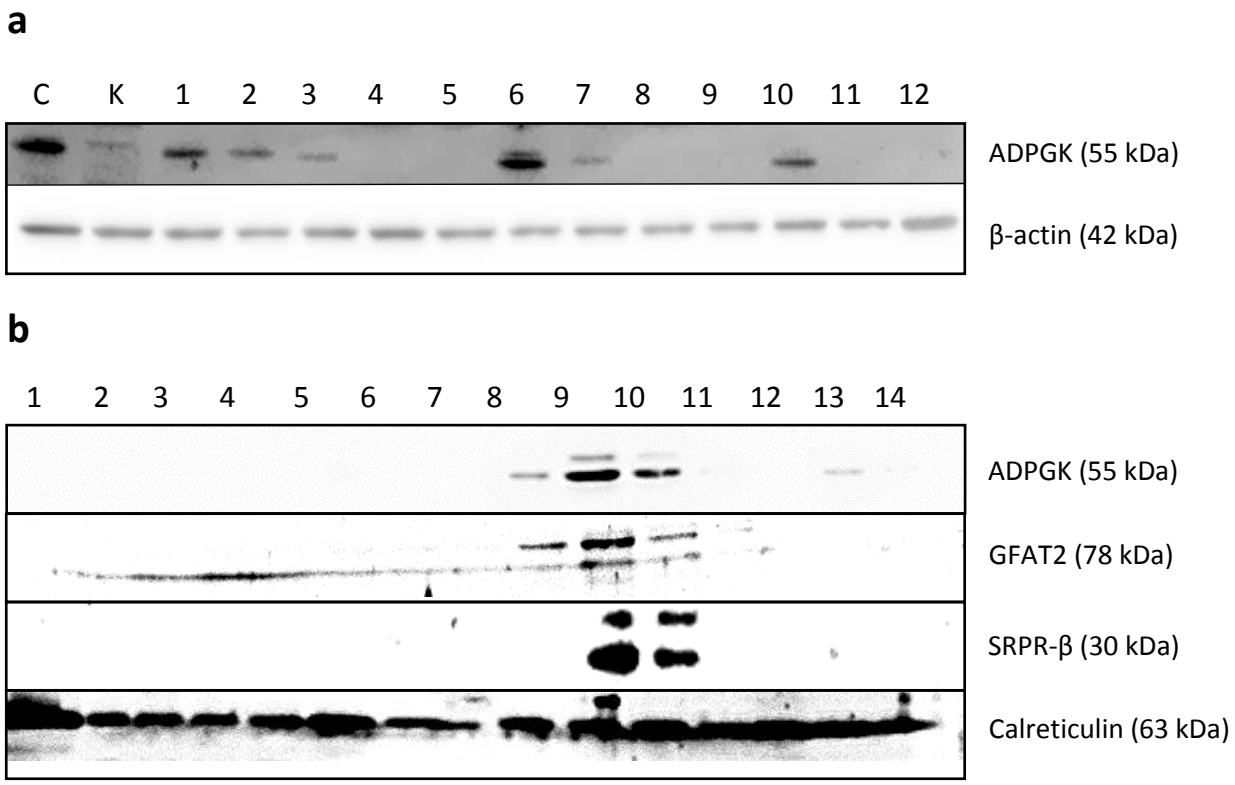

Figure 3.1: ***ADPGK* knock-out and localization studies**. *ADPGK* knock-outs were generated via CRISPR/Cas9 technology targeting exon-2 of *ADPGK*. For localization studies, ER (endoplasmic reticulum) fraction was ultra-centrifuged in a sucrose density gradient and 14 fractions isolated from the gradient were analyzed for ADPGK and ER markers. ***a***: ADPGK (ADP dependent glucokinase) knock-out selection via western blot using 55 kDa band as reference. β-actin is the loading control. (1-12) depict 12 analyzed clones ***b***: Result of sucrose gradient centrifugation for 14 fractions isolated from ER (Endoplasmic reticulum) with calreticulin as control. C is positive control and K negative control for ADPGK. Numbers 1-14 show the 14 isolated fractions with increasing order of density.

ADPGK expression upon B-cell activation

B-cells stimulated with PMA are known to follow an initial course of activation and proliferation followed by differentiation into plasmablasts leading to Memory B-cells or Plasma cells (Benjamin et al., 1984; Ghamlouch et al., 2014; Ho, Subhendu, & Hsu, 1987). A burst of aerobic glycolysis marks the proliferative phase providing necessary energy and metabolites for growth. We wanted to see the expression changes of ADPGK in Ramos BL cells upon activation with a known protein kinase-C (PKC) based inducer of B-cell activation, phorbol 12-myristate 13-acetate (PMA) (Benjamin et al., 1984; Ghamlouch et al., 2014; Ho et al., 1987; Krappmann, Patke, Heissmeyer, & Scheidereit, 2001; Rousset et al., 1989; Valentine, Cotner, Gaur, Torres, & Clark, 1987).

Ramos cells were stimulated with PMA for up to seven days and we measured ADPGK expression/activity at D2 and D7 representing the proliferating and differentiated cells respectively (Fig. 3.2a, b). The expression of *ADPGK* increased several folds upon stimulation and peaked at D2 where after it was found to decrease until D7 and became even lower than basal levels. ADPGK enzyme activity was on the other hand undetectable in unstimulated cells but displayed significant increase in kinetics at D2 before again becoming undetectable at D7.

This depicted the correlation of ADPGK with proliferating cells and at the same time displaying its near-redundant nature in quiescent cells.

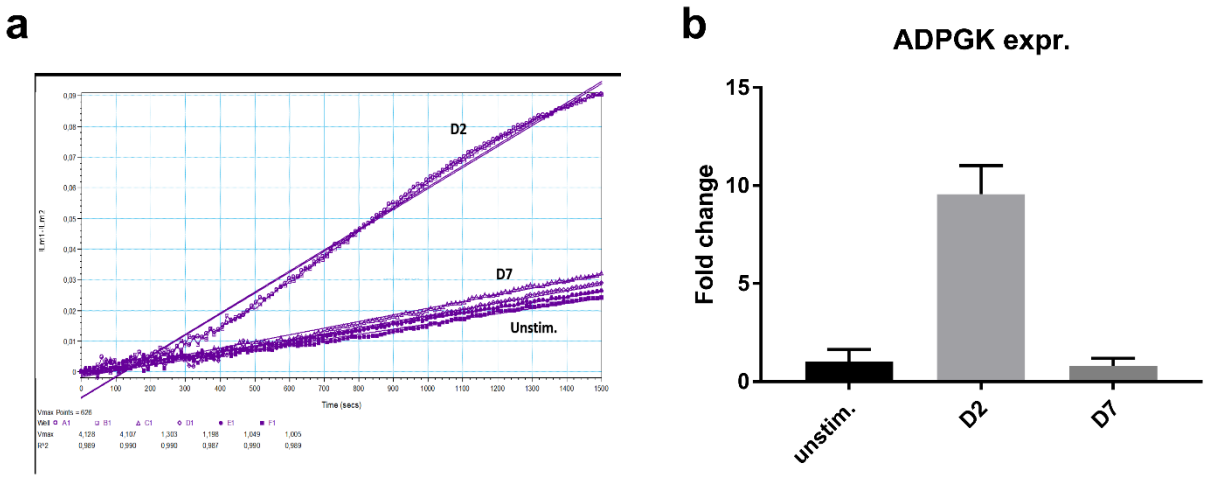

Figure 3.2: **ADPGK activity and expression upon activation**. Ramos BL (Burkitt's lymphoma) cells were stimulated with PMA (phorbol-12 myristate 13-acetate) for a period of seven days and analyzed at D2 (two days post stimulation) and D7 (seven days post stimulation). ***a***: Enzyme kinetics of ADPGK at D2, D7 and unstim. (unstimulated) states. *X-axis* represents time in seconds and *y-axis* is difference in absorbance between 340 nm and 400 nm. ***b***: Change in ADPGK expression upon stimulation at D2, D7 and unstimulated states using RT-qPCR. Data is representative of three individual experiments. Error bars represent standard deviation.

PMA stimulation induced differentiation is hampered in *ADPGK* KO cells

Flow cytometric profiling signalled stalled differentiation and increased apoptosis in *ADPGK* KO cells

CD20 and CD138 (Syndecan-1) are important markers for following B-cell differentiation (Jourdan et al., 2011; Tedder, Boyd, Freedman, Nadler, & Schlossman, 1985). Mature unstimulated B-cells are $CD20^{+}/CD138^{-}$. When stimulated by antigens they undergo cell surface changes to activated $CD20^{+}/CD138^{+}$ B-cells, and finally differentiate into $CD20^{-}/CD138^{+}$ plasma cells or recently classified $CD20^{-/low}$ pre-plasmablasts (Ghamlouch et al., 2014; Jourdan et al., 2011; Kaminski, Wei, Qian, Rosenberg, & Sanz, 2012; Tedder & Engel, 1994). Flow cytometric analysis of CD20 on D0, D2, and D7 post stimulation showed a normal differentiation related expression of this molecule on WT Ramos cells. With high quantity of CD20 detected in the unstimulated state, the levels of this molecule were upregulated until D2 post PMA stimulation, and exhibited a drastic decrease on D7 reflecting differentiation of WT cells (Fig. 3.3a, b). CD138 (Syndecan-1), undetected at D2, increased in expression at D7, though remaining at low levels but signifying a population positive for this plasma cell marker.

ADPGK KO cells exhibited nearly equal concentration of CD20 in the unstimulated state as the WT cells and were stable till D2. On D7, the KO cells exhibited low CD20 expression, but levels were still much higher than WT cells. CD138 was slightly upregulated at D7 but overall levels of CD138 remained almost at half the values for WT cells, signifying a reduced capacity of these cells to differentiate into plasma cells (Fig. 3.3a, b).

Another piece of information conveyed by flow cytometric analysis of *ADPGK* KO and WT cells was the FSC (forward scatter) and SSC (side scatter) data representing cell size and granularity, respectively (Ghamlouch et al., 2014). We found a consistent increase in FSC and SSC values in both cell lines (WT and KO) post stimulation, showing a large increase in size and increased cytoplasm:nucleus content for both types of cells (Fig. 3.3c). Increase in SSC usually represents a higher cytoplasm to nucleus ratio and thus points towards differentiated cells, however higher values of side scatter may also represent membrane blebs common in an apoptotic cell. SSC values gradually increased both for KO and WT cells till day 7 reflecting increased granularity and morphological changes related to differentiation. However, on D7 there was a significant increase in side scatter for KOs

compared to WT (Fig. 3.3c) most likely depicting higher number of apoptotic cells in the stimulated KOs which failed to differentiate.

The morphological changes linked with apoptosis in KO cells were confirmed with Annexin V staining (Schutte, Nuydens, Geerts, & Ramaekers, 1998) where KO cells showed almost 70 percent higher staining of the apoptotic marker compared to WT cells. The stained cells were additionally observed under a microscope and clearly depicted a much higher number of FITC stained cells in case of *ADPGK* KO cells (Fig. 3.3a, b, e).

The increased apoptosis cell death in *ADPGK* KO cells seven days post stimulation was also confirmed by a novel marker of Ca^{2+} induced apoptosis, the IP3 receptor. Protein levels of IP3R increased dramatically for *ADPGK* KO cells seven days post stimulation (Fig. 3.4b, e). Though the levels were increased for wild type cells also, but the change was many folds lower than KO cells.

Activation associated homotypic aggregation is lost in *ADPGK* KO cells

B-cells are known to form homotypic aggregates due to crosslinking of CD-40 molecules or mediated by LFA-1 upon stimulation by appropriate antigen (L. H. Dang & Rock, 1991; Rousset et al., 1989) and the interaction supports the clonal expansion and activation of lymphocytes (Burger & Peled, 2009). We indeed found large aggregates of cells starting to form as early as 48 hours post stimulation with PMA in WT Ramos cells, which increased several folds in size up to D7. Very few individual free cells were present in the media. KO cells, on the other hand, were only able to form small collections of cells when compared to the aggregates observed in case of WTs, providing a visible evidence of hindered differentiation in these cells (Fig. 3.3f). The aggregates even seemed to dissociate around D7 and only free individual cells were found in the culture after this point.

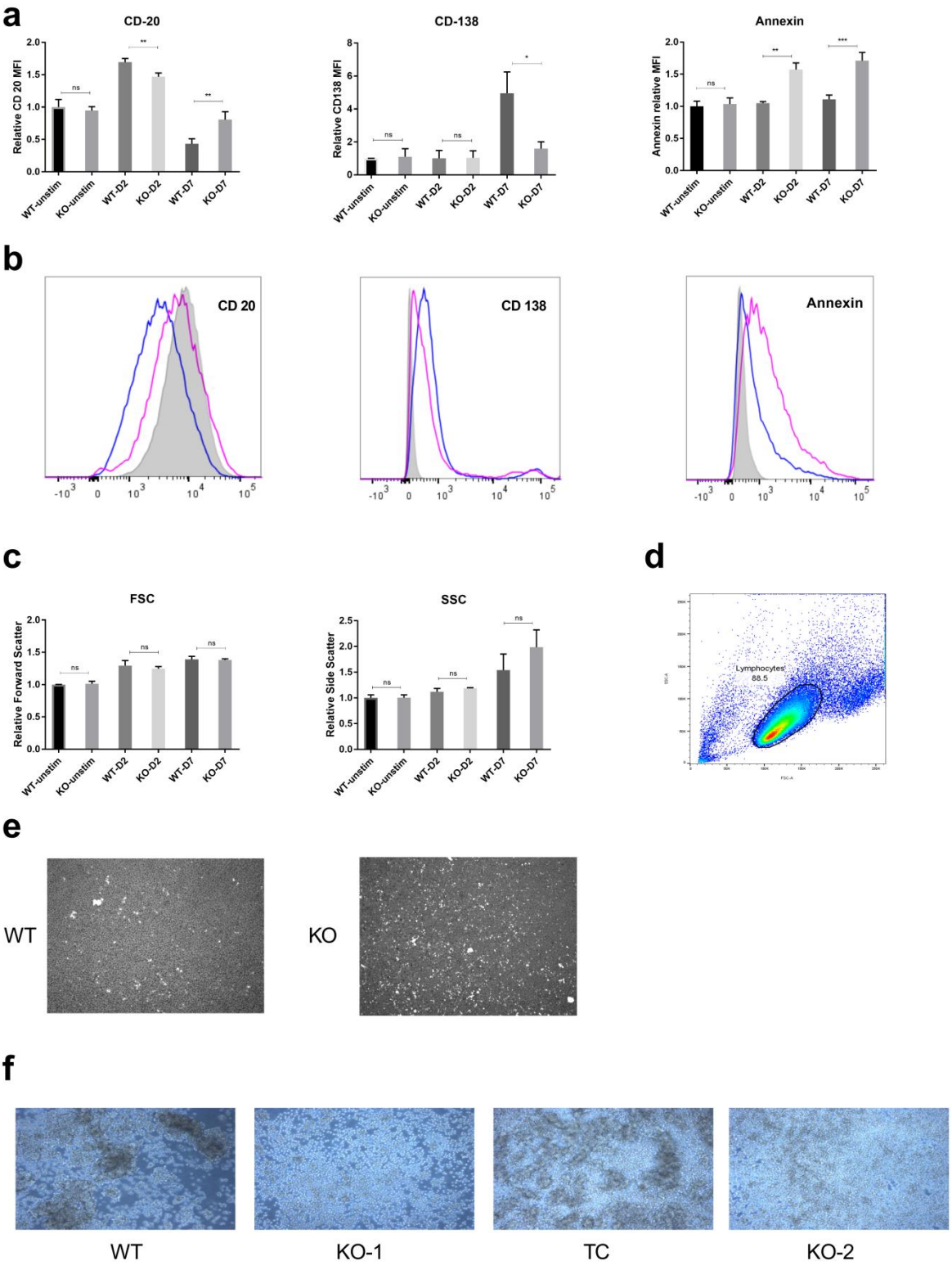

Figure 3.3: **PMA stimulation induced differentiation is hampered in *ADPGK* KO cells.** *ADPGK* (ADP dependent glucokinase) KO (knock out) and WT (wild type) cells were treated with 50 ng/ml PMA (phorbol-12 myristate 13-acetate) and cultured for seven days under standard conditions. Flow cytometric analysis was performed for cells collected at D0, D2

and D7 (unstimulated, 2 day stimulated, and 7 day stimulated) post stimulation. Panel ***a*** shows the change in Relative Fluorescence Intensity (RFI), which is the ratio of the Median fluorescence intensity (MFI) of cells labelled with a specific Ab to that of unlabelled cells over seven days, representing signal obtained from PE (CD20 and CD138) or FITC (AnnexinV) tagged fluorescent antibodies. ***b*****:** The same data represented as histogram of D7 (differentiation phase) fluorescence intensities for respective markers; pink line represents KO cells, blue WT and shaded area as unstimulated WT cells serving as control. ***c*****:** Forward and side scatter values generated by the flow cytometry experiments on various days for WT and KO cells. Gating strategy for the experiments is represented in ***d*** for excluding cell debris and clumps from analysis with automated area selection for lymphocytes using FlowJo software. Percentage of gated cells used for further analysis is shown by the number in the box. ***e*****:** Microscopic images of cells collected at D7 and displaying fluorescence for AnnexinV at 5x magnification. ***f***: Homotypic aggregates observed at 5x magnification under a light microscope at D7 in PMA stimulated WT and KO cells. Error bars represent standard deviation of mean of RFI (for CD20, CD138 and AnnexinV) or FSC/SSC values obtained from three independent experiments. WT, KO: mean of values from two wild-type and two *ADPGK* knock-out cell lines. *y-axis* for bar-graphs represents mean values of each sample normalized to unstimulated WT cells. *x-axis* in histograms shows fluorescence intensity. 100,000 events were recorded for each flow cytometry experiment. (*=$p < 0.05$; **=$p < 0.01$, ***=$p < 0.001$, calculated using Welch's t-test for significance)

ER stress-based differentiation markers are more expressed in *ADPGK* WT cells

Independent of the well-known role of XBP1 (X-box binding protein 1) in ER stress, cell proceeding through the terminal stages of differentiation is bound to have increased content of the XBP1(s) transcript compared to the unspliced XBP1 mRNA (Reimold et al., 2001; Todd et al., 2009) and thereby we wanted to analyse the levels of spliced/unspliced XBP1 in WT Ramos and *ADPGK* KO cells to decipher the activation induced differentiation status of these cells.

We measured the transcript content of spliced and unspliced XBP1 in unstimulated, 2 day and 7-day PMA stimulated WT Ramos and *ADPGK* KO cells. We found the ratio of spliced to unspliced XBP1 to be higher in KO cells compared to WT in unstimulated state (almost two folds) (Fig. 3.4a), which is uncharacterized of Burkitt's lymphoma. Previous studies have shown the very low or absent transcript levels of XBP-1 in Burkitt's lymphoma patient biopsies, typical of an undifferentiated lymphoma (Maestre et al., 2009). This signalled stressed cellular machinery in *ADPGK* KO cells even in unstimulated state, as also observed with metabolic data for these cells. At day two post stimulation, we observed a decrease in XBP1 splicing in both WT and KO cells, which could be explained by increased proliferative, glycolytic phenotype in the activation phase post stimulation with PMA. Further, at seven days post stimulation with PMA, the trend reversed dramatically in favour of a differentiated state with almost six to eight-fold increase in XBP-1 spliced/unspliced level for *ADPGK* WT cells. The KO cells, though, exhibited a much lower comparative increase, with two folds higher spliced mRNA levels of XBP1, again signalling an incomplete differentiation owing to hampered metabolism in activation phase.

The XBP1 splicing mechanism is completed by an ER resident protein IRE-1 and its levels in the cell could further shed light on the ER stress signalling operating in the cell (He, 2010; Tsuru, Imai, Saito, & Kohno, 2016). We thus measured phosphorylated IRE-1 protein levels in WT and *ADPGK* KO cells at the same stimulation points as for XBP1 mRNA levels. Western blot quantification seemed to strengthen our mRNA splicing data for XBP1 as the seven day stimulated cells had higher levels of IRE-1 than the two-day activated and unstimulated state for all cells (Fig. 3.4b, c). We were however not able to discriminate between the IRE-1 levels for *ADPGK* WT and KO cells based on the protein blots.

Immunoglobulins, secreted by differentiated B-cells or antibody secreting cells (ASCs), are rich in disulphide bonds, whose formation in the endoplasmic reticulum (ER) is catalysed by protein disulphide isomerase (PDI) (Lilie, McLaughlin, Freedman, & Buchner, 1994). With several studies pointing to a correlation between the levels of PDI and the differentiated state of a cell (Bertolotti et al., 2010; Miyaishi et al., 1998; Paver, Freedman, & Parkhouse, 1989), we quantified the protein content of PDI in WT and *ADPGK* KO unstimulated, D2 and D7 cells. The protein blots revealed a gradual increase in PDI levels in all cell lines upon activation, with levels increasing up to four-folds at D7 for WT cells (Fig. 3.4b, d). At all the measured time points, PDI protein levels in WT cells remained significantly higher than *ADPGK* KO cells. Overall, PDI known to act as an important mediator of protein folding for secreted proteins such as Ig's and a regulator of ER stress via its chaperone activity, was thus found in accordance with the increased differentiation status of WT cells.

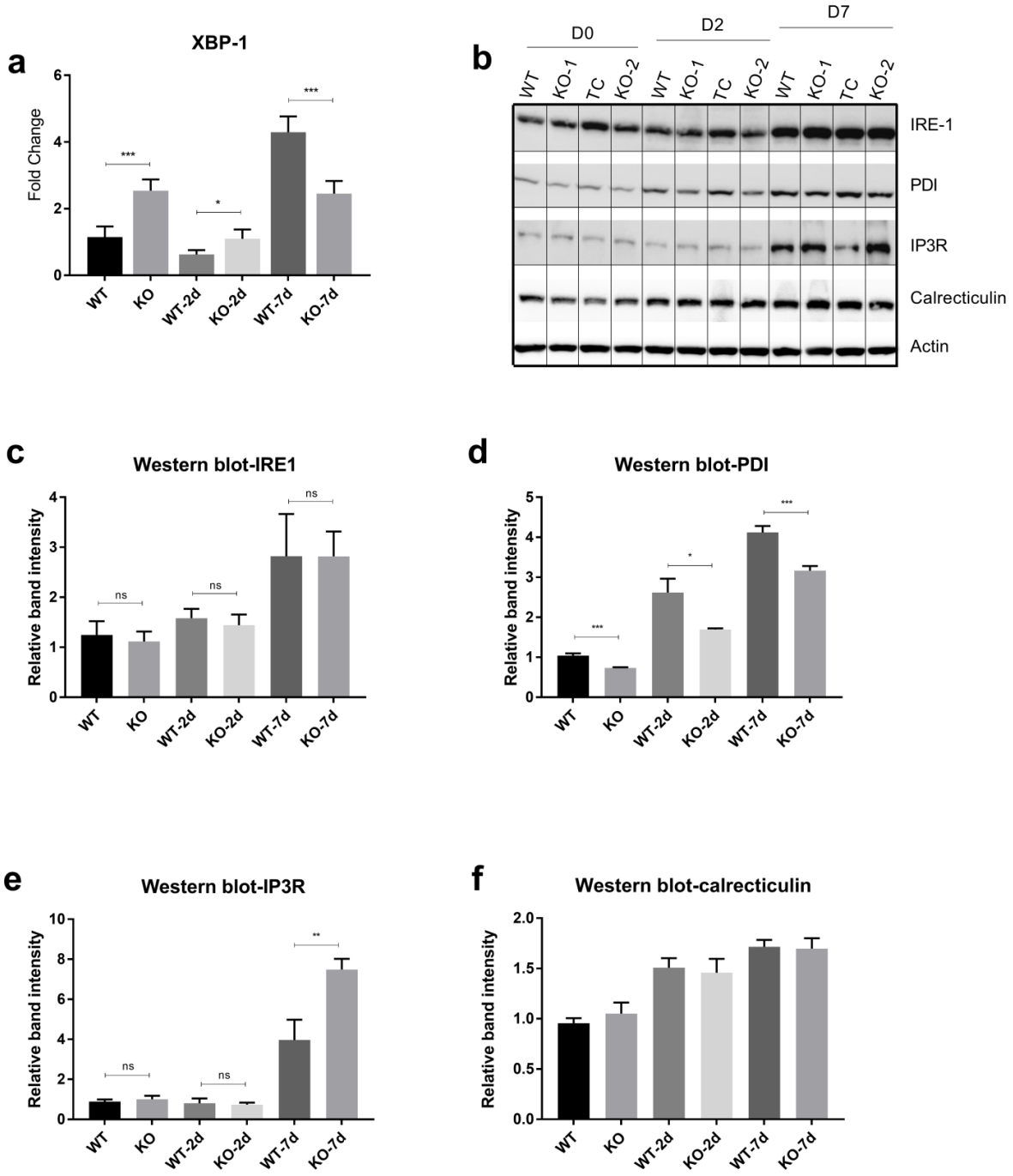

Figure 3.4: **ER stress-based differentiation markers are more expressed in *ADPGK* WT cells.** *ADPGK* KO and WT cells, treated with PMA and cultured for seven days under standard conditions were analyzed via western blot and RT-qPCR at D0, D2 and D7 post stimulation. ***a***: results of RT-qPCR performed for detecting ratio of spliced:unspliced XBP1 transcript in KO and WT cells at different conditions. y-axis represents fold change in expression of all samples normalized to unstimulated WT cells. ***b***: Western blots for WT and KO cells at D0, 2

and 7 with beta-Actin as loading control. ***c-f:*** quantification of band intensities using ImageJ software. All graphs are representative of three independent experiments. WT, KO: mean of values from two wild-type and two *ADPGK* knock-out cell lines. For western blots, TC is transfection control and the two knock-out lines as KO-1 and KO-2. *y-axis* in all graphs represents respective raw values normalized to unstimulated WT cells. Error bars represent standard deviation of mean for three individual experiments (*=$p < 0.05$; **=$p < 0.01$, ***=$p < 0.001$, calculated using Welch's t-test for significance)

ADPGK KO B-cells are metabolically toxified

ADPGK KO cells display reduced glycolysis in initial phases of stimulation driven differentiation

We measured cytosolic enzyme activities of Hexokinase-2 (HK2) and Glucose 6-phosphate dehydrogenase (G6PDH) (Jiang, Du, & Wu, 2014) in WT and KO Ramos cells 48 hours and seven days post stimulation with PMA. WT cells stimulated with PMA showed significantly increased, 2.5-3 folds, glycolytic enzyme activities (Hexokinase-2 and G6PDH) whereas the *ADPGK* KO cells displayed a significantly reduced activation-based increase in glycolytic enzyme activities compared to WT cells post two days (Fig. 3.5a, d). At seven days, the activity values dropped to almost 20 percent of the unstimulated state activities in both cell type but with WT cells displaying a higher residual activity than KOs. Gene expression values measured via RT-QPCR for Hexokinase-2 followed the same pattern as enzymatic activities and suggested a stably reduced glycolytic phenotype of KO cells (Fig. 3.5b).

ADPGK KO cells are less 'glucoholic' than the wild type Ramos cells

Detection of fluorescently labelled glucose is a common non-invasive method of detecting aggressively growing tumors using PET-CT scan. The amount of glucose uptake by most cancers being much higher than the normal body cells, the glucose uptake rate correlates well with the aggressiveness of a growing tumor (Zou, Wang, & Shen, 2005). The same holds true also for rapidly proliferating cells such as activated lymphoblasts. We thus detected NBD-glucose in four hour-PMA stimulated WT and KO Ramos cells to adjudge their malignant potential and activation phenotype. Post stimulation for 48 hours and seven days, NBD glucose was provided to the cells and its accumulation in cells was measured via flow cytometry. Glucose was provided for 10 minutes duration to the cells to detect the small changes in rapid glucose uptake. As shown in Fig. 3.5c, in the 48 hour stimulated cells, we observed an increased uptake in all cells with respect to unstimulated cells but wild-type cells exhibiting significantly higher amounts of glucose compared to KO's. At D7, we observed no significant difference in glucose uptake between wild type and KO, however there was a noteworthy reduction in uptake rate compared to unstimulated state in all cells. The results, further confirming the metabolic changes seen through enzymatic measurements, showed that the *ADPGK* KO cells were not progressing to a fully activated

state and were not able to upregulate glucose metabolism in the times of increased energy demands.

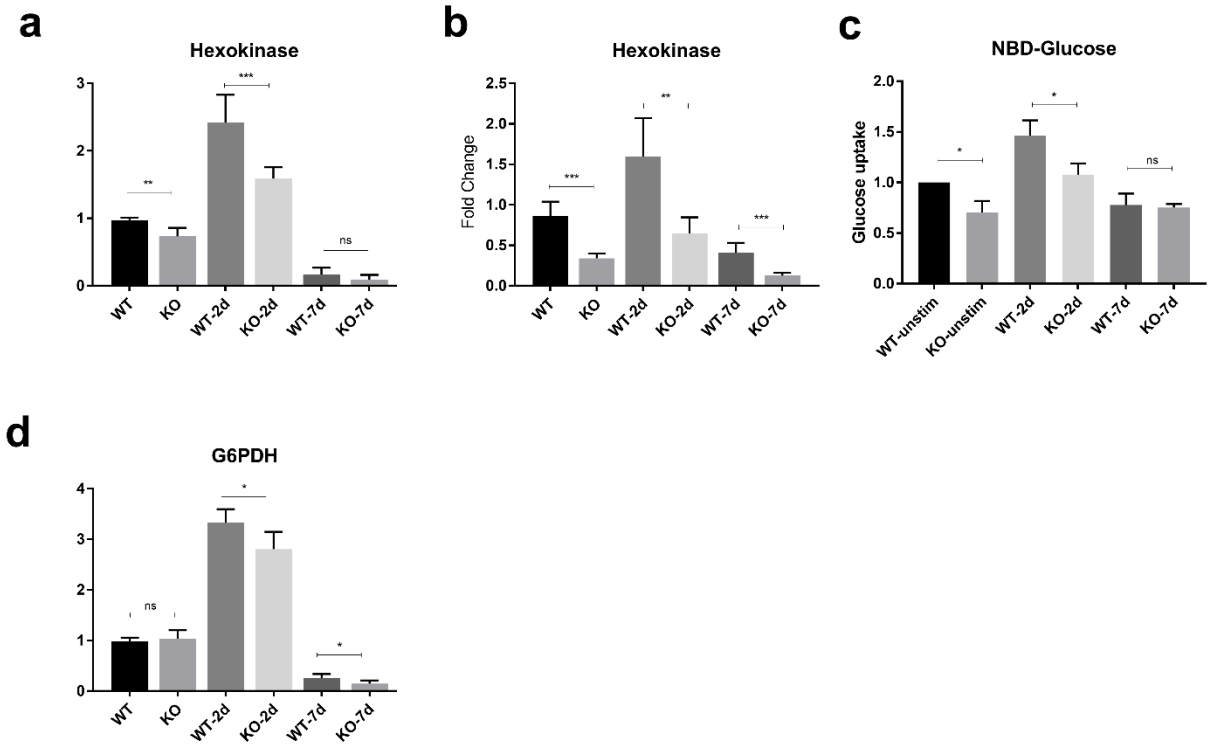

Figure 3.5: ***ADPGK* KO B-cells are metabolically toxified.** *ADPGK* KO and WT cells were analyzed for aerobic glycolysis upon stimulation with PMA by measurement of enzyme activities ***a, d*** of Hexokinase and G6PDH (Glucose 6-phophate dehydrogenase) spectrophotometrically; RT-qPCR for hexokinase-2 ***b*** for gene expression, and accumulated FITC-NBD-glucose (2-(*N*-(7-Nitrobenz-2-oxa-1,3-diazol-4-yl) Amino)-2-Deoxyglucose) ***c*** via flow cytometry for glucose uptake. All graphs are representative of three independent experiments. WT, KO: mean of values from two wild-type and two *ADPGK* knock-out cell lines. *y-axis* in all graphs represents respective raw values normalized to unstimulated WT cells. Error bars represent standard deviation of mean (*=$p < 0.05$; **=$p < 0.01$, ***=$p < 0.001$, calculated using Welch's t-test for significance)

Amino-acid uptake and metabolite secretion is remnant of activation driven metabolism in *ADPGK* KO cells

Amino acids form the building blocks of proteins, lipids, nucleotides, and participate in almost all major energy generating reactions in the cell. Importance of several amino acids like glutamine and serine is further highlighted in times of stress and high proliferation (Mattaini, Sullivan, & Vander Heiden, 2016; Tsun & Possemato, 2015). After detection of low glycolytic profile of *ADPGK* KO cells, we thus next wanted to investigate the amino acid uptake rate of these cells as replenishment for hampered glucose processing.

The results, as shown in Figures 3.6a, b depict significantly higher consumption of serine and glutamine by WT Ramos cells, compared to *ADPGK* KOs, at 2 days post PMA stimulation. Noteworthy was the higher increase in consumption of glutamine in stimulated state compared to unstimulated state (ratio, two days stimulated : unstimulated) in *ADPGK* KO cells. This could be explained by the compensatory use of glutamine in response to reduced glucose uptake and metabolism by these cells. However, taken as a quantitative uptake value, glutamine uptake levels for KO cells remained below the corresponding values for WT cells (1.48:1 for WT:KO). High dependence on glutamine as metabolite was further reflected by dramatic increase in free NH_3 (ammonia) levels in media of *ADPGK* KO cells in unstimulated and stimulated states, which reflected clearly the consumption of glutamine (Fig. 3.6c). Ornithine, which is originally not present in media formulation used for these cells, and was probably a by-product of glutamine metabolism, was also detected at values correlating with NH3 levels and fortifies the theory of glutamine dependent energy generation and biosynthesis by *ADPGK* KO cells.

Measurement of accumulated lactate and pyruvate levels in culture media of growing cells provides an estimate about the aerobic glycolysis where higher levels of lactate:pyruvate correspond to a more aerobic glycolytic phenotype and is a common occurrence in aggressively growing tumors (J. Xie et al., 2014; D. Q. Yang et al., 2016). To this end, we measured the lactate and pyruvate content in culture media obtained from 2 day and seven day stimulated cells. The levels of lactate:pyruvate rose in all cells at 2 days post stimulation by at least two folds, signifying actively proliferating cells (Fig. 3.6c). However, the comparative data again hinted towards a much-reduced aerobic glycolysis occurring in *ADPGK* KO cells with the levels of lactate:pyruvate in 2 day stimulated cells almost half of

that in WT Ramos cells (Fig. 3.6c). At seven days post stimulation, lactate:pyruvate values dropped for all cells signifying again the resting differentiated phase but as seen with other glycolytic data, WT Ramos cells still exhibited higher values of lactate secretion than their KO counterparts.

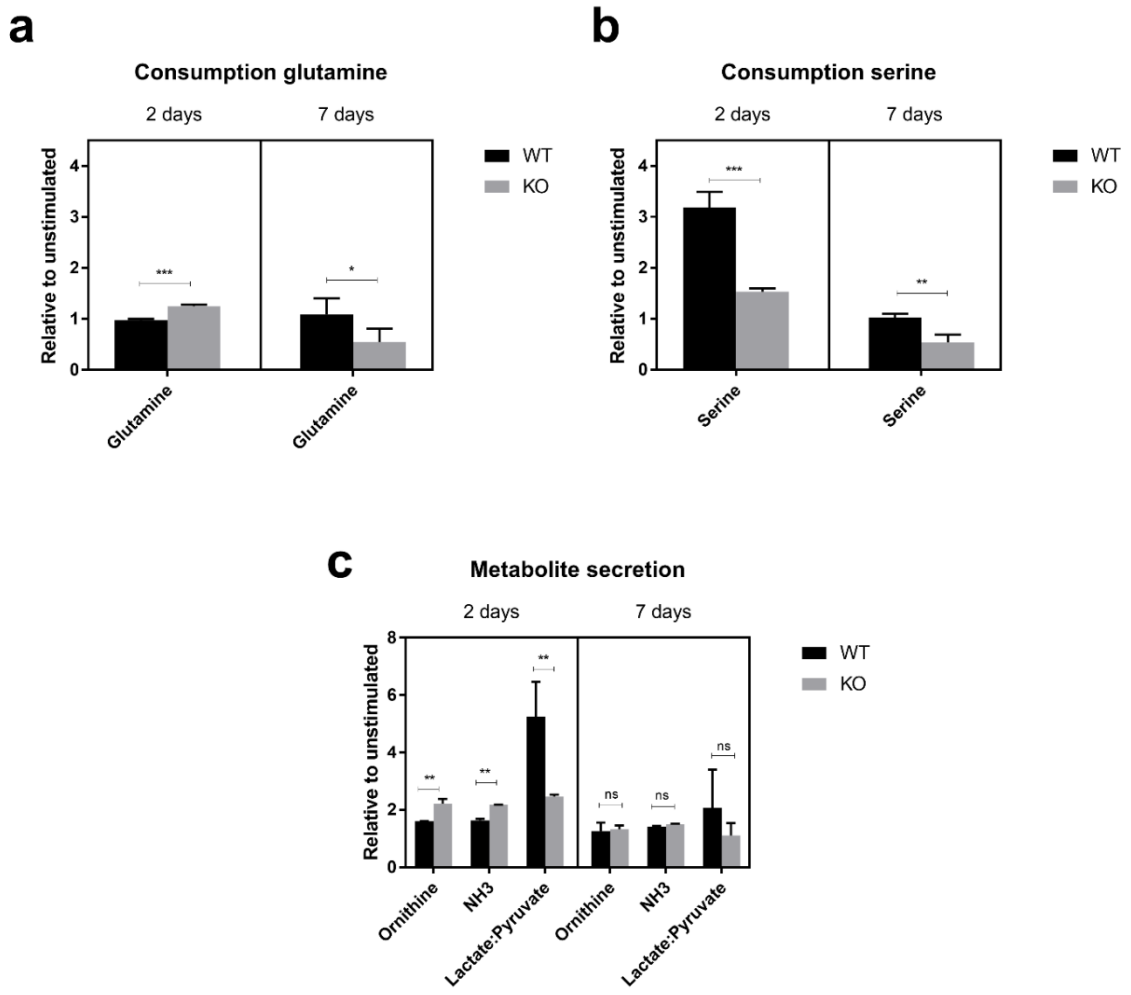

Figure 3.6: ***ADPGK* KO B-cells are metabolically toxified.** *ADPGK* KO and WT cells were analyzed for aerobic glycolysis upon stimulation with PMA by measurement of amino-acids and metabolites in culture media at D2 and D7 post stimulation. ***a, b***: Serine and Glutamine consumption in WT and KO cells at D2, D7 normalized to their respective unstimulated values. ***c***: secreted metabolites in culture media at D2, D7; lactate:pyruvate levels for estimation of Warburg phenotype and Ornithine, NH_3 values for glutamine metabolism, normalized to respective unstimulated conditions. All graphs are representative of three independent experiments. WT, KO: mean of values from two wild-type and two *ADPGK*

knock-out cell lines. *y-axis* in all graphs, represents respective raw values normalized to their unstimulated counterparts. Error bars represent standard deviation of mean (*=$p < 0.05$; **=$p < 0.01$, ***=$p < 0.001$, calculated using Welch's t-test for significance)

c-*MYC* expression and mutational status are dependent on glucose metabolism

We wanted to assess the effect of PMA stimulation on expression of c-*MYC* transcript (both wild type and translocated). cDNA primers used in the study were designed to obtain 3' region of exon 1 and 5' plus middle section of exon 2, which is also the coding sequence of c-Myc protein. Analysis of this coding region would provide a direct cue to action of c-Myc as a transcriptional regulator.

***ADPGK* KO cells exhibit a near complete loss of c-Myc post activation**

We performed c-*MYC* expression analysis of two days and seven days PMA stimulated cells, where the RT-qPCR results showed a significant increase in c-*MYC* transcript levels at two days post activation (Fig. 3.7a), signifying metabolically active proliferating cells and the change was similar in *ADPGK* KO and WT cells. However, at day seven post stimulation, we observed a strong reduction in c-*MYC* transcript levels, to almost 30 percent of base level values in WT cells but, to our astonishment, to nearly 10 percent of base level in *ADPGK* KO cells.

The results were verified by protein blots for c-Myc protein as well (Fig. 3.7b, c); however, we failed to detect c-Myc in unstimulated state in all samples via western blot. The reason for missing c-Myc protein in unstimulated cells had yet to be determined at that point and has been discussed below.

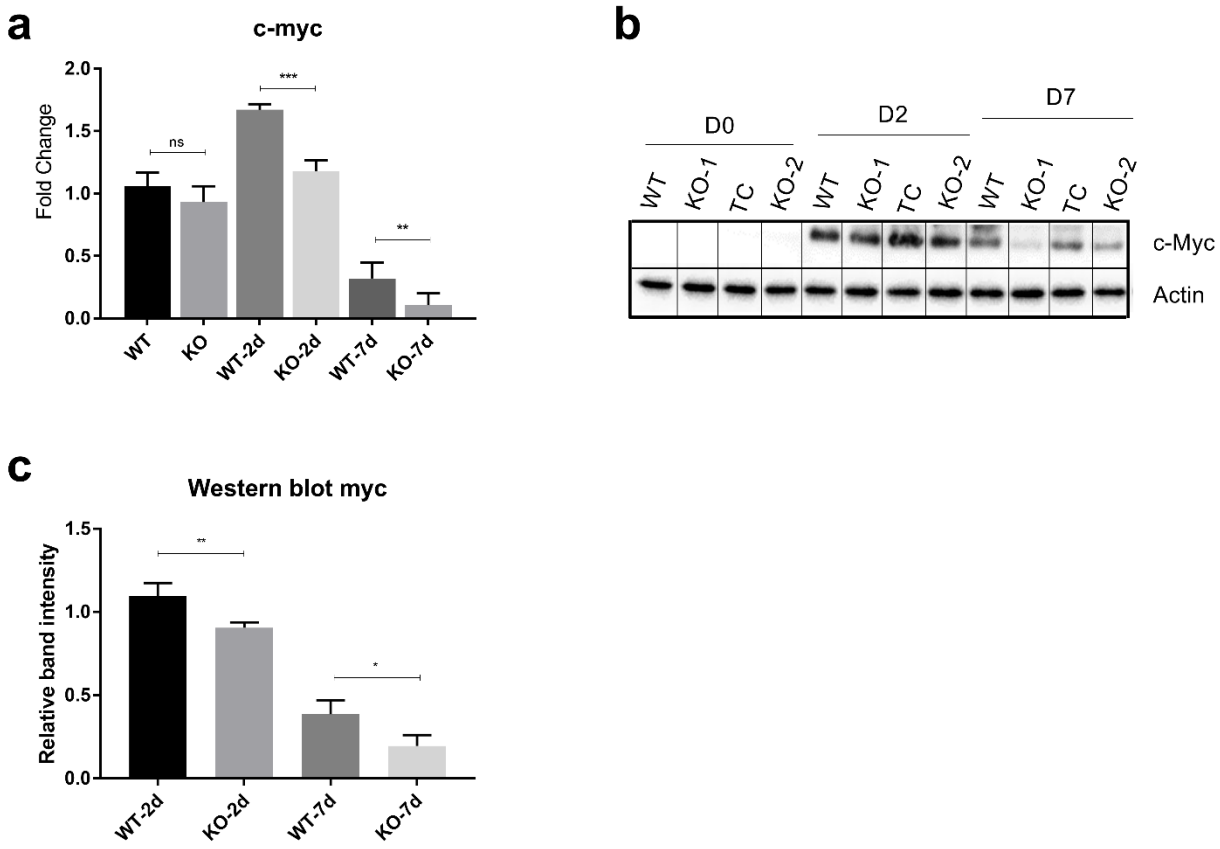

Figure 3.7: **c-*MYC* expression is dependent on glucose metabolism.** c-*MYC* (translocated and wild-type) expression in *ADPGK* KO and WT cells at different time points post stimulation was measured via RT-qPCR and protein content via western blots. ***a***: expression of *MYC* at D0, D2 and D7 post stimulation. *y-axis* represents fold change normalized to unstimulated WT cells. ***b***: protein blot of c-MYC and beta-Actin loading control, with quantification of bands in ***c*** using ImageJ software. Expression analysis and protein blots are representative of three individual experiments. WT, KO: mean of values from two wild-type and two *ADPGK* knock-out cell lines. Error bars show standard deviation of mean. (*=$p < 0.05$; **=$p < 0.01$, ***=$p < 0.001$, calculated using Welch's t-test for significance)

Translocated and wild-type c-*Myc* are expressed differentially in Ramos cells

We also wanted to know the mutational status of the transcripts being produced at different time points post PMA based stimulation. We thus sequenced the *MYC* transcripts and aligned the resulting sequences with known sequences of translocated c-Myc in Ramos and to the wild type transcript. The results depicted as per expectations, a vast number of mutations accumulated in *MYC* transcript of Ramos cells (both WT and KO) (Fig. 3.8c, d). Several of the mutations were conserved throughout the sequences analysed and most of them matching with the known mutations in translocated *MYC* allele of Ramos cells and patient biopsy samples of Burkitt's lymphoma (Bemark & Neuberger, 2000; Cowling et al., 2014). However, some of the conserved mutations were novel and depicted additional effect of hypermutation during culture of these cells, as also known from previous studies (Bemark & Neuberger, 2000). Insertions and deletions of several bases were observed along with point mutations. To our surprise though, upon sequencing of two day and seven day stimulated Ramos BL cells (both WT and KO), we obtained wild type c-*Myc* sequence in almost 50 percent of cases. This finding is in first sight, in contradiction to previous studies which reported that only the translocated c-*Myc* allele is expressed in Ramos BL cells (Bemark & Neuberger, 2000). However, the sequences used in previous studies were only obtained from unstimulated cells and true to that, we obtained only translocated c-*Myc* allele from non-PMA stimulated cells.

This result however answered the question of failure to detect c-Myc protein in the unstimulated state. The translocated c-*Myc* being highly mutated compared to wild type c-*Myc* and that being the only transcript produced in unstimulated cells, the commercial antibody used for detection of c-Myc will most likely not be able to bind to the desired peptide. Further, upon stimulation, as the expression of wild type c-*Myc* increases in all cells, we were able to detect the protein in western blots.

Translocated c-*Myc* is highly mutated in WT cells compared to *ADPGK* KO

Having discovered the variations in c-*Myc* expression levels, we were interested in random non-conserved point mutations which had likely accumulated due to culturing and PMA based activation of *ADPGK* wild type and KO cell lines in the lab. Analysis of 65 WT and KO sequences revealed astonishing results where we found 38 independent mutations in WT

cells and just 10 mutations in KO cells (Fig. 3.8a, b). Moreover, out of the 38 point mutations in WT cells, 30 were found in PMA stimulated conditions (two day + seven day). More than 2/3rd of these (21 precisely) were found in seven day stimulated cells, clearly pointing to a role of activation induced hypermutation in the observation. On the other hand, *ADPGK* KO cells displayed half (5/10) mutations in the stimulated state, out of which just two were in seven day stimulated cells (Fig. 3.8). Knowing that 'AGC triplets' are a hotspot for AID targeted mutations in activated GC B-cells (Bemark & Neuberger, 2000; Betz, Rada, Pannell, Milstein, & Neuberger, 1993), we analysed the location of mutations with respect to AGC (or GCT, reverse complement) sites. Indeed, 20/38 or almost 52 percent mutations were at AGC triplets (Fig. 3.8c), out of which 18 were found in sequences from stimulated Ramos cells. A random mutational targeting with respect to the consensus translocated *MYC* sequence would have yielded maximum 13 percent hits on AGC triplets. Also, 36/38 targets, or almost 95 percent mutations, were at G/C sites. There was also a preference for transitions overs transversions with 50 percent observed mutations occurring as transitions (randomly expected 33 percent). Such highly specific and preferential mutational targeting is a characteristic of immunoglobulin hypermutation (Bemark & Neuberger, 2000; Xu-Monette et al., 2016) and clearly reflected a much higher degree of organized mutations in *ADPGK* WT cells compared to the KOs.

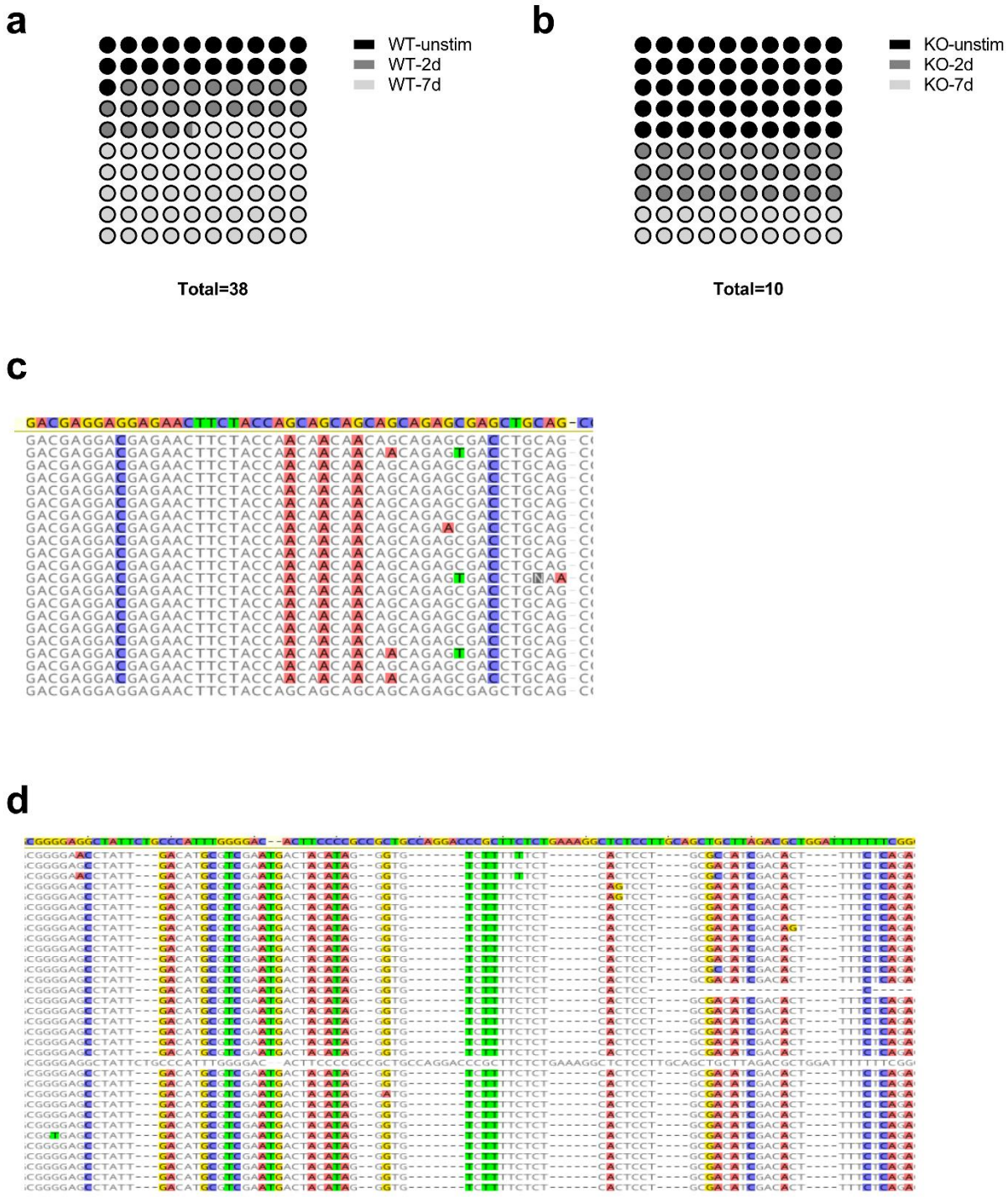

Figure 3.8: **c-*MYC* mutational status is dependent on glucose metabolism.** Transcripts obtained at D0, D2 and D7 post stimulation with PMA for *ADPGK* WT and KO cells were sequenced and aligned with wild type *MYC* to analyse mutations in translocated allele. ***a, b:*** 10 x 10 dot plot for representation of observed mutations in WT and KO cells at D0, D2 and D7 post stimulation. Each dot corresponds to one percent and thus the percentage of mutations for various time points can be calculated. Total number of observed mutations

for each cell line are given below the plots. ***c:*** Representative figure showing the distribution of random mutations and their preferential targeting to AGC sites with respect to wild type *MYC* (topmost highlighted sequence). ***d:*** figure shows the vast accumulation of conserved mutations in translocated *MYC* obtained from WT and KO cells. Mutational analysis was performed with over sixty individual *MYC* transcripts obtained from WT and KO cells at different time points. Sequences were aligned in Geneious software and figures exported are depicted.

ADPGK KO leads to reduced migration of macrophages to tumor

Immune cell, especially macrophage, migration to Burkitt's lymphoma microenvironment is often considered as one of the most important factors contributing to aggressiveness of the disease (Coussens & Werb, 2002; Liu & Cao, 2015). The macrophages which are chemotactically or otherwise attracted towards the tumor niche, the Tumor Associated Macrophages (TAMs), are more often than not, are polarized to and serve as tumor growth promoting, anti-inflammatory, M2 macrophages (Genard, Lucas, & Michiels, 2017). To study the effect of *ADPGK* KO on regulation of immune cell chemotaxis, the migration of THP-1 monocyte/macrophages was studied in presence of wild type Ramos or *ADPGK* KO cells. The quantification of migrated THP cells post 6 hours of incubation showed a marked difference between WT and *ADPGK* KOs, with the latter displaying a much-reduced number of THP cells which underwent migration, the number of migrated cells even approaching those observed with the negative control (only media, no cells) (Fig. 3.9e, f). Wild type Ramos exhibited migration rates more than double compared to its KO counterparts, indicating a significant loss in chemotactic attraction capabilities of Burkitt's lymphoma cells upon removal of *ADPGK*.

Macrophage M1 polarization increases with KO of *ADPGK*

We aimed at replicating the tumor-immune cell interaction at an *in-vitro* level to understand the phenotype bestowed upon the macrophages by lymphoma cells. PMA activated THP-1 monocytes were co-cultured with stimulated WT Ramos or *ADPGK* KO cells for a period of 48 hours, which corresponds to the activation state of B-cells signifying high proliferation and high glycolytic activity found in aggressively growing lymphomas. Monocyte-

macrophages collected post co-culture with Ramos WT or KO cells displayed a greater shift towards the M2 polarized state when incubated with WT Ramos cells compared to KOs as evident by the reduced expression of glycolytic enzymes (HK), M1 marker iNOS1 (Inducible nitric oxide synthase) and pro-inflammatory cytokine IL8, and increased expression of M2 marker Arg1 (Arginase 1) (Fig. 3.9a-d) (Colegio et al., 2014; Galvan-Pena & O'Neill, 2014; Genard et al., 2017; Varney et al., 2002). Macrophages collected from *ADPGK* KO cells co-culture on the other hand displayed enhanced expression of glycolytic enzymes (HK), which were significantly increased compared to the cells stimulated with PMA alone and not incubated in a co-culture setup, depicting a shift towards high glycolytic, M1 polarized state. Expression of IL8, and iNOS were also upregulated in cells collected from *ADPGK* KO co-culture. On the other hand, a potent M2 marker, Arg1, was much reduced in expression in macrophages obtained from *ADPGK* KO co-culture. Overall, the expression data for M1/M2 markers clearly showed that only macrophages co-cultured with WT Ramos cells were increasingly polarized to a tumor-assisting M2 phenotype, as also known in case of most aggressive tumors.

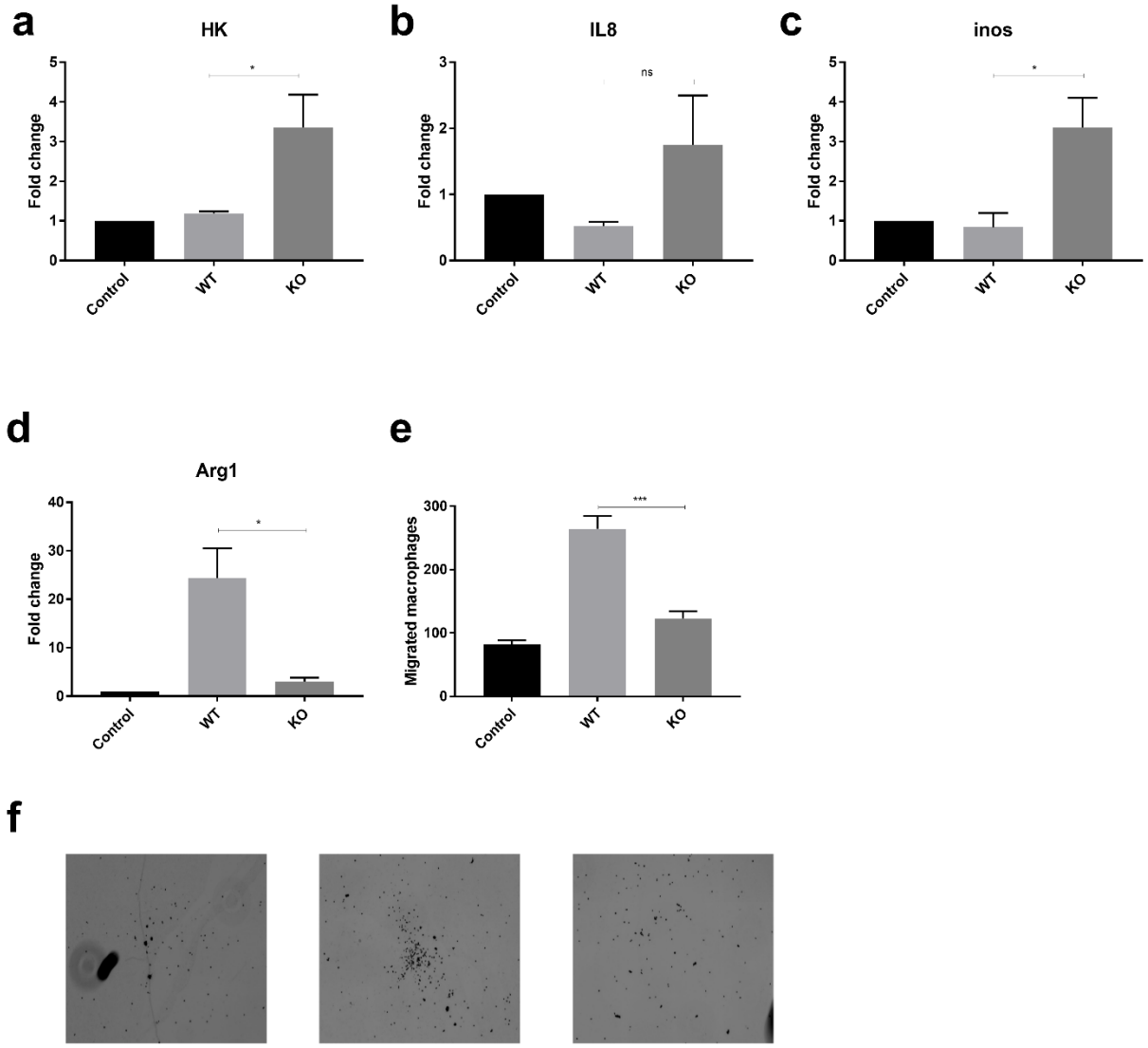

Figure 3.9: ***In-vitro*** **analysis of tumor aggressiveness in *ADPGK* KO and WT cells. *a-d*:** PMA activated THP-1 monocytes were co-cultured with stimulated WT Ramos or *ADPGK* KO cells for a period of 48 hours. Monocyte-macrophages collected post co-culture with Ramos WT or KO cells were analyzed via RT-qPCR for expression of M1, M2 markers in form of Hexokinase, IL-8, iNOS (inducible nitric oxide synthase) and Arginase 1. PMA activated THP-1 cells without a co-culture setup served as control for the experiment. ***e***: the migration of THP-1 monocyte/macrophages was studied in presence of WT or *ADPGK* KO cells. Media without WT/KO cells served as control. The quantification of migrated THP-1 cells post 6 hours of incubation is represented as actual cell numbers on *y-axis*. ***f:*** Microscopic images representing migrated THP-1 cells upon co-culture with WT and KO cells at magnification 2.5x. WT, KO: mean of values from two wild-type and two *ADPGK* knock-out cell lines in all

bar-graphs. Error bars show standard deviation of mean. (*=$p < 0.05$; **=$p < 0.01$, ***=$p < 0.001$, calculated using Welch's t-test for significance)

ADPGK KO affects the growth of lymphoma xenografts in Zebrafish larvae

To monitor the development of lymphoma xenografts in zebrafish larvae over a period of two days, we injected PMA activated WT Ramos and *ADPGK* KO cells in the yolk of *kdrl:GFP* zebrafish larvae 48 hpf (hours post fertilization). Images were taken over 48 hours (D0 and D2) and the growth of tumor was quantified. Images taken immediately after injection (D0), showed a near equal distribution of WT Ramos and KO xenografted cells in zebrafish yolk. Post 48 hours (D2), we observed a significant increase (up to 50 percent increase than D0) in the size of xenografted mass in 43/50 zebrafish larvae in case of WT Ramos cells (Fig. 3.10a, b). Larvae injected with *ADPGK* KO cells showed growth of the xenografted mass only in 16/50 injections, plus the growth was significantly hampered compared to their WT counterparts. In remaining injected zebrafish, the xenografted mass surprisingly shrank in most of the larvae (21/34) while being consistent in size in others, likely reflecting the inability of KO cells to grow in an external environment owing to impeded regulators of aerobic glycolysis.

This, being the first study ever with establishing of Burkitt's Lymphoma xenografts in zebrafish, successfully replicated our *in-vitro* data and strengthened the hypothesis that *ADPGK* KO Ramos cells fail to adapt into the activation phase associated with differentiation and due to low Warburg phenotype, undergo apoptosis, which overall makes them less aggressive as a xenografted tumor when compared to WT Ramos cells.

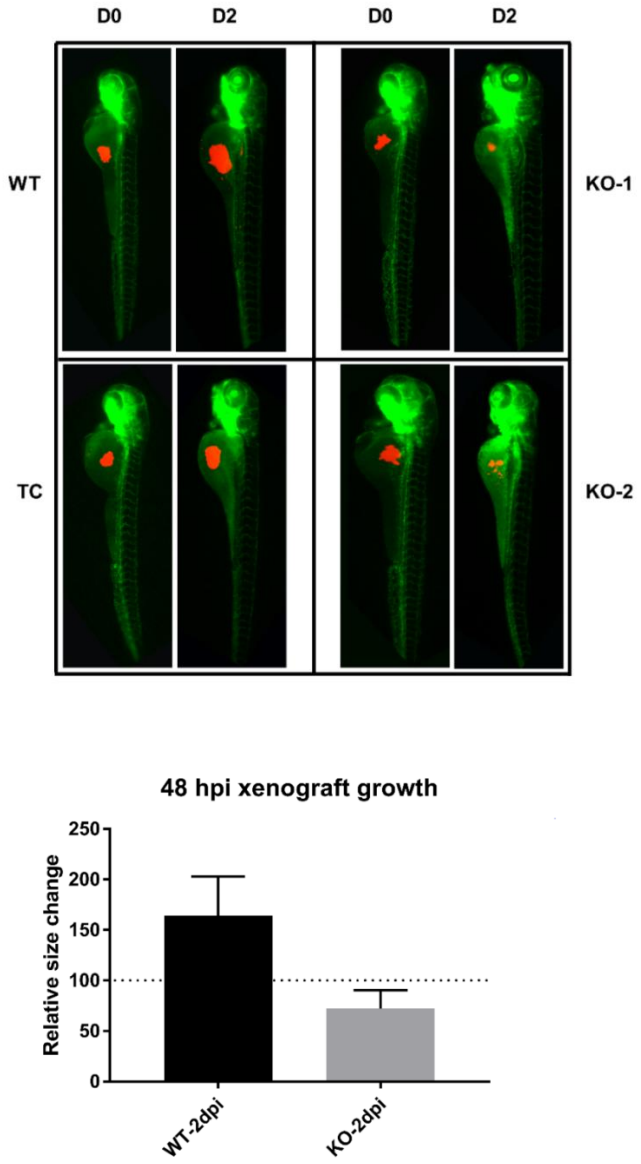

Figure 3.10: ***In-vivo*** **analysis of tumor aggressiveness in *ADPGK* KO and WT cells.** Approximately 200-250 CM-dil labelled cells (WT or KO) were injected in yolk of 48 hpf (hours post fertilization) *kdrl:GFP* zebrafish larvae. Images in ***a*** show the progression of xenografted cells over two days post injection (D0 – D2) in wild type (WT, TC) and *ADPGK* knock-out (KO-1, KO-2) cells. Xenograft area quantified using ImageJ for 50 injected larvae with WT and KO cells each and a mean calculated over three individual experiments is shown in ***b***. WT, KO: mean of values from two wild-type and two *ADPGK* knock-out cell lines in all bar-graphs. Error bars show standard deviation of mean. (*=$p < 0.05$; **=$p < 0.01$, ***=$p < 0.001$, calculated using Welch's t-test for significance)

DISCUSSION

In this study we aimed at analysing the effect of ADPGK mediated glucose shuttling on regulation of aerobic glycolysis in Ramos BL cells, reflected by their malignant and differentiated status upon activation. We found invariably reduced tumor aggressiveness upon activation, both *in-vitro* and *in-vivo* zebrafish, and a hindered activation mediated differentiation of *ADPGK* KO cells. The data was cemented by strikingly large reduction in *MYC* transcript and protein levels in KO cells and plummeted accumulation of mutations in the translocated *MYC* allele.

Perturbation of differentiation markers in *ADPGK* KO and WT cells

Markers of differentiation in form of CD20, CD138, XBP1, increase in cell size and granularity, and homotypic aggregation provided a clear view of well-differentiated WT cells and a delayed entry to differentiation of KO cells which ultimately ended with apoptosis.

B-lymphocyte antigen, CD20, is expressed on the surface of pre-B cells and as an important glycosylated phosphoprotein, is expressed throughout the development of B-cells except on terminally differentiated cells. The precise function of this protein still not elucidated, it is hypothesized to play a role in regulating calcium flux through the cell via its association with BCR (B-cell receptor) (Walshe et al., 2008). The expression of CD20 is variable upon activation and depends on the amount and type of antigen provided to the cell. It is often found to increase during the proliferative phase after stimulation but later becomes low/negative upon terminal differentiation into plasma cells (Jourdan et al., 2011; Tedder & Engel, 1994; Valentine et al., 1987). The low but non-negative values observed for CD20 in WT cells proceeding towards differentiation, signified a population not characteristic of plasma cells but probably a plasmablast transition state as also discussed in several other studies (Ghamlouch et al., 2014; Jourdan et al., 2011; D. A. Kaminski et al., 2012). However, the *ADPGK* KO cells displayed a much higher percentage of population positive for this marker and signalled towards a stalled differentiation pathway in these cells. The higher residual expression of CD20 in *ADPGK* KO cells is important in the light of using chemotherapeutics such as Rituximab which bind to surface CD20 on lymphomas and thereby enhances the efficacy of Natural Killer (NK) cells in destroying these malignant cells (Rudnicka et al., 2013).

Likewise, CD138 (Syndecan-1), a marker highly specific for differentiated cells, was found upregulated several folds in WT cells compared to KOs. Though, the overall levels of CD138 remained low and it needs to be investigated if longer PMA based stimulation in combination with other cytokines is needed to upregulate the expression even further. Again, this signified cells proceeding through a differentiation pathway but possibly till a plasmablast state, as seen for CD20. The protein CD138, is a transmembrane type I proteoglycan, glycosylated with a heparan sulphate (HS) moiety (Kharabi Masouleh et al., 2009). The heparan sulphate domain forms the major functional part of CD138, by binding to several extracellular ligands responsible for cell adhesion, morphogenesis, survival, tumor growth, migration and even inflammation (Kharabi Masouleh et al., 2009; McCarron, Park, & Fooksman, 2017). Expression of CD138 has been related to several cancers such as multiple myeloma, where the binding of pro-survival factor APRIL promotes cancer cell survival and proliferation (McCarron et al., 2017). A much reduced expression of CD138 on *ADPGK* KO cells thus explains partially the greater number of apoptotic cells observed via AnnexinV staining and SSC (side scatter) studies, and the inability to form homotypic aggregates mediated by cell-cell adhesion. The marker has been recently shown to translocate to the nucleus, delivering growth signals and thereby promoting tumor-stromal cross talk (Stewart, Ramani, & Sanderson, 2015). This might explain the low levels of marker observed on cell surface of both wild type and KO cells at day 7, however proving its importance in promoting tumor aggressiveness, as observed by its increased levels in WT Ramos cells.

XBP1, which is an important component of the unfolded protein response (UPR) and promotes a balance between the adaptive and apoptotic pathways in a differentiating cell (He, 2010), was found to be active in unstimulated KO cells, which is otherwise unknown of (Maestre et al., 2009), signifying an underlying stressed ER machinery in these cells. Analysis of differentiation state at day 7 depicted much reduced expression of XBP1(s) in KO cells compared to WT, signalling strongly the reduced differentiation capability of *ADPGK* KO cells. XBP-1(s) being one of the major factors upregulated upon differentiation in plasma cells, we were prompted to measure the levels of its regulatory enzyme, IRE-1. With IRE-1 protein levels undoubtedly increasing at day 7 but with no obvious difference between WT and KO cells, the observed variations in XBP1(s) expression remain elusive. However, recently discovered relationship of XBP1 with MYC, acting as partners in a transcriptional

complex (H. Xie et al., 2018; N. Zhao et al., 2018), demands further research in the subject and would provide key to the prevailing query. PDI (protein disulphide isomerase), found in ER lumen, catalyses the switch between thiol-disulphide in proteins and helps in the formation of disulphide bonds during protein folding (Oka & Bulleid, 2013). Immunoglobulin (Ig) formation in plasma cells or antibody secreting cells (ASCs) involves a high load of proteins shuttling though the ER and requiring disulphide bond formation to constitute a function Ig molecule (Lilie et al., 1994; Miyaishi et al., 1998; Oka & Bulleid, 2013). Though the overall levels of PDI were found to increase several folds at D7, starting as early as D2, in all cells, the WT cells showed a significantly higher content of this protein at all stages of activation. This depicted a marked difference in response to increased unfolded protein content in the ER between WT and *ADPGK* KO cells, with the latter hampered in their ability to cope up with the highly increased flux of proteins (Ig's) associated with B-cell activation and differentiation.

The pathway to terminal differentiation was clearly stalled in ADPGK KO cells, as studied via various markers, and ultimately pushed these cells to apoptosis as observed from SSC, Annexin V and the novel IP3R study.

Metabolic catastrophe was bestowed upon *ADPGK* KO cells

A reduced Warburg phenotype upon activation for *ADPGK* KO cells was one of the effects reflected by study of glycolytic enzyme activities (HK2, G6PDH) and expression (HK2), and pointed to a direct link between ADPGK and BL cell metabolism. The study involved enzymatic and expression analysis of hexokinase-2, which is the sole isoform of hexokinase overexpressed in cancer (Katabi, Chan, Karp, & Batist, 1999; Mathupala, Ko, & Pedersen, 2006; Patra et al., 2013). With HK2 expression/activity in WT cells significantly higher than KOs at all times but most evident at D2, depicted a low glycolytic profile of *ADPGK* KO cells post stimulation in the proliferative phase. We measured G6PDH enzyme activity, as the protein is involved in pentose-phosphate pathway for providing NADPH to proliferating cells, preventing them from oxidative damage, besides initiating the generation of nucleotides. The role of G6PDH activity in leukemia cell lines has been recently highlighted (S. N. Xu, Wang, Li, & Wang, 2016) and thus the observed differences in G6PDH activity between *ADPGK* KO and WT cells point to a reduced cancer metabolism upon removal of ADPGK. Detection of fluorescently labelled glucose, which is a common non-invasive

method of detecting aggressively growing tumors using PET-CT scan (Cox et al., 2015), displayed a reduced glucose uptake by *ADPGK* KO cells, further confirming and reflecting the metabolic changes seen through enzymatic measurements. Overall the glycolytic study showed that the *ADPGK* KO cells were not able to upregulate glucose metabolism in the times of increased energy demands during the proliferation phase.

Amino acids form the building blocks of proteins, lipids, nucleotides, and participate in almost all major energy generating reactions in the cell. Importance of several amino acids like glutamine and serine is further highlighted in times of stress and high proliferation (Mattaini et al., 2016; Tsun & Possemato, 2015). Serine, a major source of one-carbon units, is employed for the replenishment of ATP, NAD(P)H and *S*-adenosyl-methionine (SAM) majorly by cancer cells (Newman & Maddocks, 2017) and true to that we observed significantly increased uptake of this non-essential amino acid in activated WT cells compared to KOs. Relative to unstimulated state, the increased Glutamine uptake in KO cells compared to WT cells could be explained by the compensatory use of glutamine in response to reduced glucose uptake and metabolism by these cells. High dependence on glutamine as metabolite was further reflected by dramatic increase in free NH_3 (ammonia) levels in media of *ADPGK* KO cells in activated states, which reflected clearly the consumption of glutamine. Ornithine, which is originally not present in media formulation used for these cells, and was probably a by-product of glutamine metabolism, was also detected at values correlating with NH_3 levels and fortified the theory of glutamine dependent energy generation and biosynthesis by *ADPGK* KO cells.

Measurement of accumulated lactate and pyruvate levels in culture media of growing cells provides an estimate about the aerobic glycolysis (J. Xie et al., 2014; D. Q. Yang et al., 2016), with a higher lactate:pyruvate value correlating with increased aerobic glycolysis in increased cancer metabolism. The almost three-fold higher lactate:pyruvate levels observed upon stimulation at D2 (proliferative phase) in WT Ramos cells compared to KOs, further fortified the metabolic study, pointing to a highly diminished Warburg phenotype of *ADPGK* KO cells.

Overall, the presented data suggests that hampered induction of Warburg effect is underlying the failure of *ADPGK* KO cells to fully proliferate and differentiate upon PMA activation.

c-*MYC* expression and mutational status are hampered by *ADPGK* KO

We found wild type *MYC* expression increasing upon activation and going down upon differentiation to stop cellular proliferation, as also known from B-cell differentiation models (Cole, 1986; C. V. Dang, 1999; Habib et al., 2007; Lin, Lin, & Calame, 2000). The reduction of overall levels of c-Myc at day seven signified a differentiated status of these cells (Lin et al., 2000; Shaffer et al., 2002). The repression of c-Myc upon differentiation signals the cell to stop proliferating and assume an antibody secreting phenotype (Shaffer et al., 2002).

Activation of B-cells triggers AID (Activation induced cytidine deaminase) mediated somatic hypermutation (Clark et al., 2006; Peled et al., 2008) in the IgH locus which is required for creating diversity in repertoire of antibodies after contact with an antigen. In case of Burkitt's lymphoma, translocated *MYC* becomes a target of SHM and AID mediated mutational activity (Adams et al., 1985; Bemark & Neuberger, 2000). However, accumulation of mutations, besides depending on AID activity, more importantly depend on the transcriptional rate of the target locus with a highly transcribing locus accumulating proportionally higher number of mutations (Ramiro, Stavropoulos, Jankovic, & Nussenzweig, 2003). With AID expression levels nearly the same in WT and KO cells, it is evident that a higher transcriptional activity of translocated *MYC* under the IgH promoter was responsible for the intriguingly large difference in accumulated mutations between WT and *ADPGK* KO cells, thereby showing the increased proliferative, activated phenotype of WT cells upon stimulation. With majority of the mutations observed at D2 and D7 post stimulation, it is obvious that activation induced hypermutation, acting though transcriptionally active WT cells, was responsible for the mutational status of these cells. Also, with several observed mutations in *MYC*, known to provide a growth advantage to cancer cells (P57, T58, S62, S67, R83, F138 etc.), by stabilizing the MYC protein (increased half-life) (Bhatia et al., 1993; Cowling et al., 2014; Hemann et al., 2005; Xu-Monette et al., 2016), future research could aim at introducing one or more of these mutations through transgenic *MYC* in Burkitt's lymphoma cells and observing their effects on proliferation and/or differentiation status of cells in which the endogenous *MYC* has been silenced.

***ADPGK* KO cells resemble a nutrient starved condition**

With a combined overview of metabolism, differentiation and mutational status of *MYC*, the situation observed in *ADPGK* KO cells is not very different from a nutrient starved cell, which fails to garner energy for upregulation of metabolic activity and synthesis of biomolecules. The desired upregulation in energy metabolism lacking in KO cells, they fail to transform into differentiated cells and are left with less available resources to spend for accumulating mutations in translocated *MYC*. The differentiation of B-cells into plasma cell phenotype requiring immense energy turnover and synthesis of thousands of proteins per minute (Bertolotti et al., 2010; Garcia-Manteiga et al., 2011), a healthy metabolic state becomes essential for cells proceeding through this pathway and the non-competent ones are pushed to apoptosis (Lam & Bhattacharya, 2018). A metabolically functional cell, represented in our study by *ADPGK* WT cells, will have enough energy stocks to upregulate proliferation and synthesis of proteins necessary for differentiating into an ASC (Antibody secreting cell) and also for providing evolutionary advantage to its progenies through accumulation of mutations. Overall, the nutrient state of the cell, acting in this case via the glucose sensor ADPGK, seems to be the interlinking factor between the threads of metabolism, differentiation and mutation accumulation.

***In-vitro* and *in-vivo* models of reduced tumor aggressiveness in ADPGK KO cells**

The co-culture and migration system provided added information about the oncogenic and transformation state of WT cells with KO cells showing reduced macrophage transforming capability *in-vitro*. Heterogenous populations of B and T lymphocytes have been shown to affect the polarization status of myeloid cells (de Visser, Eichten, & Coussens, 2006; DeNardo, Andreu, & Coussens, 2010) and hence the study provided another insight into the development of tumor-microenvironment with the activation status of B-cells regulating the immune response to tumor. We observed that activated germinal-centre B-cells can chemotactically attract macrophages, through migration, and transform these TAMs (tumor associated macrophages) to M2, tumor promoting phenotype, and that removal of a crucial regulator of aerobic glycolysis, ADPGK, abolishes this effect. We quantified this effect by measuring the expression of several important M1/M2 markers such as Hexokinase, IL8, iNOS and Arginase-1. Hexokinase expression which goes down upon PMA stimulation of THP-1 cells, went further down when the cells were incubated with WT Ramos cells,

signifying low glycolytic, pro-tumor M2 macrophages (Galvan-Pena & O'Neill, 2014). In *ADPGK* KO cells a contrary of this, upregulation of hexokinase levels, signified M1, anti-tumor macrophages. Interleukin-8, responsible for chemotaxis of immune cells to tumor and often related with anti-tumor-phenotype (Colegio et al., 2014; Varney et al., 2002), was found to increase upon incubation with *ADPGK* KO cells, signifying their reduced tumor aggressiveness *in-vitro*. iNOS and Arg1 are a set of complementary macrophage polarization markers, with their role depending on differential utilization of arginine. With iNOS metabolizing the arginine to nitric oxide (NO), a potential anti-tumor free radical, Arginase-1 leads to production of proline, involved in wound healing and tissue growth (Colegio et al., 2014; Galvan-Pena & O'Neill, 2014; Z. Yang & Ming, 2014). True to their roles, we found increased iNOS levels in *ADPGK* KO cells and increased Arg1 levels in WT Ramos cells, displaying clearly their macrophage M1 and M2 polarization potential respectively. Overall, the study was a novel design to study Burkitt's lymphoma-macrophage microenvironment *in-vitro* and thereby provided a quantitative measure of reduced macrophage polarizing capability and tumor aggressiveness of *ADPGK* KO cells.

The study, extended to *in-vivo* model in zebrafish, proved further the diminished tumor aggressiveness of *ADPGK* KO cells failing to grow in an otherwise natural environment for tumor growth. With an undeveloped adaptive immune system until at least 4 weeks post fertilization (Novoa & Figueras, 2012), the zebrafish larvae provided us a perfect model to study the growth of aggressive cancers in a much shorter period of time and with enhanced imaging possibilities than other experimental animals (Avci et al., 2018). Consistent to this, the use of *kdrl*:*GFP* zebrafish line (Abrial et al., 2017; Jin, Beis, Mitchell, Chen, & Stainier, 2005) enabled us to accurately monitor the growth of CM-dil tagged xenografted cells over a period of two days, corresponding to the activated proliferative state of Ramos BL cells. The KO cells showing a striking reduction in growth of xenograft, correlating with the metabolic and *in-vitro* studies, made evident the role of *ADPGK* as an important regulator of tumor growth *in-vivo* zebrafish yolk. The model is superior to commercially available 2D/3D-tumor culture models by providing an alternative natural environment with interacting stroma and vasculature along with the possibility of studying angiogenesis and immune cell involvement in the growth of tumor. This has been achieved by employing transgenic zebrafish lines for studying neovascularization, angiogenesis and metastasis of xenografts

implanted at different body locations in zebrafish larvae (Chiavacci et al., 2015; Nicoli & Presta, 2007; Tobia, Gariano, De Sena, & Presta, 2013; C. Zhao et al., 2011). These models of zebrafish xenograft provide real time imaging possibilities and monitoring dynamic changes in vasculature and/or tumor microenvironment (C. Zhao et al., 2011). Chemotherapeutic could be easily administered into larval water or directly to the tumor site by microinjection, providing rapid responses and precise quantification of tumor regression (Fior et al., 2017; Wu et al., 2017). Overall, the yolk microinjection and xenograft development model provide a basic but depending on components involved (neovascularization, micro-environment, metastasis, drug targeting etc.), a diverse system for future advances in rapid tumor profiling and targeting.

Outlook

In this study we found that Burkitt's lymphoma cells are not permanently frozen in an undifferentiated state of malignancy but could be induced to follow an aerobic glycolysis-driven activation pathway, which in the end leads to its own suppression. The study, though lacking the precise signalling pathway involved which leads to the observed metabolic catastrophe upon *ADPGK* knock-out, proved the importance of this protein in regulating glucose homeostasis and thereby acting as an important mediator in B-cell activation. Though indirectly, we managed to relate the suppression of an important proto-oncogene, *MYC*, with the loss of ADPGK activity. We observed the effects knowing that ER biosynthesis is highly upregulated in B-cells upon stimulation and a missing ER glucose sensor in form of ADPGK, could stall the metabolism and consequently the pathway to differentiation. Additionally, the reduction in glucose metabolism in knock-out cells being present even at unstimulated state, where ADPGK activity was undetectable, prompt us to investigate the possible interacting partners of ADPGK, irrespective of its catalytic function.

The development of inhibitors against ADPGK has found success as demonstrated by a recent study utilizing 8-bromoadenosine phosphate (Grudnik et al., 2018), however with the physiological role of ADPGK still not fully deciphered, drug targets against ADPGK still await discovery and deployment.

Overall, knowing the role of ADPGK in cancer metabolism and immune cell activation, as demonstrated by our study, the discovery of antibodies/inhibitors against ADPGK can have far reaching consequences against autoimmune diseases and immunological cancers.

Conclusion

We successfully identified the role of ADPGK in regulation of aerobic glycolysis in Burkitt's Lymphoma cells and showed that its knock-out leads to reduced tumor aggressiveness, as measured *in-vitro* and *in-vivo* Zebrafish. We found reduced *MYC* transcription in *ADPGK* knock-out Burkitt's lymphoma cells and several folds reduction in accumulated random mutations in translocated *MYC* in these cells. We additionally observed a stalled pathway to differentiation of ADPGK knock out B-cells into plasma cells upon stimulation by mitogenic signals. Overall, ADPGK was found to act as a regulator of cell-differentiation and cancer aggressiveness in Burkitt's lymphoma cells.

Bibliography

1. Abrial, M., Paffett-Lugassy, N., Jeffrey, S., Jordan, D., O'Loughlin, E., Frederick, C. J., 3rd, . . . Burns, C. E. (2017). TGF-beta Signaling Is Necessary and Sufficient for Pharyngeal Arch Artery Angioblast Formation. *Cell Rep, 20*(4), 973-983. doi:10.1016/j.celrep.2017.07.002
2. Adams, J. M., Harris, A. W., Pinkert, C. A., Corcoran, L. M., Alexander, W. S., Cory, S., . . . Brinster, R. L. (1985). The c-myc oncogene driven by immunoglobulin enhancers induces lymphoid malignancy in transgenic mice. *Nature, 318*(6046), 533-538.
3. Alberts, B. (2017). Molecular Biology of the Cell.
4. Allavena, P., Sica, A., Solinas, G., Porta, C., & Mantovani, A. (2008). The inflammatory micro-environment in tumor progression: the role of tumor-associated macrophages. *Crit Rev Oncol Hematol, 66*(1), 1-9. doi:10.1016/j.critrevonc.2007.07.004
5. Andrade-Filho, J. S. (2014). ANALOGIES IN MEDICINE: STARRY-SKY. *Rev Inst Med Trop Sao Paulo, 56*(6), 541-542. doi:10.1590/s0036-46652014000600015
6. Antinucci, P., & Hindges, R. (2016). A crystal-clear zebrafish for in vivo imaging. *Sci Rep, 6*, 29490. doi:10.1038/srep29490
7. Avci, M. E., Keskus, A. G., Targen, S., Isilak, M. E., Ozturk, M., Atalay, R. C., . . . Konu, O. (2018). Development of a novel zebrafish xenograft model in ache mutants using liver cancer cell lines. *Sci Rep, 8*(1), 1570. doi:10.1038/s41598-018-19817-w
8. Barriuso, J., Nagaraju, R., & Hurlstone, A. (2015). Zebrafish: a new companion for translational research in oncology. *Clin Cancer Res, 21*(5), 969-975. doi:10.1158/1078-0432.ccr-14-2921
9. Bemark, M., & Neuberger, M. S. (2000). The c-MYC allele that is translocated into the IgH locus undergoes constitutive hypermutation in a Burkitt's lymphoma line. *Oncogene, 19*(30), 3404-3410. doi:10.1038/sj.onc.1203686
10. Benjamin, D., Magrath, I. T., Triche, T. J., Schroff, R. W., Jensen, J. P., & Korsmeyer, S. J. (1984). Induction of plasmacytoid differentiation by phorbol ester in B-cell lymphoma cell lines bearing 8;14 translocations. *Proc Natl Acad Sci U S A, 81*(11), 3547-3551.
11. Bertolotti, M., Yim, S. H., Garcia-Manteiga, J. M., Masciarelli, S., Kim, Y. J., Kang, M. H., . . . Sitia, R. (2010). B- to plasma-cell terminal differentiation entails oxidative stress and profound reshaping of the antioxidant responses. *Antioxid Redox Signal, 13*(8), 1133-1144. doi:10.1089/ars.2009.3079
12. Betz, A. G., Rada, C., Pannell, R., Milstein, C., & Neuberger, M. S. (1993). Passenger transgenes reveal intrinsic specificity of the antibody hypermutation mechanism: clustering, polarity, and specific hot spots. *Proc Natl Acad Sci U S A, 90*(6), 2385-2388.
13. Bhatia, K., Huppi, K., Spangler, G., Siwarski, D., Iyer, R., & Magrath, I. (1993). Point mutations in the c-Myc transactivation domain are common in Burkitt's lymphoma and mouse plasmacytomas. *Nat Genet, 5*(1), 56-61. doi:10.1038/ng0993-56
14. Bradbury, J. (2004). Small fish, big science. *PLoS Biol, 2*(5), E148. doi:10.1371/journal.pbio.0020148
15. Brand, K., Leibold, W., Luppa, P., Schoerner, C., & Schulz, A. (1986). Metabolic alterations associated with proliferation of mitogen-activated lymphocytes and of

lymphoblastoid cell lines: evaluation of glucose and glutamine metabolism. *Immunobiology, 173*(1), 23-34. doi:10.1016/s0171-2985(86)80086-9

16. Bransteitter, R., Pham, P., Scharff, M. D., & Goodman, M. F. (2003). Activation-induced cytidine deaminase deaminates deoxycytidine on single-stranded DNA but requires the action of RNase. *Proc Natl Acad Sci U S A, 100*(7), 4102-4107. doi:10.1073/pnas.0730835100
17. Burger, J. A., & Peled, A. (2009). CXCR4 antagonists: targeting the microenvironment in leukemia and other cancers. *Leukemia, 23*(1), 43-52. doi:10.1038/leu.2008.299
18. Buttgereit, F., Burmester, G. R., & Brand, M. D. (2000). Bioenergetics of immune functions: fundamental and therapeutic aspects. *Immunol Today, 21*(4), 192-199.
19. Cairns, R. A., Harris, I. S., & Mak, T. W. (2011). Regulation of cancer cell metabolism. *Nat Rev Cancer, 11*(2), 85-95. doi:10.1038/nrc2981
20. Chiavacci, E., Rizzo, M., Pitto, L., Patella, F., Evangelista, M., Mariani, L., & Rainaldi, G. (2015). The zebrafish/tumor xenograft angiogenesis assay as a tool for screening anti-angiogenic miRNAs. *Cytotechnology, 67*(6), 969-975. doi:10.1007/s10616-014-9735-y
21. Clark, L. A., Ganesan, S., Papp, S., & van Vlijmen, H. W. (2006). Trends in antibody sequence changes during the somatic hypermutation process. *J Immunol, 177*(1), 333-340.
22. Cole, M. D. (1986). The myc oncogene: its role in transformation and differentiation. *Annu Rev Genet, 20*, 361-384. doi:10.1146/annurev.ge.20.120186.002045
23. Colegio, O. R., Chu, N. Q., Szabo, A. L., Chu, T., Rhebergen, A. M., Jairam, V., . . . Medzhitov, R. (2014). Functional polarization of tumour-associated macrophages by tumour-derived lactic acid. *Nature, 513*(7519), 559-563. doi:10.1038/nature13490
24. Coussens, L. M., & Werb, Z. (2002). Inflammation and cancer. *Nature, 420*(6917), 860-867. doi:10.1038/nature01322
25. Cowling, V. H., Turner, S. A., & Cole, M. D. (2014). Burkitt's lymphoma-associated c-Myc mutations converge on a dramatically altered target gene response and implicate Nol5a/Nop56 in oncogenesis. *Oncogene, 33*(27), 3519-3527. doi:10.1038/onc.2013.338
26. Cox, B. L., Mackie, T. R., & Eliceiri, K. W. (2015). The sweet spot: FDG and other 2-carbon glucose analogs for multi-modal metabolic imaging of tumor metabolism. *Am J Nucl Med Mol Imaging, 5*(1), 1-13.
27. Dang, C. V. (1999). c-Myc Target Genes Involved in Cell Growth, Apoptosis, and Metabolism. *Mol Cell Biol, 19*(1), 1-11.
28. Dang, L. H., & Rock, K. L. (1991). Stimulation of B lymphocytes through surface Ig receptors induces LFA-1 and ICAM-1-dependent adhesion. *J Immunol, 146*(10), 3273-3279.
29. de Visser, K. E., Eichten, A., & Coussens, L. M. (2006). Paradoxical roles of the immune system during cancer development. *Nat Rev Cancer, 6*(1), 24-37. doi:10.1038/nrc1782
30. DeBerardinis, R. J., Lum, J. J., Hatzivassiliou, G., & Thompson, C. B. (2008). The biology of cancer: metabolic reprogramming fuels cell growth and proliferation. *Cell Metab, 7*(1), 11-20. doi:10.1016/j.cmet.2007.10.002
31. DeFranco, A. L., Raveche, E. S., & Paul, W. E. (1985). Separate control of B lymphocyte early activation and proliferation in response to anti-IgM antibodies. *J Immunol, 135*(1), 87-94.

32. DeNardo, D. G., Andreu, P., & Coussens, L. M. (2010). Interactions between lymphocytes and myeloid cells regulate pro- versus anti-tumor immunity. *Cancer Metastasis Rev, 29*(2), 309-316. doi:10.1007/s10555-010-9223-6
33. Di Noia, J. M., & Neuberger, M. S. (2007). Molecular mechanisms of antibody somatic hypermutation. *Annu Rev Biochem, 76*, 1-22. doi:10.1146/annurev.biochem.76.061705.090740
34. Ding, B. B., Bi, E., Chen, H., Yu, J. J., & Ye, B. H. (2013). IL-21 and CD40L synergistically promote plasma cell differentiation through upregulation of Blimp-1 in human B cells. *J Immunol, 190*(4), 1827-1836. doi:10.4049/jimmunol.1201678
35. Dozzo, M., Carobolante, F., Donisi, P. M., Scattolin, A., Maino, E., Sancetta, R., . . . Bassan, R. (2017). Burkitt lymphoma in adolescents and young adults: management challenges. *Adolesc Health Med Ther, 8*, 11-29. doi:10.2147/ahmt.s94170
36. Duquette, M. L., Pham, P., Goodman, M. F., & Maizels, N. (2005). AID binds to transcription-induced structures in c-MYC that map to regions associated with translocation and hypermutation. *Oncogene, 24*(38), 5791-5798. doi:10.1038/sj.onc.1208746
37. Eick, D., & Bornkamm, G. W. (1989). Expression of normal and translocated c-myc alleles in Burkitt's lymphoma cells: evidence for different regulation. *Embo j, 8*(7), 1965-1972.
38. Ellett, F., Pase, L., Hayman, J. W., Andrianopoulos, A., & Lieschke, G. J. (2011). mpeg1 promoter transgenes direct macrophage-lineage expression in zebrafish. *Blood, 117*(4), e49-56. doi:10.1182/blood-2010-10-314120
39. Escuin-Ordinas, H., Elliott, M. W., Atefi, M., Lee, M., Ng, C., Wei, L., . . . Ribas, A. (2013). PET imaging to non-invasively study immune activation leading to antitumor responses with a 4-1BB agonistic antibody. *J Immunother Cancer, 1*, 14. doi:10.1186/2051-1426-1-14
40. Fior, R., Povoa, V., Mendes, R. V., Carvalho, T., Gomes, A., Figueiredo, N., & Ferreira, M. G. (2017). Single-cell functional and chemosensitive profiling of combinatorial colorectal therapy in zebrafish xenografts. *Proc Natl Acad Sci U S A, 114*(39), E8234-e8243. doi:10.1073/pnas.1618389114
41. Fouad, Y. A., & Aanei, C. (2017). Revisiting the hallmarks of cancer. *Am J Cancer Res, 7*(5), 1016-1036.
42. Galvan-Pena, S., & O'Neill, L. A. (2014). Metabolic reprograming in macrophage polarization. *Front Immunol, 5*, 420. doi:10.3389/fimmu.2014.00420
43. Garcia-Manteiga, J. M., Mari, S., Godejohann, M., Spraul, M., Napoli, C., Cenci, S., . . . Sitia, R. (2011). Metabolomics of B to plasma cell differentiation. *J Proteome Res, 10*(9), 4165-4176. doi:10.1021/pr200328f
44. Gatenby, R. A., & Gillies, R. J. (2004). Why do cancers have high aerobic glycolysis? *Nat Rev Cancer, 4*(11), 891-899. doi:10.1038/nrc1478
45. Genard, G., Lucas, S., & Michiels, C. (2017). Reprogramming of Tumor-Associated Macrophages with Anticancer Therapies: Radiotherapy versus Chemo- and Immunotherapies. *Front Immunol, 8*. doi:10.3389/fimmu.2017.00828
46. Gensel, J. C., Kopper, T. J., Zhang, B., Orr, M. B., & Bailey, W. M. (2017). Predictive screening of M1 and M2 macrophages reveals the immunomodulatory effectiveness of post spinal cord injury azithromycin treatment. *Sci Rep, 7*, 40144. doi:10.1038/srep40144

47. Ghamlouch, H., Ouled-Haddou, H., Guyart, A., Regnier, A., Trudel, S., Claisse, J. F., . . . Gubler, B. (2014). Phorbol myristate acetate, but not CD40L, induces the differentiation of CLL B cells into Ab-secreting cells. *Immunol Cell Biol, 92*(7), 591-604. doi:10.1038/icb.2014.37
48. Ghesquiere, B., Wong, B. W., Kuchnio, A., & Carmeliet, P. (2014). Metabolism of stromal and immune cells in health and disease. *Nature, 511*(7508), 167-176. doi:10.1038/nature13312
49. Grudnik, P., Kaminski, M. M., Rembacz, K. P., Kuska, K., Madej, M., Potempa, J., . . . Dubin, G. (2018). Structural basis for ADP-dependent glucokinase inhibition by 8-bromo-substituted adenosine nucleotide. *J Biol Chem, 293*(28), 11088-11099. doi:10.1074/jbc.RA117.001562
50. Habib, T., Park, H., Tsang, M., de Alboran, I. M., Nicks, A., Wilson, L., . . . Iritani, B. M. (2007). Myc stimulates B lymphocyte differentiation and amplifies calcium signaling. *J Cell Biol, 179*(4), 717-731. doi:10.1083/jcb.200704173
51. He, Y. (2010). Emerging Roles for XBP1, a sUPeR Transcription Factor. *15*(1), 13-25.
52. Hemann, M. T., Bric, A., Teruya-Feldstein, J., Herbst, A., Nilsson, J. A., Cordon-Cardo, C., . . . Lowe, S. W. (2005). Evasion of the p53 tumour surveillance network by tumour-derived MYC mutants. *Nature, 436*(7052), 807-811. doi:10.1038/nature03845
53. Ho, Y. S., Subhendu, C., & Hsu, S. M. (1987). Induction of differentiation of African Burkitt's lymphoma cells by phorbol ester: possible relation with early B cells. *Cancer Invest, 5*(2), 101-107.
54. Ibrahim, M., & Richardson, M. K. (2017). In vitro development of zebrafish vascular networks. *Reprod Toxicol, 70*, 102-115. doi:10.1016/j.reprotox.2017.02.008
55. Jiang, P., Du, W., & Wu, M. (2014). Regulation of the pentose phosphate pathway in cancer. *Protein Cell, 5*(8), 592-602. doi:10.1007/s13238-014-0082-8
56. Jin, S. W., Beis, D., Mitchell, T., Chen, J. N., & Stainier, D. Y. (2005). Cellular and molecular analyses of vascular tube and lumen formation in zebrafish. *Development, 132*(23), 5199-5209. doi:10.1242/dev.02087
57. Jourdan, M., Caraux, A., Caron, G., Robert, N., Fiol, G., Reme, T., . . . Klein, B. (2011). Characterization of a transitional preplasmablast population in the process of human B cell to plasma cell differentiation. *J Immunol, 187*(8), 3931-3941. doi:10.4049/jimmunol.1101230
58. Kalueff, A. V., Stewart, A. M., & Gerlai, R. (2014). Zebrafish as an emerging model for studying complex brain disorders. *Trends Pharmacol Sci, 35*(2), 63-75. doi:10.1016/j.tips.2013.12.002
59. Kaminski, D. A., Wei, C., Qian, Y., Rosenberg, A. F., & Sanz, I. (2012). Advances in human B cell phenotypic profiling. *Front Immunol, 3*, 302. doi:10.3389/fimmu.2012.00302
60. Kaminski, M. M., Sauer, S. W., Kaminski, M., Opp, S., Ruppert, T., Grigaravicius, P., . . . Gulow, K. (2012). T cell activation is driven by an ADP-dependent glucokinase linking enhanced glycolysis with mitochondrial reactive oxygen species generation. *Cell Rep, 2*(5), 1300-1315. doi:10.1016/j.celrep.2012.10.009
61. Katabi, M. M., Chan, H. L., Karp, S. E., & Batist, G. (1999). Hexokinase type II: a novel tumor-specific promoter for gene-targeted therapy differentially expressed and regulated in human cancer cells. *Hum Gene Ther, 10*(2), 155-164. doi:10.1089/10430349950018959

62. Kengen, S. W., de Bok, F. A., van Loo, N. D., Dijkema, C., Stams, A. J., & de Vos, W. M. (1994). Evidence for the operation of a novel Embden-Meyerhof pathway that involves ADP-dependent kinases during sugar fermentation by Pyrococcus furiosus. *J Biol Chem, 269*(26), 17537-17541.
63. Kharabi Masouleh, B., Ten Dam, G. B., Wild, M. K., Seelige, R., van der Vlag, J., Rops, A. L., . . . Gotte, M. (2009). Role of the heparan sulfate proteoglycan syndecan-1 (CD138) in delayed-type hypersensitivity. *J Immunol, 182*(8), 4985-4993. doi:10.4049/jimmunol.0800574
64. Krappmann, D., Patke, A., Heissmeyer, V., & Scheidereit, C. (2001). B-cell receptor- and phorbol ester-induced NF-kappaB and c-Jun N-terminal kinase activation in B cells requires novel protein kinase C's. *Mol Cell Biol, 21*(19), 6640-6650.
65. Lam, W. Y., & Bhattacharya, D. (2018). Metabolic Links between Plasma Cell Survival, Secretion, and Stress. *Trends Immunol, 39*(1), 19-27. doi:10.1016/j.it.2017.08.007
66. Li, Z., Woo, C. J., Iglesias-Ussel, M. D., Ronai, D., & Scharff, M. D. (2004). The generation of antibody diversity through somatic hypermutation and class switch recombination. *Genes Dev, 18*(1), 1-11. doi:10.1101/gad.1161904
67. Liberti, M. V., & Locasale, J. W. (2016). The Warburg Effect: How Does it Benefit Cancer Cells? *Trends Biochem Sci, 41*(3), 211-218. doi:10.1016/j.tibs.2015.12.001
68. Lilie, H., McLaughlin, S., Freedman, R., & Buchner, J. (1994). Influence of protein disulfide isomerase (PDI) on antibody folding in vitro. *J Biol Chem, 269*(19), 14290-14296.
69. Lin, K. I., Lin, Y., & Calame, K. (2000). Repression of c-myc Is Necessary but Not Sufficient for Terminal Differentiation of B Lymphocytes In Vitro. *Mol Cell Biol, 20*(23), 8684-8695.
70. Liu, Y., & Cao, X. (2015). The origin and function of tumor-associated macrophages. *Cell Mol Immunol, 12*(1), 1-4. doi:10.1038/cmi.2014.83
71. Maestre, L., Tooze, R., Canamero, M., Montes-Moreno, S., Ramos, R., Doody, G., . . . Roncador, G. (2009). Expression pattern of XBP1(S) in human B-cell lymphomas. *Haematologica, 94*(3), 419-422. doi:10.3324/haematol.2008.001156
72. Mantovani, A., Sozzani, S., Locati, M., Allavena, P., & Sica, A. (2002). Macrophage polarization: tumor-associated macrophages as a paradigm for polarized M2 mononuclear phagocytes. *Trends Immunol, 23*(11), 549-555.
73. Mao, C., Jiang, L., Melo-Jorge, M., Puthenveetil, M., Zhang, X., Carroll, M. C., & Imanishi-Kari, T. (2004). T cell-independent somatic hypermutation in murine B cells with an immature phenotype. *Immunity, 20*(2), 133-144.
74. Mathupala, S. P., Ko, Y. H., & Pedersen, P. L. (2006). Hexokinase II: cancer's double-edged sword acting as both facilitator and gatekeeper of malignancy when bound to mitochondria. *Oncogene, 25*(34), 4777-4786. doi:10.1038/sj.onc.1209603
75. Mattaini, K. R., Sullivan, M. R., & Vander Heiden, M. G. (2016). The importance of serine metabolism in cancer. *J Cell Biol, 214*(3), 249-257. doi:10.1083/jcb.201604085
76. McCarron, M. J., Park, P. W., & Fooksman, D. R. (2017). CD138 mediates selection of mature plasma cells by regulating their survival. *Blood, 129*(20), 2749-2759. doi:10.1182/blood-2017-01-761643
77. Miyaishi, O., Kozaki, K., Iida, K., Isobe, K., Hashizume, Y., & Saga, S. (1998). Elevated expression of PDI family proteins during differentiation of mouse F9 teratocarcinoma cells. *J Cell Biochem, 68*(4), 436-445.

78. Molyneux, E. M., Rochford, R., Griffin, B., Newton, R., Jackson, G., Menon, G., . . . Bailey, S. (2012). Burkitt's lymphoma. *Lancet, 379*(9822), 1234-1244. doi:10.1016/s0140-6736(11)61177-x
79. Murdoch, C., Muthana, M., Coffelt, S. B., & Lewis, C. E. (2008). The role of myeloid cells in the promotion of tumour angiogenesis. *Nat Rev Cancer, 8*(8), 618-631. doi:10.1038/nrc2444
80. Newman, A. C., & Maddocks, O. D. K. (2017). Serine and Functional Metabolites in Cancer. *Trends Cell Biol, 27*(9), 645-657. doi:10.1016/j.tcb.2017.05.001
81. Nicoli, S., & Presta, M. (2007). The zebrafish/tumor xenograft angiogenesis assay. *Nat Protoc, 2*(11), 2918-2923. doi:10.1038/nprot.2007.412
82. Novoa, B., & Figueras, A. (2012). Zebrafish: model for the study of inflammation and the innate immune response to infectious diseases. *Adv Exp Med Biol, 946*, 253-275. doi:10.1007/978-1-4614-0106-3_15
83. Oka, O. B., & Bulleid, N. J. (2013). Forming disulfides in the endoplasmic reticulum. *Biochim Biophys Acta, 1833*(11), 2425-2429. doi:10.1016/j.bbamcr.2013.02.007
84. Patra, K. C., Wang, Q., Bhaskar, P. T., Miller, L., Wang, Z., Wheaton, W., . . . Hay, N. (2013). Hexokinase 2 is required for tumor initiation and maintenance and its systemic deletion is therapeutic in mouse models of cancer. *Cancer Cell, 24*(2), 213-228. doi:10.1016/j.ccr.2013.06.014
85. Paver, J. L., Freedman, R. B., & Parkhouse, R. M. (1989). Induction of expression of protein disulphide-isomerase during lymphocyte maturation stimulated by bacterial lipopolysaccharide. *FEBS Lett, 242*(2), 357-362.
86. Peled, J. U., Kuang, F. L., Iglesias-Ussel, M. D., Roa, S., Kalis, S. L., Goodman, M. F., & Scharff, M. D. (2008). The biochemistry of somatic hypermutation. *Annu Rev Immunol, 26*, 481-511. doi:10.1146/annurev.immunol.26.021607.090236
87. Phan, L. M., Yeung, S. C. J., & Lee, M. H. (2014). Cancer metabolic reprogramming: importance, main features, and potentials for precise targeted anti-cancer therapies. *Cancer Biol Med, 11*(1), 1-19. doi:10.7497/j.issn.2095-3941.2014.01.001
88. Pieper, K., Grimbacher, B., & Eibel, H. (2013). B-cell biology and development. *J Allergy Clin Immunol, 131*(4), 959-971. doi:10.1016/j.jaci.2013.01.046
89. Proia, P., Di Liegro, C. M., Schiera, G., Fricano, A., & Di Liegro, I. (2016). Lactate as a Metabolite and a Regulator in the Central Nervous System. *Int J Mol Sci, 17*(9). doi:10.3390/ijms17091450
90. Ramiro, A. R., Stavropoulos, P., Jankovic, M., & Nussenzweig, M. C. (2003). Transcription enhances AID-mediated cytidine deamination by exposing single-stranded DNA on the nontemplate strand. *Nat Immunol, 4*(5), 452-456. doi:10.1038/ni920
91. Reimold, A. M., Iwakoshi, N. N., Manis, J., Vallabhajosyula, P., Szomolanyi-Tsuda, E., Gravallese, E. M., . . . Glimcher, L. H. (2001). Plasma cell differentiation requires the transcription factor XBP-1. *Nature, 412*(6844), 300-307. doi:10.1038/35085509
92. Richter, J. P., Goroncy, A. K., Ronimus, R. S., & Sutherland-Smith, A. J. (2016). The Structural and Functional Characterization of Mammalian ADP-dependent Glucokinase. *J Biol Chem, 291*(8), 3694-3704. doi:10.1074/jbc.M115.679902
93. Richter, S., Richter, J. P., Mehta, S. Y., Gribble, A. M., Sutherland-Smith, A. J., Stowell, K. M., . . . Wilson, W. R. (2012). Expression and role in glycolysis of human ADP-dependent glucokinase. *Mol Cell Biochem, 364*(1-2), 131-145. doi:10.1007/s11010-011-1212-8

94. Roth, K., Oehme, L., Zehentmeier, S., Zhang, Y., Niesner, R., & Hauser, A. E. (2014). Tracking plasma cell differentiation and survival. *Cytometry A, 85*(1), 15-24. doi:10.1002/cyto.a.22355
95. Rousset, F., Billaud, M., Blanchard, D., Figdor, C., Lenoir, G. M., Spits, H., & De Vries, J. E. (1989). IL-4 induces LFA-1 and LFA-3 expression on Burkitt's lymphoma cell lines. Requirement of additional activation by phorbol myristate acetate for induction of homotypic cell adhesions. *J Immunol, 143*(5), 1490-1498.
96. Rudnicka, D., Oszmiana, A., Finch, D. K., Strickland, I., Schofield, D. J., Lowe, D. C., . . . Davis, D. M. (2013). Rituximab causes a polarization of B cells that augments its therapeutic function in NK-cell-mediated antibody-dependent cellular cytotoxicity. *Blood, 121*(23), 4694-4702. doi:10.1182/blood-2013-02-482570
97. Schmitz, R., Ceribelli, M., Pittaluga, S., Wright, G., & Staudt, L. M. (2014). Oncogenic mechanisms in Burkitt lymphoma. *Cold Spring Harb Perspect Med, 4*(2). doi:10.1101/cshperspect.a014282
98. Schutte, B., Nuydens, R., Geerts, H., & Ramaekers, F. (1998). Annexin V binding assay as a tool to measure apoptosis in differentiated neuronal cells. *J Neurosci Methods, 86*(1), 63-69.
99. Scott, D. W., & Gascoyne, R. D. (2014). The tumour microenvironment in B cell lymphomas. *Nat Rev Cancer, 14*(8), 517-534. doi:10.1038/nrc3774
100. Semmel, M., Hanania, N., Huet, S., Pavloff, N., Gay, F., & Biquard, J. M. (1988). Differentiation of Burkitt lymphoma cells by hexamethylenbisacetamide. *Mol Biol Rep, 13*(3), 151-157.
101. Shaffer, A. L., Lin, K. I., Kuo, T. C., Yu, X., Hurt, E. M., Rosenwald, A., . . . Staudt, L. M. (2002). Blimp-1 orchestrates plasma cell differentiation by extinguishing the mature B cell gene expression program. *Immunity, 17*(1), 51-62.
102. Shapiro-Shelef, M., & Calame, K. (2005). Regulation of plasma-cell development. *Nat Rev Immunol, 5*(3), 230-242. doi:10.1038/nri1572
103. Spence, R., Gerlach, G., Lawrence, C., & Smith, C. (2008). The behaviour and ecology of the zebrafish, Danio rerio. *Biol Rev Camb Philos Soc, 83*(1), 13-34. doi:10.1111/j.1469-185X.2007.00030.x
104. Stewart, M. D., Ramani, V. C., & Sanderson, R. D. (2015). Shed syndecan-1 translocates to the nucleus of cells delivering growth factors and inhibiting histone acetylation: a novel mechanism of tumor-host cross-talk. *J Biol Chem, 290*(2), 941-949. doi:10.1074/jbc.M114.608455
105. Subei, A. M., & Cohen, J. A. (2015). Sphingosine 1-Phosphate Receptor Modulators in Multiple Sclerosis. *CNS Drugs, 29*(7), 565-575. doi:10.1007/s40263-015-0261-z
106. Szulzewsky, F., Pelz, A., Feng, X., Synowitz, M., Markovic, D., Langmann, T., . . . Kettenmann, H. (2015). Glioma-associated microglia/macrophages display an expression profile different from M1 and M2 polarization and highly express Gpnmb and Spp1. *PLoS One, 10*(2), e0116644. doi:10.1371/journal.pone.0116644
107. Tedder, T. F., Boyd, A. W., Freedman, A. S., Nadler, L. M., & Schlossman, S. F. (1985). The B cell surface molecule B1 is functionally linked with B cell activation and differentiation. *J Immunol, 135*(2), 973-979.
108. Tedder, T. F., & Engel, P. (1994). CD20: a regulator of cell-cycle progression of B lymphocytes. *Immunol Today, 15*(9), 450-454. doi:10.1016/0167-5699(94)90276-3

109. Tobia, C., Gariano, G., De Sena, G., & Presta, M. (2013). Zebrafish embryo as a tool to study tumor/endothelial cell cross-talk. *Biochim Biophys Acta, 1832*(9), 1371-1377. doi:10.1016/j.bbadis.2013.01.016
110. Todd, D. J., McHeyzer-Williams, L. J., Kowal, C., Lee, A. H., Volpe, B. T., Diamond, B., . . . Glimcher, L. H. (2009). XBP1 governs late events in plasma cell differentiation and is not required for antigen-specific memory B cell development. *J Exp Med, 206*(10), 2151-2159. doi:10.1084/jem.20090738
111. Tsun, Z. Y., & Possemato, R. (2015). Amino acid management in cancer. *Semin Cell Dev Biol, 43*, 22-32. doi:10.1016/j.semcdb.2015.08.002
112. Tsuru, A., Imai, Y., Saito, M., & Kohno, K. (2016). Novel mechanism of enhancing IRE1alpha-XBP1 signalling via the PERK-ATF4 pathway. *Sci Rep, 6*, 24217. doi:10.1038/srep24217
113. Valentine, M. A., Cotner, T., Gaur, L., Torres, R., & Clark, E. A. (1987). Expression of the human B-cell surface protein CD20: alteration by phorbol 12-myristate 13-acetate. *Proc Natl Acad Sci U S A, 84*(22), 8085-8089.
114. van der Ent, W., Burrello, C., Teunisse, A. F., Ksander, B. R., van der Velden, P. A., Jager, M. J., . . . Snaar-Jagalska, B. E. (2014). Modeling of human uveal melanoma in zebrafish xenograft embryos. *Invest Ophthalmol Vis Sci, 55*(10), 6612-6622. doi:10.1167/iovs.14-15202
115. Varney, M. L., Olsen, K. J., Mosley, R. L., Bucana, C. D., Talmadge, J. E., & Singh, R. K. (2002). Monocyte/macrophage recruitment, activation and differentiation modulate interleukin-8 production: a paracrine role of tumor-associated macrophages in tumor angiogenesis. *In Vivo, 16*(6), 471-477.
116. Vincent, C., Truffinet, V., Fiancette, R., Petit, B., Cogne, N., Cogne, M., & Denizot, Y. (2009). Uncoupling between Ig somatic hypermutation and oncogene mutation in mouse lymphoma. *Biochim Biophys Acta, 1793*(2), 418-426. doi:10.1016/j.bbamcr.2008.10.011
117. Wagner, S. D., & Neuberger, M. S. (1996). Somatic hypermutation of immunoglobulin genes. *Annu Rev Immunol, 14*, 441-457. doi:10.1146/annurev.immunol.14.1.441
118. Walshe, C. A., Beers, S. A., French, R. R., Chan, C. H., Johnson, P. W., Packham, G. K., . . . Cragg, M. S. (2008). Induction of cytosolic calcium flux by CD20 is dependent upon B Cell antigen receptor signaling. *J Biol Chem, 283*(25), 16971-16984. doi:10.1074/jbc.M708459200
119. Wu, J. Q., Zhai, J., Li, C. Y., Tan, A. M., Wei, P., Shen, L. Z., & He, M. F. (2017). Patient-derived xenograft in zebrafish embryos: a new platform for translational research in gastric cancer. *J Exp Clin Cancer Res, 36*. doi:10.1186/s13046-017-0631-0
120. Xie, H., Tang, C. H., Song, J. H., Mancuso, A., Del Valle, J. R., Cao, J., . . . Simon, M. C. (2018). IRE1alpha RNase-dependent lipid homeostasis promotes survival in Myc-transformed cancers. *J Clin Invest, 128*(4), 1300-1316. doi:10.1172/jci95864
121. Xie, J., Wu, H., Dai, C., Pan, Q., Ding, Z., Hu, D., . . . Hu, X. (2014). Beyond Warburg effect – dual metabolic nature of cancer cells. *Sci Rep, 4*. doi:10.1038/srep04927
122. Xu-Monette, Z. Y., Deng, Q., Manyam, G. C., Tzankov, A., Li, L., Xia, Y., . . . Young, K. H. (2016). MYC mutation profiling and prognostic significance in de novo diffuse large B-cell lymphoma. *Clin Cancer Res, 22*(14), 3593-3605. doi:10.1158/1078-0432.ccr-15-2296

123. Xu, M. L., & Fedoriw, Y. (2016). Lymphoma Microenvironment and Immunotherapy. *Surg Pathol Clin, 9*(1), 93-100. doi:10.1016/j.path.2015.10.001
124. Xu, S. N., Wang, T. S., Li, X., & Wang, Y. P. (2016). SIRT2 activates G6PD to enhance NADPH production and promote leukaemia cell proliferation. *Sci Rep, 6*, 32734. doi:10.1038/srep32734
125. Yang, D. Q., Freund, D. M., Harris, B. R. E., Wang, D., Cleary, M. P., & Hegeman, A. D. (2016). Measuring relative utilization of aerobic glycolysis in breast cancer cells by positional isotopic discrimination. *FEBS Lett, 590*(18), 3179-3187. doi:10.1002/1873-3468.12360
126. Yang, Z., & Ming, X. F. (2014). Functions of arginase isoforms in macrophage inflammatory responses: impact on cardiovascular diseases and metabolic disorders. *Front Immunol, 5*, 533. doi:10.3389/fimmu.2014.00533
127. Zhang, Y., Garcia-Ibanez, L., & Toellner, K. M. (2016). Regulation of germinal center B-cell differentiation. *Immunol Rev, 270*(1), 8-19. doi:10.1111/imr.12396
128. Zhao, C., Wang, X., Zhao, Y., Li, Z., Lin, S., Wei, Y., & Yang, H. (2011). A novel xenograft model in zebrafish for high-resolution investigating dynamics of neovascularization in tumors. *PLoS One, 6*(7), e21768. doi:10.1371/journal.pone.0021768
129. Zhao, N., Cao, J., Xu, L., Tang, Q., Dobrolecki, L. E., Lv, X., . . . Chen, X. (2018). Pharmacological targeting of MYC-regulated IRE1/XBP1 pathway suppresses MYC-driven breast cancer. *J Clin Invest, 128*(4), 1283-1299. doi:10.1172/jci95873
130. Zou, C., Wang, Y., & Shen, Z. (2005). 2-NBDG as a fluorescent indicator for direct glucose uptake measurement. *J Biochem Biophys Methods, 64*(3), 207-215. doi:10.1016/j.jbbm.2005.08.001